LCH Laboratoire de Constructions Hydrauliques
Laboratory of Hydraulic Constructions

ÉCOLE POLYTECHNIQUE
FÉDÉRALE DE LAUSANNE

Communication 62

Time-dependent failure analysis of large block size riprap as bank protection in mountain rivers

Mona Jafarnejad Chaghooshi

Editeur : Prof. Dr A. Schleiss

Lausanne, 2016

Communications du Laboratoire de Constructions Hydrauliques ISSN 1661-1179
Ecole Polytechnique Fédérale de Lausanne
Editeur: Prof. Dr A. Schleiss

PREFACE

The protection of riverbanks with blocks, called riprap, is the most used method in alpine rivers to avoid uncontrolled lateral erosion. For rivers with significant bed slopes large boulders have to be used in order to withstand high flow forces. Such large boulders cannot be dumped anymore, like in the case of lowland rivers, but they have to be placed individually by machines because of their weight. Consequently the blocks are better interlocked even if a rough surface of the riprap is required. Thus a higher resistance of such individually placed or "compressed" riprap may be expected. The existing design methods have been developed for dumped riprap with relatively small block sizes.

Dr. Mona Jafarnejad studied for the first time systematically the effect of compressed riprap, that means with individually placed blocks having a good interlocking, on the failure resistance. Based on a relative roughness and modified Froude number, Dr. Jafarnejad proposed an empirical relationship which can assess the limit between stable and failure conditions of the blocks and thus gives a criterion for the required minimum block size. Furthermore, and also for the first time, the time-dependant failure was analysed which is also not considered in existing design methods. Dimensionless empirical relationships between the time to failure and the bed shear stress as well as flow depth were developed. The results revealed that for a total failure of the compressed riprap a relatively high number of blocks have to be eroded. In loose dumped riprap, normally the erosion of a few blocks results in a fast failure knowing that the time to failure is very important in practice since the flood peaks have only a limited duration.

Additionally Dr. Jafarnejad studied the effect of a second layer of individually placed riprap on the time-dependant failure process, which is novel. She developed also an empirical relationship, which takes into account the influence of such a second layer. For the same longitudinal channel slope and side bank slopes, the second layer stabilizes the section and postpones failure. The effect of a second layer is more significant for higher bed slopes and bank side slopes.

Finally, compared to the traditional design methods, using a safety factor approach, Dr. Jafarnejad developed a probabilistic failure analysis method for riprap, which considers uncertainties of the design parameters and the future evolution of bed load transport under climate change.

We thank the members of the jury Prof. Antonio Cardoso from IST Lisbon, Portugal; Prof. Juan Pedro Martin-Vide from Technical University of Catalonia, Spain as well as Dr. Dieter Rickenmann from Swiss Federal Institute for Forest, Snow and Landscape Research WSL, Switzerland, for their valuable comments and helpful suggestions. Finally we also thank gratefully the Swiss Federal Office of Environment for their financial support under project "SEDRIVER".

Prof. Dr. Anton Schleiss Prof. Dr. Eugen Brühwiler

Abstract

Time-dependent failure analysis of large block size riprap as bank protection in mountain rivers

Erodible river banks need to be safe against the possible scouring during flood events in mountain rivers. The consequences of the bank failure are probably lateral uncontrolled erosion and flooding with disastrous losses in residential areas or damage of infrastructures.

Among all flood protection measures that keep the riverbank safe against erosion and damage, riprap revetment is one of the most commonly used structures. Some of the advantages of utilizing riprap are flexibility, a tendency to be self-restorative, relative ease of installation, long lasting and easy to repair. In order to ensure the safest design, determining the required riprap size is one of the most important factors. Several methods of riprap sizing exist which are mostly evolved for dumped median size blocks. However, in mountain rivers and steep channels, the extra stability has to be ensured by using the large, heavy blocks as bank riprap protection, which have to be individually placed because of their weight. Such arrangement generates additional resistance against flow erosion since the space between the blocks is minimized, and the interlocking forces among the blocks are increased. The behavior of the latter protection was rarely studied for alpine river conditions, and no adapted design criteria exist.

Therefore, an experimental study was carried out focusing on the stability of such compressed riprap as river bank protection. This research investigates the effect of packed placement of riprap on sizing, the resistance to failure and the time to failure of riprap. Comparison with the existing design methods is also performed considering the effect of riprap thickness and bank slope. This is studied by means of 121 series of systematic tests of compressed riprap and 34 tests of dumped ones. The experiments were carried out using a 10 m long and 1.5 m wide flume with a rough fixed bed at the Laboratory of

Hydraulic Constructions (LCH) at École Polytechnique Fédérale de Lausanne (EPFL). Riprap was reproduced with uniform crushed blocks with three block sizes namely D_{50} = 0.037, 0.042 and 0.047 m. Tests were conducted on streamwise bed slopes of S = 0.015, 0.03 and 0.055, and riprap bank slopes of 35°, 31° and 27° under supercritical flow conditions and for a maximum of three hours of test duration. The porosity which is an effective factor on the stability is assessed and the results show a reduction of 2% for smallest size to 10% for the largest size of packed blocks. Compared to dumped small size riprap, the failure mechanism of packed blocks is different, since the erosion of one single block is hardly the reason for a total failure of this kind of riprap. Failure happens if a group of blocks slides and provokes an instability of the river banks. In the present study, the total collapse of all blocks in a section over the whole bank height is considered as failure. This failure is the result of slumping or sliding down of riprap from top to the toe of the embankment producing a full exposure of the filter to the flowing water.

Firstly, the detailed analysis and comparison of the results of the systematic experimental tests of dumped and compressed riprap is presented. It was observed that the compressed riprap increased the stability of the bank protections considerably. The existing design formulae suggest block sizes of up to three times larger than what is observed for the compressed riprap. An empirical relationship between relative roughness and modified Froude number is discussed. Then a sizing riprap empirical formula for large blocks individually placed on supercritical flow is herein developed; considering the riprap thickness and bank slope. This empirical relationship is compared with existing formulae.

As a further step based on a time-based analysis of the failure process, a relationship between time to failure, shear velocity, and dimensionless bed shear stress is established. An empirical relationship was established which allows to estimate the time to failure of the riprap bank protections. Consequently, it can be used as a failure forecasting model for compressed riprap in the range of application of the model tests.

The influence of a second layer on the time to the failure and on the bank stability is also analyzed. The results reveal that, for the same longitudinal channel slope and bank slope, the second layer significantly stabilizes the bank protection and postpones its failure time. Nevertheless, during the test, the block erosion rate is increased significantly

(almost twice) for two layers comparing to one layer riprap. The thickness of the riprap has a considerable influence on riprap protection for higher bank slope than the flatter ones. It means that the second layer has more stabilizing role when the riprap bank slope gets closer to the angle of repose of the blocks. Furthermore, the effect of the riprap thickness is smaller for higher channel slopes comparing to lower channel slopes.

Finally, a probabilistic failure analysis method of riprap is developed considering that existing riverbank riprap revetments could be exposed to higher risk of failure if flood and sediment regime changes in future. The potential failure probabilities of riprap are evaluated by using Monte Carlo Simulation and Moment Analysis Methods as well as Rosenblueth Point Estimation Method. The advantages of this probabilistic model are that it can cover different failure mechanisms and make use of the multivariate probabilistic method. The probability of failure in various modes, namely direct block erosion, toe scouring and overtopping, has been defined. Therefore, bed level variation is used in the model based on bedload transport described with a probabilistic function of the peak discharge. This probabilistic simulation method can be directly implemented in water surface and bed load calculation models. The method was applied to two rivers in Switzerland; namely Kleine Emme and Brenno. The probability of failure for different mechanisms based on the expected sediment transport regime under climate change is defined for these two rivers as a case study.

Keywords: bank erosion; direct block erosion; failure mechanisms; flood protection measure; Monte Carlo simulation; overtopping; probabilistic simulation; riprap design; sediment transport; stability; time-dependent analysis; toe scouring.

Résumé

Analyse en fonction du temps de la ruine d'enrochements à large blocs protégeant les rives des rivières de montagne

Pendant les crues dans les rivières de montagnes, les berges des rivières doivent être protégées contre les possibilités d'érosion. Les conséquences d'effondrement de berges englobent surtout l'érosion latérale non contrôlée et les inondations causant des dégâts désastreux dans les zones résidentielles ou endommageant les infrastructures.

Parmi les différentes mesures de protection contre les crues afin d'éviter l'érosion et l'endommagement des berges de rivières, le revêtement par enrochement est la plus utilisée. Les principaux avantages de l'utilisation des structures en enrochement sont la flexibilité, la tendance à l'auto-restauration, la facilité relative de la mise en place et de la réparation ainsi que la durabilité. Afin d'assurer un dimensionnement le plus sûr, la taille de l'enrochement est le facteur le plus important. Plusieurs méthodes de dimensionnement existent, les plus avancées étant celles des blocs déposés à taille moyenne. Toutefois, dans les rivières de montagnes à fortes pentes, une stabilité supplémentaire doit être assurée en utilisant de larges et lourds blocs pour la protection en enrochement. Ces derniers doivent être mis en place un à un en raison de leurs poids. Une telle disposition assure une plus grande résistance contre l'érosion produite par l'écoulement vu que l'espace entre les blocs est minimisé et les forces d'emboîtement entre les blocs sont augmentées. Le comportement d'une telle protection a été rarement étudié pour le cas de rivières alpines et aucun critère de dimensionnement adapté n'existe.

Par conséquent, une étude expérimentale a été menée se concentrant sur la stabilité de tels enrochements compactés en tant que moyens de protection des berges riveraines. La présente recherche étudie l'effet des enrochements compactés sur le dimensionnement, la résistance à la rupture et le temps jusqu'à la rupture. La comparaison avec d'autres méthodes de dimensionnement a été faite basée sur l'effet de la largeur de

l'enrochement ainsi que la pente de la berge. Cela est accompli en effectuant 121 séries de tests systématiques avec enrochements compactés ainsi que 34 tests avec enrochements déposés. Les tests ont eu lieu dans un canal de 10 m de long et de 1.5 m de large avec un fond rugueux fixe au sein du Laboratoire de Constructions Hydrauliques (LCH) de l'Ecole Polytechnique Fédérale de Lausanne (EPFL). Les enrochements ont été reproduits à l'aide de pierres uniformes concassées de trois diamètres différents D_{50} = 0.037, 0.042 et 0.047 m. Les pentes du lit testées sont dirigées dans le sens de l'écoulement et trois pentes différentes ont été testées S = 0.015, 0.03 et 0.055. Les pentes des enrochements sont de 35°, 31° et 27° sous des conditions d'écoulement torrentiel et pendant un maximum de trois heures de test. La porosité, qui est un facteur à forte influence sur la stabilité, est évaluée et les résultats montrent une réduction de 2% pour les blocs compactés les plus petits et de 10% pour les plus larges. En comparaison avec les petits enrochements déposés le mécanisme de rupture des blocs compactés est différent, dans la mesure où l'érosion d'un seul bloc peut difficilement causer une rupture totale de ce genre d'enrochement. La rupture a lieu si un groupe de blocs glisse et provoque une instabilité des berges de la rivière. Dans la présente étude, l'effondrement total de tous les blocs d'une section sur toute la hauteur de la berge est considéré comme le rupture. Cette dernière est le résultat de l'affaissement ou du glissement de l'enrochement depuis le sommet jusqu'aux pieds de la digue exposant ainsi complètement le filtre à l'écoulement de l'eau.

En premier lieu, une analyse détaillée et une comparaison des résultats des tests expérimentaux systématiques effectués avec des enrochements déposés et ceux compactés sont présentées. Il a été observé que les enrochements compactés augmentent considérablement la stabilité des protections de berges. La formule de dimensionnement existante suggère des blocs de taille trois fois plus large que ce qui est observé pour le cas d'enrochement compacté. Une relation empirique entre la rugosité relative et le nombre de Froude modifié est discutée. Ensuite, une formule empirique pour les blocs larges placés individuellement dans un écoulement torrentiel est développée en tenant en compte de l'épaisseur des enrochements ainsi que de la pente des berges. Cette relation empirique est comparée avec la formule existante.

En outre, et suivant une analyse basée sur le temps du processus de rupture, une relation entre le temps jusqu'à la rupture, la vitesse de cisaillement, et la contrainte de

cisaillement adimensionnelle du lit est établie. Une relation empirique a été établie permettant l'estimation du temps jusqu'à la rupture de l'enrochement. Par conséquent, ce résultat peut être utilisé comme modèle de prévision de rupture pour les enrochements compactés, dans le champ d'application des tests sur modèle.

L'effet d'une seconde couche sur le temps à la rupture et sur la stabilité des berges est également analysé. Les résultats montrent que pour la même pente longitudinale du canal et de la berge, la seconde couche stabilise considérablement la digue et retarde le moment de rupture. Néanmoins, pendant le test, le taux d'érosion de blocs a augmenté (environ deux fois) pour le cas avec deux couches par rapport à celui avec une seule couche d'enrochement. L'épaisseur de l'enrochement a une influence plus importante sur la protection en enrochement pour les grandes pentes de berge que pour les petites. Cela implique que la seconde couche a un rôle stabilisant plus important lorsque la pente d'enrochement est plus proche de l'angle de frottement interne des blocs. De plus, l'effet de l'épaisseur d'enrochement est plus important pour les grandes pentes de canal que pour les petites.

Finalement, une méthode d'analyse de rupture probabiliste des enrochements est développée en prenant en considération que les digues de rivières existantes peuvent être exposées à plus de risque si le régime de crue et de sédiments change dans le futur. Les probabilités du potentiel de rupture des enrochements sont évaluées en utilisant la méthode de simulation de Monte Carlo, les méthodes d'Analyse de Moment, ainsi que la méthode d'Estimation Ponctuelle de Rosenblueth. Les avantages de ce modèle probabiliste sont dans le fait qu'il couvre les différents mécanismes de rupture et utilise la méthode probabiliste multivariée. La probabilité de rupture par différents modes, notamment l'érosion directe de blocs, l'érosion des pieds et la submersion a été définie. Ainsi, la variation du niveau du lit est utilisée dans ce modèle basée sur le charriage du lit décrit à l'aide d'une fonction probabiliste de débit de pointe. Cette méthode de simulation probabiliste peut être directement mise en place dans les modèles de calculs de surface d'eau et de charriage. La méthode a été appliquée à deux rivières en Suisse: Kleine Emme et Brenno. La probabilité de rupture pour différents mécanismes basée sur le régime attendu du transport de sédiment dans le cas de changement climatique est définie pour ces deux rivières en tant qu'étude de cas.

Mots-clés : l'érosion des berges; l'érosion directe de blocs; mécanismes de rupture; mesure de protection contre les crues; simulation de Monte Carlo; débordement; simulation probabiliste; conception d’enrochement; transport des sédiments; stabilité; analyse en fonction du temps; érosion du pieds.

Acknowledgement

The present PhD dissertation is the output of spending about four years with the wonderful group of the Laboratory of Hydraulic Constructions at Ecole Polytechnique Fédérale de Lausanne. The study was supported by the Swiss Federal Office for the Environment (FOEN) under contract no. A2111.0239/10-0019.PJ/J372-1192 and in the framework of project SEDRIVER.

First of all, I would like to express my sincerest thanks and appreciation to Professor Anton J. Schleiss, who trusted in my capacity to perform this research in such a challenging and interesting subject and accepted to guide and lead my work. Prof. Schleiss combines perfectly engineering knowledge and management skills, and guides a great team which I had the honour to work with. LCH has always a positive atmosphere, with magnificent and motivated people who like to work together and it for sure comes from the way it is managed. I do thank also my co-advisor Prof. Eugen Brühwiler who supported and advised me based on his outstanding experiences and knowledge.

I am deeply thankful to Dr. Mário J. Franca for his guidance provided during this PhD. He supported me both scientifically and personally, when I was feeling frustrated and doubted to finish this huge work. Thank you Mário!

I would like also to appreciate great helps and supports from Dr. Michael Pfister from the first day I started my work at LCH till today. I learned a lot from his experience and knowledge in doing research and helping me to write scientific articles.

I would like to thank Prof. Cardoso, Martin Vide and Rickenmann who accepted being members of the jury of my thesis and for reading and evaluating this dissertation. I equally thank Prof. Wüest for being the president of the jury.

Many thanks to Dr. Giovanni De Cesare, Dr. Pedro Manso, and very special one to my dear friend Dr. Azin Amini who patiently read my thesis. Thank you Azin, you are adorable.

It is a pleasure for me to acknowledge my friends and colleagues at LCH who are graduated now: Fadi Hachem, Martin Bieri, Michael Müller, Violaine Dugué, Tamara Ghilardi, Milad Daneshvari, Raphael Sprenger (who helped me a lot during the experiments), Ana Margarida Ricardo, Ramona Receanu, Théodora Cohen Liechti,; and to the amazing new crew that I leave formed by Stéphane Terrier, Sebastian Schwindt, Alex Pachoud, Fränz Zeimetz, Elena Battisacco, Davide Würthrich, Nicolas Adam, Mélanie Baehler, Felix Oberrauch, Carmelo Juez Jiménez, David Ferràs, Irene Samora, Paloma Furlan, severin stähly, Ana Clara Santos, Mohammad Ostad Mirza, Reyhaneh Ghazanfari and mon-ami Sebastian Guillén. I thank my two lovely office mates Sabine Chamoun and Jessica Zordan who always supported me in difficult days with their kindness and patience. Particularly, thanks to José Pedro Matos for his friendliness and his availability to help me in many technical aspects of the thesis.

Thanks to Cédric Bron, Michel Teuscher, Marc-Eric Pantillon and the particularly skilled people who really make a difference when working at LCH: Laurent Morier, David,and specially Sasan who assisted me in most of the heavy experiments.

I wish to express my warmest thanks to my beloved parents, Dr. Ahmad Jafarnejad and Dr. Mina Safiri; my sisters, Zoha and Sama and my brother in law Nima, who gave me the extra strength, motivation and love to get things done and finally, my sincere gratitude to my dear Vafa, for his endless love, enormous patience, and persistent supports.

Table of Contents

List of Symbols and Acronyms

Symbol	*Description*	*Unit*
A	Wetted area	m^2
C_i	Isbash constant	–
C_{ti}	Coefficient depends on turbulence intensity	–
$C_{refernce}$	A numerical coefficient, usually based on experimental data	–
C_T	Blanket thickness coefficient	–
D	Block size	m
D_{50}	Median diameter of spherical blocks	m
D_c	Characteristic particle size (D_{30} or D_{90} depending on investigator)	m
D_m	Median diameter of blocks	m
Fr	Froude number	–
g	Acceleration of gravity	ms^{-2}
h	Flow depth	m
H	Local water depth	m
h_{avg}	Average depth in the main channel	m
K_h	Depth factor dependent on velocity profile	–
K_{sl}	Slope factor	–
K_{slc}	Side slope correction factor	–
K_t	Turbulence factor	–
n_p	Porosity	–
Q	Water discharge	m^3s^{-1}
q	Unit discharge	$m^3s^{-1}m^{-1}$
R	Hydraulic radius	m
R_a	Centerline radius of bend	m
S	Longitudinal channel slope	–
S_B	Specific gravity of blocks	–
t^*	Normalized time to failure	–
$T_D{}^*$	Normalized time to failure characterizing block size	–
t_f	Time to failure	min
$T_h{}^*$	Normalized time to failure characterizing flow depth	–
u^*	Shear velocity	ms^{-1}
U_b	Mean velocity measured at a point 10% of flow depth above bed	ms^{-1}
V	Depth average velocity	ms^{-1}
V_c	Characteristic velocity	ms^{-1}
V_m	Mean velocity	ms^{-1}
V_{ss}	Characteristic velocity, depth averaged velocity at point 20% upslope from toe	ms^{-1}
W_i	Minimum weight of blocks which resists force of flowing water and remains stable on slope of river banks	lb
W	Water surface width at upstream end of bend	m

Symbol	***Description***	***Unit***
α	Angle for determining side slope effect	deg
γ	Specific weight of water	kgm^{-3}
γ_s	Specific weight of blocks	kgm^{-3}
γ_w	Specific weight of water	kgm^{-3}
Δ	Relative submerged density of blocks	–
η	Stability number	–
θ	Bank angle	deg
ρ	Water density	kgm^{-3}
ρ_s	Blocks density	kgm^{-3}
τ_0	Shear stress on the side slope	kgm^{-2}
φ	Riprap angle of response	deg
φ_c	Geometry correction factor to account for edges or transitions	–
ψ_{cr}	Shields parameter	–
τ	Bed shear stress	Nm^{-2}
τ^*	Dimensionless bed shear stress	–

Acronyms

CDF	Cumulative Distribution Function
EPFL	Ecole Polytechnique Fédérale de Lausanne
FORM	First Order Reliability Method
FOSM	First Order Second Moment
FRV	Function of Random Variables
LCH	Laboratory of Hydraulic Constructions
MAM	Moment Analysis Method
MCSM	Monte Carlo Simulation Method
PDF	Probability Distribution Function
PE	Point Estimation
RPEM	Rosenblueth Point Estimation Method
RV	Random Variables
SF	Safety Factor
SOSM	Second Order Second Moment
UVP	Ultrasonic Velocity Profiler

List of Figures

List of Tables

Chapter 1

Introduction

This chapter introduces the topic of this research study, gives its objectives and methods, and presents the structure of the thesis.

1.1 Motivation

Stream power in mountain rivers potentially carries the possibility of scouring the channel bed and bank. Constructions along rivers also increase significantly this risk of failure by increasing the cost of destabilization. Destruction or collapsing of river banks will result in uncontrolled flooding and lateral erosion with a displacement of meanders and the formation of braided river patterns. These processes can have catastrophic consequences on urban areas and infrastructures especially along mountain rivers. Therefore, the erodible river banks need to be protected against the possible erosion practically during the flood events. As such an optimum design which provide a safe condition is crucial. Among all kind of river bank protection measures, riprap is one of the most frequently used protections to avoid bank erosion (Maynord et al. 1989). Riprap design has been developed for a long time. Several methods of riprap sizing exist which are mostly derived for dumped median size blocks. However, in mountain rivers and steep channels, extra stability should be provided by packing the large blocks and individually positioned riprap. Therefore, most of the existent design methods over-estimate the size of large blocks which is not economical in this case of application.

The packed and individually placed model of riprap installation has been rarely studied. The motivation of current study is to analyze the stability and design of such packed riprap.

It is expected that climate change will have impact on flooding and sediment transport in mountain rivers and catchments of Switzerland in future. Changing the atmospheric circulation will influence the amount of precipitation and its regional distribution, thus possibly the magnitude and frequency of extreme events and the duration of their occurrence will change respectively. The result changes sediment transport dynamics as well. Sediment yield in a catchment is dependent both on transport capacity of the stream and availability of loose material. Therefore, sediment transport flow will be influenced by change of extreme events. These changes will affect the behavior and performance of flood protection measures and may increase their risk of failure.

Figure 1.1 The view of large block size riprap and residential area in Switzerland (Kleine Emme 2011)

Current consists of two main parts. First part focuses on the design of large blocks individually placed riprap in mountain rivers. Other part of this study is related to the risk of failure in riprap according to the flood uncertainties.

1.2 Objectives and methods

Many research projects concerning riprap design were carried out in the past decades. However, failure risk of large blocks in mountain streams is poorly understood compared to the knowledge existing on lowland rivers. The present study aims at understanding the behavior of large blocks individually placed in terms of stability. The research was carried out by means of laboratory experiments in a flume at the Laboratory of Hydraulic Constructions (LCH) of the Ecole Polytechnique Fédérale de Lausanne (EPFL). The failure time of packed blocks is studied as a function of several relevant parameters: 1. Water discharges (several scenarios) 2. Flume slope (three slopes) 3. The size of blocks (three sizes) 4. Bank slope (three slopes) 5. The thickness of the riprap revetment.

The objectives of this study are to address the lack of investigation and answer to the following questions:

- What is the minimum block size required to remain stable on the bank slope when the riprap is packed? (Chapters 4 and 6)
- What is the effect of side slope angle ranging from 2.5V-5H to 3.5V-5H on the stability of the packed riprap? (Chapters 4 and 6)
- What is the influence of flow duration on the riprap stability? (Chapters 5 and 6)
- How does the thickness of the riprap revetments influence the time of failure or stabilizing riprap? (Chapter 6)

In terms of failure risk of riprap protection the question would be:

- What is the probability of failure for a river bank riprap in different mechanisms? (Chapters 7 and 8)

Then the objective of this research is to assess the risk evolution as a function of changed hydraulics and sediment transport condition due to flood uncertainties (e.g. climate change). For this purpose, various probabilistic simulation and assessment models to define the failure risk of riverbank protection structures. These probabilistic simulations estimate the resistance regarding the varied flood and sediment transport in future.

1.3 Structure of the report

This thesis report is organized into three parts with a total of nine chapters, as outlined in Figure 1.2. The main points of this study development and analysis of riprap failure is presented in Figure 1.3.

In the first part, the context, motivation, objectives, background and methods of the thesis are presented in three chapters:

Chapter 1 highlights the importance of study the behavior of packed river bank riprap in mountain rivers. In this chapter, the main objectives of this study, the methodology and the structure of the report are presented.

Chapter 2 compiles the existent knowledge on riprap design and points out the gaps to be filled by this study. The literature review is made by focusing on designing procedures.

Chapter 3 outlines the experimental facilities, measurement equipment and experimental setup.

Second part presents the results of the current research study. It is composed of five complementary studies that correspond to the chapters 4 to 8 of this report.

Chapters 4 to 7 were written as scientific articles. Chapter 5 and 7 are submitted to peer-reviewed journals. A brief description of Chapters 4 to 7 is given below:

Chapter 4 addresses the sizing of large block riprap built in mountain rivers with the minimum possible spaces among the blocks. It specifically deals with the diameter of the riprap blocks *D*, longitudinal channel slope *S*, side slope of the riprap and hydraulic conditions. A new empirical relationship is developed to define the block size and also re-evaluate the stability of existing packed riprap facings. The equation for designing the optimum block size for individually placed riprap, based on Froude number, relative roughness and bank slope is modified by repose angle of blocks.

Chapter 5 contains the effect of block sizes and channel slope on the time of failure. As a further step based on a time-based analysis of the failure process, a relationship between time to failure, shear velocity, and dimensionless bed shear stress is established. An empirical relationship was established which allows to estimate the time to failure of the riprap bank protections. Consequently, it can be used as a failure forecasting model for packed riprap in the range of application of the model tests.

In Chapter 6, the influence of a second layer at the time of the failure and on the bank stability is analyzed in this chapter. The thickness of the riprap influence on the stability of riprap protection in different bank slope has been studied. Furthermore, the effect of the riprap thickness on the slopes of the channel is investigated in this chapter.

In Chapter 7, a probabilistic failure analysis method of riprap is developed considering that existing riverbank riprap revetments could be exposed to higher risk of failure if flood and sediment regime changes in the future. The potential failure

probabilities of riprap are evaluated and compared by using Monte Carlo Simulation, Moment Analysis Methods and Rosenblueth Point Estimation Method.

In Chapter 8, the method is applied here to two rivers in Switzerland; namely Kleine Emme and Brenno. The probability of failure for different mechanisms based on the expected sediment transport regime under flood uncertainties is defined for these two rivers as a case study.

In the last part, the main conclusions with some recommendations for future research are given in Chapter 9.

The annexes at the end of the document contain the graphical representation of the Experiments, Sensitivity analysis of Monte Carlo simulations and the results of the probabilistic model application on two rivers in Switzerland: Kleine Emme and Brenno.

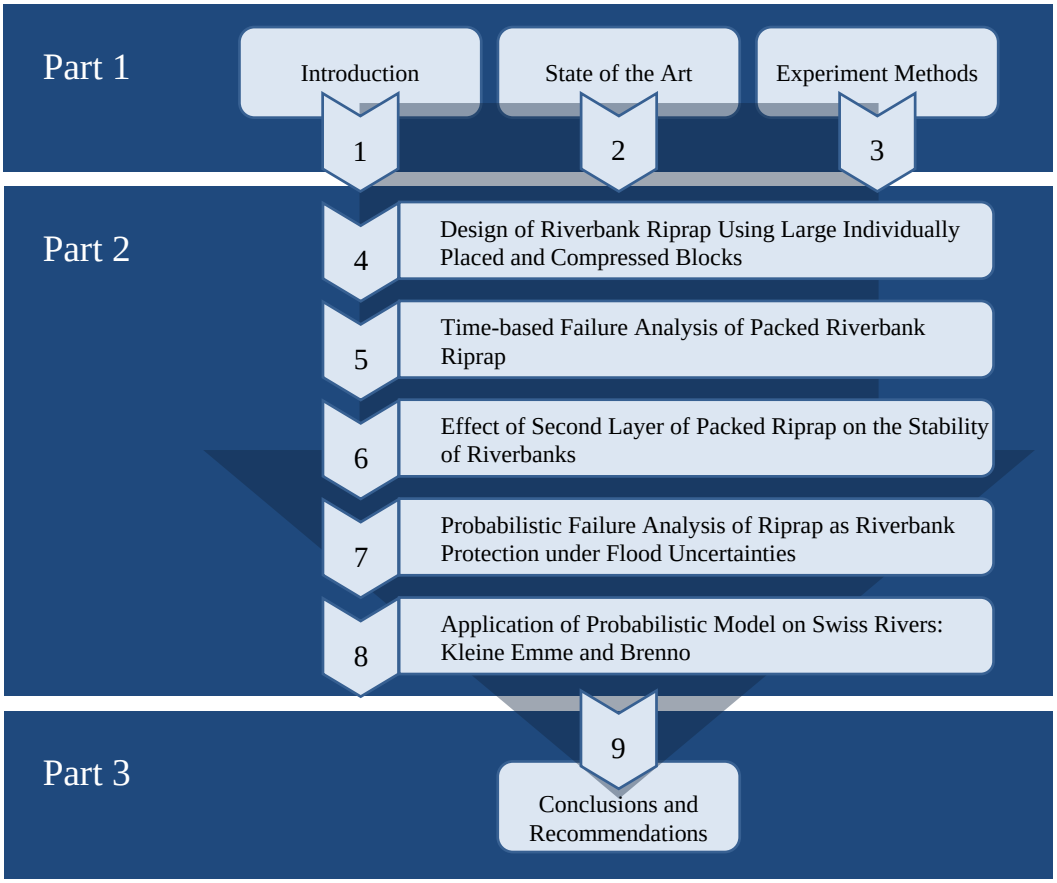

Figure 1.2 Outline of thesis research

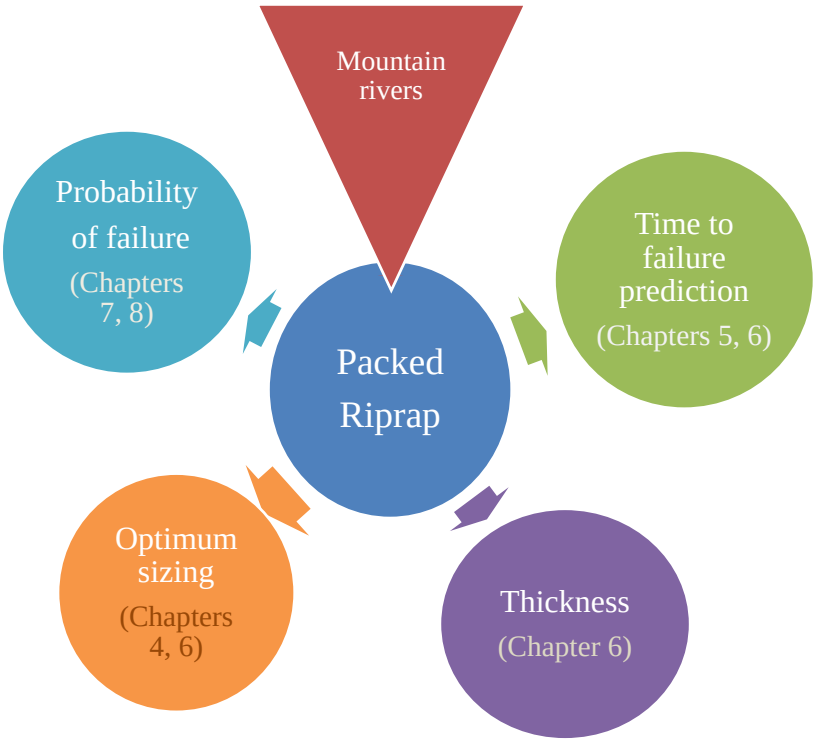

Figure 1.3 Main points of this study development and analysis of riprap failure

Chapter 2

State of the Art

This chapter gives an overview about the characteristics of the riprap as a river bank protection and the failure mechanisms. It also describes the main previous developments on design of riprap revetments.

2.1 Introduction

River protection measures are designed to protect the riverbanks and prevent lateral migration of channels through bank erosion. River-stabilization methods can be classified according to two different approaches:

1. *Strengthening the bank and bed* like riprap, windrows and trenches, vegetation, sacks and blocks, gabions mattresses, soil-cement, retaining walls and bed protection measures (e.g. sills, block ramps and traverse).

2. *Reducing hydrodynamic forces* such as hard points, spurs or groynes, guide banks, dikes, fences, vane, and brushwood fences.

Factors affecting stream bank failure include hydraulic parameters that control the active forces such as discharge magnitude and duration, velocity, and applied shear stress magnitude and orientation. Additional active forces that are due to seepage, piping, surface waves, and ice can also contribute to bank erosion. Artificially-induced activities such as urbanization, drainage, floodplain farming and development, boating and commercial navigation, and water-level fluctuations from hydropower generation can have detrimental effects on bank stability (Julien, 2002).

2.2 Riprap

Riprap is the most commonly used structure for bank protection when it is available in adequate size and quantity. The construction is supposed not to be complicated and extraordinary equipment and training are not required. A local damage or loss is easily repaired by the placement of more blocks. Riprap is usually durable and recoverable. Locally available riprap usually provides a cost-effective alternative to many other types of bank protection.

2.2.1 Failure mechanisms in riprap

According to Julien (2002) and Lagasse et al (2006) riprap failure mechanisms are identified as direct block erosion, translational slide, modified slump, and side-slope failure. Direct block erosion by flowing water is the mostly considering erosion mechanism in the literature. Direct block erosion can be the result of abrasion, reverse flow, local flow acceleration, or toe scouring. The size of blocks might be a reason for

direct erosion. Steep slope of a riverbank and too uniform gradation of riprap also are the other causes of direct block erosion. Figure 2.1 shows the direct erosion of individual blocks by flowing water.

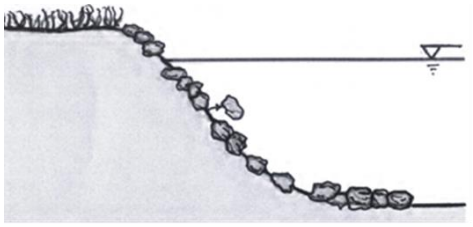

Figure 2.1 Direct block erosion (according to Julien 2002)

A translational slide is a failure caused by the downslope riprap material movement. The initial phase of a translational slide is shown by cracks in the upper part of the riprap blanket that extend parallel to the channel. Translational slides are caused by the steep slope of the riverbank and excessive hydrostatic pore pressure. However, this failure process mostly occurs due to toe scouring and instability of the riprap caused by the weakness in the toe foundation (Figure 2.2).

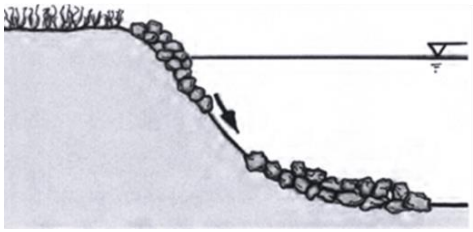

Figure 2.2 Translational slide in a riprap (according to Julien 2002)

The modified slump failure of riprap is the mass movement of material within only the riprap blanket where the blocks seem to slide on each other. The probable causes of the modified slump are the steep slope of the embankment and lack of toe support (Figure 2.3).

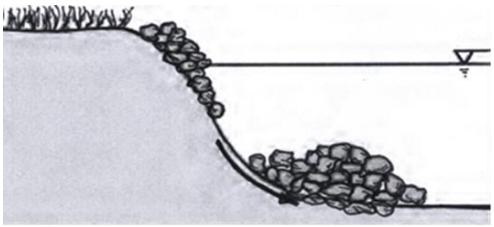

Figure 2.3 Modified slump in a riprap (according to Julien 2002)

The slope instability of the riprap is causing mostly due to overtopping. It is a rotation-gravitational movement of material along a surface of rupture. It relates to the shear failure of the underlying base material that supports the riprap. While overtopping occurs, the water saturates the riprap and the material behind it. Once the level of the water decreases, the water in the saturated part tend to move faster and the slide-slope in riverbank riprap takes place (Figure 2.4).

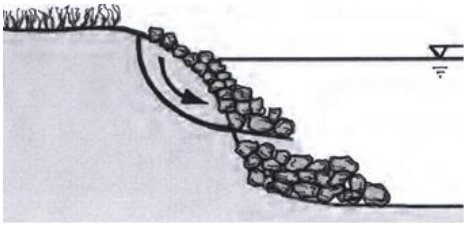

Figure 2.4 Slide-slope in riprap (according to Julien 2002)

2.2.2 Design methods of riprap

In the design of riprap revetment there are two approaches, Acceptable velocity and tractive force approaches. Acceptable velocity approach is the mostly used one as it is easier to record and calculate velocity. In the tractive force approach, it is hard to obtain force data at specific points on the bed and bank. Some of the previous studies about tractive force approach are done by Lane (1952, 1955), Carter et al. (1953), Terrell and Borland (1958), Ippen and Drinker (1962) and Monten (1988) (Maynord and Neil, 2008).

The tractive force concept was applied by Dubuat (1786) but did not become popular until Schoklitsch (1914) (Lagasse et al.,2006). Lane (1953) used the tractive force method for stable channel design in the noncohesive material. Anderson et al. (1968) developed the tractive force approach into a riprap design method which includes the effects of bank slopes and channel bend. The work of Anderson et al. is used as the basis for riprap design by the US Department of Transportation (1975). Stevens and Simons (1971) and Li et al. (1976) developed tractive force methods which combined probability and safety factors into the design method. Neil and Van Der Giessen (1966) state that turbulence intensity could be dependent on relative roughness. Thus many existing design methods may apply over only a limited range of relative roughness.

Some of the existing riprap design procedures (Li et al. 1976) used the logarithmic velocity law to change shear stress into velocity in sizing riprap. However, significant

problems appear in use of the logarithmic velocity functions to rough surfaces like riprap where relative roughness is high (Maynord et al, 1989).

In following, the detail review of some of the existing formulae is presented:

Riprap protection is endangered by the erosive effects of drag and lift forces resulting from the velocity distribution near particles. Considering riprap stability, different sizing methods were developed. The basic form of many sizing equations is given by Maynord and Neill (2008) as:

$$\frac{V_C}{[g(S_B-1)D_c]^{\frac{1}{2}}} = C_{ref}\left(\frac{h}{D_c}\right)^{P_{ref}} \tag{2.1}$$

where

V_c = Characteristic velocity (which may be near-bed velocity, depth-averaged velocity, or cross, sectional average velocity) [ms^{-1}]

g = Acceleration of gravity [ms^{-2}]

S_B = Specific gravity of blocks = ρ_s/ρ [-]

ρ_s = Blocks density [kgm^{-3}]

ρ = Water density [kgm^{-3}]

D_c = Characteristic particle size (D_{30} or D_{90}) [m]

C_{ref} = A coefficient, typically based on experimental data

h = flow depth [m]

P_{ref} = An exponent dependent on the hydraulic condition and the technique that the characteristic velocity V_c is defined.

Specific forms of riprap sizing equations for different authors are presented below. Corresponding P_{ref} and C_{ref} values are expressed in each title.

2.2.2.1 Isbash Equation

Isbash (1935) studied the river closures by dumping rocks and represented a relationship between required blocks diameter and mean velocity (equation 2.2).

$$V = C(2g(S_B-1)D_{50})^{0.5} \tag{2.2}$$

where

V = Mean velocity against blocks, ms^{-1}

C_i = Isbash constant: 0.86 for flow velocity at which loose surface blocks first begin to roll, 1.20 for flow velocity at which blocks projected by neighbor particles begin to roll until they find another place to settle

g = Acceleration of gravity, $[ms^{-2}]$

S_B = Specific gravity of blocks [-]

D_{50} = Median diameter of spherical blocks, [m]

Comparing to the basic equation (equation 2.1), Isbash (1935) equation has $P_{ref} = 0$ (no dependence on depth) and varying C_{ref} depending on the application.

2.2.2.2 Pilarczyk Equation

Pilarczyk (1990) developed an equation for stability under current attack and it is represented in CUR Manual (CUR, 1995) as:

$$\Delta D_m = \varphi_c \frac{0.035}{\psi_{cr}} K_t K_h K_{sl}^{-1} \frac{V^2}{2g} \tag{2.3}$$

where

D_m = Median diameter of blocks = $0.85 D_{50}$, [m]

Δ = Relative submerged density of blocks = $(S_B - 1)$

φ_c = Geometry correction factor to account for edges or transitions: 0.75 for continuous protection, 1.0 to 1.5 for edges and transitions, 1.5 for exposed rock on a sill

ψ_{cr} = Shields parameter = 0.035 for loose rock

K_t = Turbulence factor: 1.0 for normal river turbulence, 1.5 for increased turbulence as in bends, 2.0 for high-turbulence hydraulic jumps, sharp bends, local disturbances and 3.0 for propeller jets

K_h = Depth factor dependent on velocity profile: $2(\log h/k_s)^{-2}$ for fully developed boundary layer and $(D_m/h)^{0.2}$ for a velocity profile not fully developed where h is depth of flow above toe of bank

K_{sl} = Slope factor: product of a side slope term and a longitudinal slope term

V = Depth average velocity, [ms^{-1}]

g = Acceleration of gravity, [ms^{-2}]

In the equation 2.3, the right hand side corresponds to the disturbing forces and left hand side to resisting strength of the revetment.

In relation with basic equation form (equation. 2.1), Pilarczyk (1990) equation has varying P_{ref} and C_{ref} depending on the application. An explicit form of the Pilarczyk (1990) equation is used before in PIANC (1987b) and Hemphill and Bramley (1989).

2.2.2.3 California Bank and Shore Protection (CBSP) Manual

California Division of Highways (1970) examined primarily the special treatment of both riverbanks and highway embankments to prevent erosion by surface waters and stated the equation of stable block size for slopes no steeper than 1.5H:1V as:

$$W_i = \frac{0.00002\, V_{cbsp}^6\, S_B}{(S_B - 1)^3 sin^3(\beta - \alpha)} \tag{2.4}$$

where

W_i = Minimum weight of blocks which resists force of flowing water and remains stable on slope of stream or river banks, [kg]

V_{cbsp} = Stream velocity to which the bank is exposed, [fts^{-1}], defined as ⅔ of average channel velocity for parallel flow (in straight reaches) and ⁴⁄₃ of average velocity for impinging flow (on the outside bends)

S_B = Specific gravity of blocks [-]

β = Angle for determining side slope effect, 70° for arbitrarily placed rubble, degrees

α = Side slope, degrees

Also it is proposed by Froehlich and Benson (1996) that “practical angle of initial yield” is about 70–75° for typical gradations and Ulrich (1987) used “bearing angle” as 75°.

Racin (1996) evaluates the method relative to field data and depicted that this method emphasizes relatively uniform rock placed in two or more layers instead of graded rock.

2.2.2.4 Escarameia and May Equation

The Escarameia and May (1992) equation for sizing revetment, loose or interlocking concrete blocks and gabion mattresses is,

$$D_m = C \frac{{U_b}^2}{2g(S_B - 1)} \tag{2.5}$$

where

D_m = Characteristic size of blocks, size of equivalent cube, [m]

C = Coefficient depends on turbulence intensity = $12.3TI$ – 0.2 for riprap bank or bed protection on side slopes of 1:2 or flatter

TI = Ratio of root mean square velocity fluctuation over mean velocity measured at a point 10% of the flow depth above bed and varies from 0.12 to 0.60 for different structures

U_b = Mean velocity measured at a point 10% of flow depth above bed = $(1.04 - 1.48TI)V$, [ms^{-1}]

S_B = Specific gravity of blocks [-]

g = Acceleration of gravity, [ms^{-2}]

Escarameia and May (1992) also present an equation for specific application to the bank and bed protection which is applicable to bank slopes of 1V:2H or flatter and normal river flow:

$$D_m = C \frac{V^2}{(S_B - 1)} \tag{2.6}$$

where

C = 0.05 for continuous revetments and 0.064 for the edges of revetments

V = Depth averaged velocity and should be measured at the toe of the slope, [ms^{-1}]

In relation with basic equation form (equation 2.1), both of Escarameia and May (1992) equations has $P_{ref} = 0$ (independence of depth) and varying C_{ref} depending on the application.

2.2.2.5 Brown and Clyde Equation

Brown and Clyde (1989), also called as the reviewed HEC-11 manual, combines Manning-Strickler equation with Shields relation. Shields relation is used for incipient motion, average shear stress, Manning equation to compute friction slope and the Strickler equation to compute Manning *n* as a function of particle size. The effect of bank angle, riprap specific gravity and desired stability factor are included in the equation. Equation for English units is,

$$D_{50} = C_{sg} C_{sf} \frac{0.001\, V^3}{h_{avg}^{0.5}\, K_{sl}^{1.5}} \tag{2.7}$$

where

D_{50} = Median diameter of blocks, [ft]

C_{sg} = $2.12/(S_B - 1)^{1.5}$

C_{sf} = $(SF/1.2)^{1.5}$

SF = Stability factor dependent on the ratio R/W of radius of curvature to channel width. For $R/W > 30$, $SF = 1.2$; for $R/W = 10$, $SF = 1.3$ to 1.6; and for $R/W < 10$, $SF = 1.7$.

V = Average channel velocity, [fts^{-1}]

h_{avg} = Average depth in the main channel, [ft]

K_{sl} = $(1 - \sin^2\theta \sin^{-2}\varphi)^{0.5}$

θ = Bank angle, degrees

φ = Riprap angle of response, degrees

revised HEC-11 (equation 2.7) is only valid for English units, for metric units the constant has to be taken as 0.00594 ($0.001/0.3048^{1.5}$) (Lagasse et al., 2006).

Comparing to equation 2.1, Brown and Clyde (1989) equation has P_{ref} = ⅙ (generally applicable to complete boundary layer development) and varying C_{ref} depending on the application.

Most of the methods above examine the riprap stability without considering the stability of individual particles in detail. The following methods include a more detailed examination of forces and moments acting on the individual particle. Also these equations consider lift force which is not included in Lane (1955) equation.

2.2.2.6 Stevens et al

Stevens et al. (1976) developed a safety factor method suggesting that particle stability is depending on the moment of its submerged weight being greater than the sum of the moments acting to displace it. He considered the forces acting on a particle in the plane of the side slope. Thus equation given below (equation 2.8) is for horizontal or parallel flow on an embankment.

$$D_m = \frac{21\tau_0}{(S_B - 1)\gamma\eta} \tag{2.8}$$

where

D_m = Characteristic riprap size, m

τ_0 = Shear stress on the side slope, [Nm^{-2}]

S_B = Specific gravity of blocks

γ = Specific weight of water, [Kgm^{-3}]

η = Stability number = $(S_m^2 - SF^2)\cos\theta / SF\, S_m^2$

SF = Safety factor = $0.5S_m\left(\sqrt{\zeta^2 + 4} - \zeta\right)$

ζ = $S_m\eta\sec\theta$

S_m = $\tan\varphi/\tan\theta$

This method requires an iterative procedure as the shear stress on the side slope is a function of relative roughness, which is riprap size divided by flow depth (HDS 6-Richardson et al., 2001 and Simons and Senturk, 1992).

2.2.2.7 Wittler and Abt study

Wittler and Abt (1988) modified Steven`s analysis to additionally consider the effect of contact and frictional forces from adjacent particles. For bed slopes of 2-20%, they tested their equation and results are found to be good; however, they did not test it for flow along a side slope.

2.2.2.8 Ahmed study

Ahmed (1988) made a comparison among seven safety factor methods for flow with 1V:1.5H bank slope and found out that all these methods underestimate the stability meaningfully. He concluded that methods by Anderson et al. (1970) and by the California Division of Highways (CDH 1970) gave better results.

2.2.2.9 US Army Corps of Engineers (USACE) Manual

USACE initiated a near prototype test program conducted by S. T. Maynord (1992) to improve riprap design procedure based on shear stress. Maynord found out from the velocity profile at the exit of the bend that the depth-averaged velocity for about 30% of the distance up the slope was equal to the velocity at the toe.

The USACE (1994) method`s source data is only limited to slopes of 2% or less and to values of D_{30}/h exceeding 0.02. The USACE equation (named as EM-1601) below (equation 2.9) is valid for desiging riprap in rivers and channels and not for immediately downstream of hydraulic structures that create highly turbulent flow.

$$D_{30} = SFC_S C_V C_T h \left[\left(\frac{\gamma_w}{\gamma_s - \gamma_w} \right)^{0.5} \frac{V_{ss}}{\sqrt{K_{slc} g h}} \right]^{2.5} \tag{2.9}$$

where

D_{30} = Particle size for 30% finer, [m]

SF = Safety factor, minimum = 1.1

C_S = Stability coefficient for incipient failure = 0.30 for angular rock or 0.375 for rounded rock. A revetment thickness of D_{100} or $1.5D_{50}$, whichever is greater, is assumed, and a gradation factor D_{85}/D_{15} in the range of 1.7 to 5.2

C_V = Vertical velocity distribution coefficient = 1.0 for straight channels or inside of bends, 1.25 downstream of concrete channels or at the ends of dikes and $(1.283–0.2\log(R/W))$ for outside of the curves (1 for R/W>26)

R = Centerline radius of bend, [m]

W = Water surface width at upstream end of bend, [m]

C_T = Blanket thickness coefficient = 1.0 for a thickness of D_{100}, with smaller values for greater thickness depending on D_{85}/D_{15}

h = Local depth, defined for side slope riprap at a point 20% upslope from toe for slope

γ_w = Specific weight of water, [kgm^{-3}]

γ_s = Specific weight of the particle, [kgm^{-3}]

V_{ss} = Characteristic velocity, depth averaged velocity at point 20% upslope from toe = $V_{avg}[1.74–0.52\log(R/W)]$ for natural channels

K_{slc} = Side slope correction factor = $-0.672 + 1.492\cot\alpha - 0.449\cot^2\alpha + 0.045\cot^3\alpha$, where α is angle to the horizontal

g = Acceleration of gravity, [ms^{-2}]

In USACE equation (equation 2.9), an incipient failure criterion is used to determine the stability coefficient. It is defined as the condition when the bank material beneath the riprap is first exposed. Incipient failure was used instead of incipient motion or displacement, to cover a wide range of gradations and to allow for the effects of blanket thickness (Lagasse et al., 2006).

The differences between this method and others are the use of D_{30} as characteristic size, an empirical relation to account for side slope, a coefficient for thickness, and the provision of guidance for determining near bank velocity V_{ss}.

Comparing to equation 2.1, the USACE (1994) equation has $P_{ref} = 0.1$ (intermediate between zero and complete boundary layer development) and varying C_{ref} depending on

the application. A similar form of USACE equation (but without most of the modifying factors) is used by Neil (1967), Bogardi (1978) and Pilarczyk (1990).

2.2.2.10 Probabilistic Methods

A probabilistic approach to the designing riprap against currents is studied by Li et al. (1996), PIANC (1987b) and Froehlich and Benson (1996). The probabilistic method has the advantage of ability to merge the effects from different mechanisms. Uncertainties in risk-based design procedures are resulting mostly from hydraulic forces, estimation of block size, block density, channel depth and so.

2.2.2.11 Blodgett and McConaughy Equation (Field Data)

Blodgett and McConaughy (1986) developed an equation based on field analysis of riprap stability which is valid for straight and curved channels having side slope of 1V:1.5H or flatter. The Blodgett and McConaughy equation (equation (2.10)) does not fit the standard form of the riprap design equation.

$$D_{50} = 0.01\, V^{2.44} \tag{2.10}$$

2.3 Conclusion

All the above mentioned studies considered dumped riprap. The gap in these investigations is the factor of compaction in large blocks individually placed. Some study like Witler and Abt (1988) and Maynord et al. (1989) did a few numbers of experiments with packed blocks. The results showed rough 10% percent of increasing the stability. However, the systematic study to illustrate the effect of packing the large blocks installing in mountain rivers has not been studied yet. Furthermore, the time of failure is rarely taken into account as a significant parameter of failure. The time of failure is getting important when the installation of blocks is compact. Thus, the current study is organized to answer practically the questions regarding the gap.

Chapter 3

Experimental Methods

In this chapter the experimental methods including procedures and measurements are explained. To assess the stability of large blocks which are individually placed as bank protection in a mountain river, systematic laboratory experiments were carried out in a laboratory tilting flume. Experiments were performed with different flume slopes S, block sizes D and bank slope α, for multiple discharges constantly fed from upstream of the channel.

In chapter 3.1 the experimental setup and the instrumentation for the measurements are described. Chapter 3.2 presents the test parameters and chapter 3.3 explains the experimental procedure. Chapter 3.4 specifies the dimensional analysis to define the approach of the analysis in next steps.

3.1 Experimental setup

3.1.1 Global description

The present research is based on packed riprap laboratory experiments (Figure 3.1). The influence of the packed installation on blocks as riprap is studied for three different channel slopes, three different bank slopes, three different gradations and block sizes in one and two layers of the revetment. Experiments were carried out in a 10 m long and 1.5 m wide tilting flume. Water is fed constantly at the flume inlet. A trapezoidal section containing movable riprap is set by making the bank slope by the filter of wide grain size distribution and installing the blocks on one side of the channel. The other side of the channel is the vertical wooden wall. The bed width of the trapezoidal section was first set as one meter. However, because the flow depth was not enough to provide failure in some of the configurations, the bed width of trapezoidal section was reduced to 0.7 m. Riprap was fixed to the bank by mortar for the first 5.5 meters of flume upstream. Then four meters of the movable blanket of the blocks were installed. Then the last half a meter was fixed on the filter to avoid the deconstruction of set-up. Figure 3.1 and Figure 3.2 are the sketch of a longitudinal side view of the channel and cross section view of the channel with riprap installed at the bank.

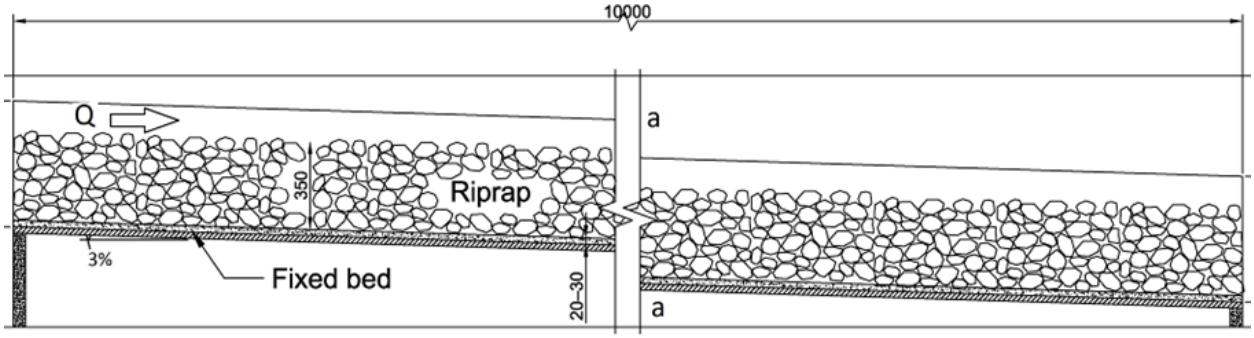

Figure 3.1 Sketch of longitudinal side view of the channel (in mm)

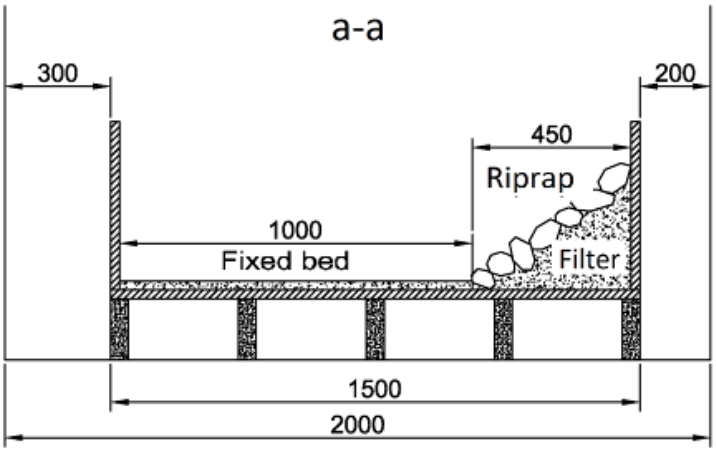

Figure 3.2 Sketch of cross section view of channel with riprap installed at the bank (in mm)

3.1.2 Experimental facility and measuring instrumentations

3.1.2.1 Set up of dumped blocks

In order to calibrate the model with the literature and existing design methods which are mostly based on dumped blocks, these series of tests are performed. First of all, the filter (Section 3.2.3) which contains a wide grain size distribution are placed as the first material on one side of the channel to produce the given bank slope. Then the blocks in given size are dumped and just released on the filter. It has been concerned that the blocks are providing the designed bank slope. The flow depth measurement equipment is installed in four positions with a distance of 2 meters.

Figure 3.3 View from downstream of the channel presenting the set-up of fixed and movable blocks parts of channel bank and the positions of ultrasonic limnimeter

3.1.2.2 Set up of packed blocks

The same procedure should be applied except that *the blocks have to be placed individually with minimum space between them*. Then the whole area of movable blocks should be packed with forces over it to reduce the void spaces and increase the interlocking forces among the blocks.

The parameter which indicates quantitatively the way of packing is the *porosity* and explained in detail in section 3.2.2.

From now on, we call packed riprap in the experiment for the individually placed blocks.

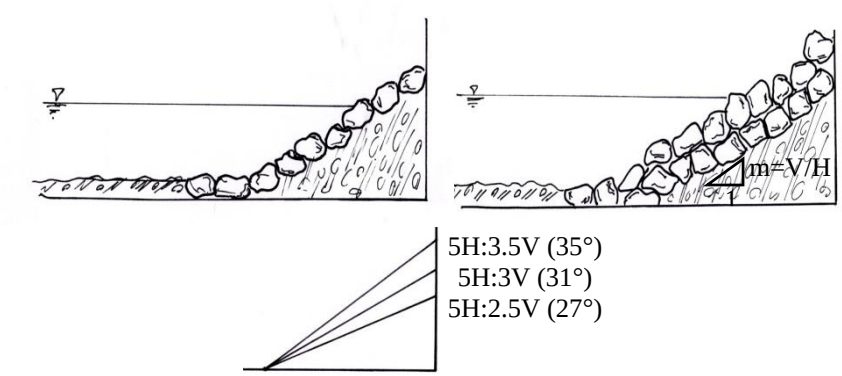

Figure 3.4 Sketch of one layer and two layers of riprap installed in three different bank slopes

Figure 3.5 Installation double layer, showing upper layer with red block

To study the effect of thickness in the application of packed riprap a series of experiments also performed for two layers of the blocks. The set-up is the same except that the amount of filter is less and the first layer is established and packed on the filter and then the second layer is installed. In this case, the interlocking between blocks and filter are more comparing upper and lower layers. The layers are installed in two different colours (red and white) but with the same size (D = 0.037 m). Figure 3.4 and Figure 3.5 present the schematic cross view of one and two layers of blocks in three different bank inclination.

3.1.2.3 Flow depth measurements

Ultrasonic limnimeters are placed above the water surface pointing down at distance of 2, 4, 6, and 8 m from upstream the channel to measure the low depth. They emit a sonic wave pulse which is reflected by an object of different density (e.g., flow surface and bed), back to the transducer. The time elapsed between emitting and receiving is proportional to the distance of the object from the sensor. For each experiment, the distance between the surface of the limnimeter transducer and the bed is first measured. When the flow passes through the channel during experiments, the distance between the transducer and the water surface is obtained. The ultrasonic limnimeters should be calibrated based on a reference distance like a dry bed for each test series (Figure 3.6).

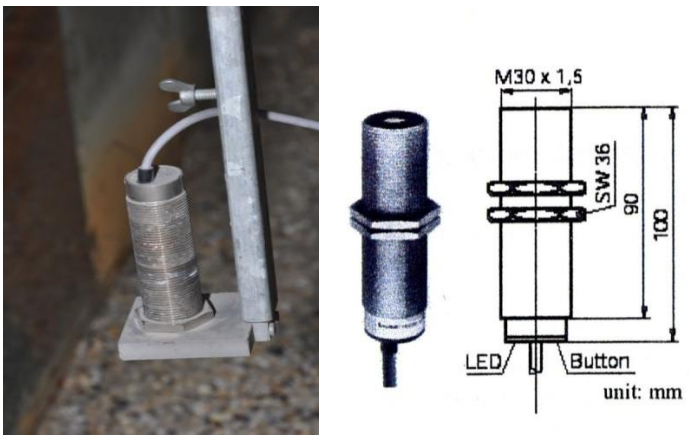

Figure 3.6 Ultrasonic limnimeter. Left side: limnimeter in the channel, right side: limnimeter with its dimensions

3.1.2.4 Camera recorder

A camcorder is placed on the top of the carriage, at a distance of 2.3 m above the channel's bed. It visualizes a longitudinal reach of the channel between 5.5 and 9.5 m long, depending on the used zoom. This recording is part of the measurements during the experiments. Counting the number of eroded blocks from upstream to downstream of movable riprap area is possible when the erosion is recorded during the tests. Defining the time of failure and understanding the location and the type of erosion is also achievable by this recording.

3.1.2.5 Velocity measurement

1D-velocity profile using the Ultrasonic Velocity Profiler (UVP) has been recorded for some of the tests in the channel axis at locations of 6, 7 and 8 m from upstream of the channel. Data acquisition has been performed by means of the Ultrasonic Velocity Profiler (UVP) instrument from Met-Flow. This instrument allows obtaining quasi-instantaneous 1D- velocity profile over the channel depth. The ultrasonic transducers had an emitting frequency of 2 MHz and an active diameter of 0.01 m. Four transducers have been installed on a support plate moving over a flow surface above the channel. They measured the velocity profile from top to bottom and pointed upstream with an angle of 18° from the vertical.

3.2 Experimental parameters

3.2.1 Block sizes and gradations

To choose the best and relative blocks for the experiments, 2 tons of a mixed lime stone crushed blocks are provided and classified in three different ranges of the weight. Each block is weighed individually then the distribution of each range of weights is defined. The specific gravity of these limestone blocks is tested as ρ_s = 2661 kgm^{-3}.

Figure 3.7 Three different size of blocks as crushed blocks categorized based on Table 3.1

Then spherical size of the blocks based on their weights are presented in Table 3.1.

Table 3.1 Grain size distribution of the blocks

Class		D_{15}	D_{30}	D_{50}	D_{65}	D_{85}	D_{max}	σ (D_{85}/D_{15}) (–)
D_a	Weight (kg)	0.057	0.065	0.073	0.077	0.083	0.090	1.18
	Size (m)	0.033	0.035	0.037	0.038	0.039	0.040	
D_b	Weight (kg)	0.093	0.100	0.107	0.115	0.0123	0.130	1.07
	Size (mm)	0.041	0.0415	0.042	0.043	0.044	0.045	
D_c	Weight (kg)	0.135	0.143	0.147	0.158	0.163	0.170	1.06
	Size (mm)	0.046	0.0465	0.047	0.048	0.049	0.05	

3.2.2 Porosity of different block sizes

The distinction between dumped and packed set-up was based on porosity measurements. Preliminary tests were performed to obtain the air volume in a defined dumped or packed riprap volume. Table 3.2 shows the porosity (n_p) of these tests, as well as the averaged values per block size and construction type. Packed porosity reduced by 2% for D_{50} = 0.037 m, by 5% for D_{50} = 0.042 m, and by 10% for D_{50} = 0.047 m when

compared with dumped riprap. The interlocking forces increase as the air volume between blocks reduces since the blocks have a closer arrangement.

Table 3.2 Porosity (n_p) of dumped and packed riprap with three different sizes of blocks

	Dumped		Packed	
D_{50} (m)	n_p (%)	Average (%)	n_p (%)	Average (%)
0.037	42.96	43.71	41.86	41.52
	43.05		42.02	
	44.62		41.00	
	44.20		41.22	
0.042	45.10	44.73	40.00	40.78
	44.20		41.13	
	44.91		40.10	
	45.00		41.86	
0.047	46.90	46.56	37.00	36.8
	47.20		36.82	
	45.95		36.50	
	46.20		36.86	

The porosity of the riprap in the experiments by Maynord and Abt (Maynord et al., 1989 and Abt, Johnson, Thornton and Trabant, 1998) was 44% to 46%, with limestones blocks of D_{50} = 0.035 m and D_{50} = 0.051 m, similar to the present blocks if dumped.

3.2.3 Filter characterization

Experiments were carried out on a rough fixed bed. The roughness of the bed is reproduced based on sediments with the grain size distribution presented in Table 3.3. The same grain size distribution has been installed to produce the bank slope. In order to represent the characteristics of mountain rivers, a wide grain size distribution was used. Hersberger (2002) analysed the grain size distribution of several alpine rivers. Herein, this grain size distribution is chosen to be used as the filter beneath the riprap and glued to the bed for these experiments. The comparison between the grain diameter distribution curve of the used sediments and typical alpine river curves is also given in Figure 3.8.

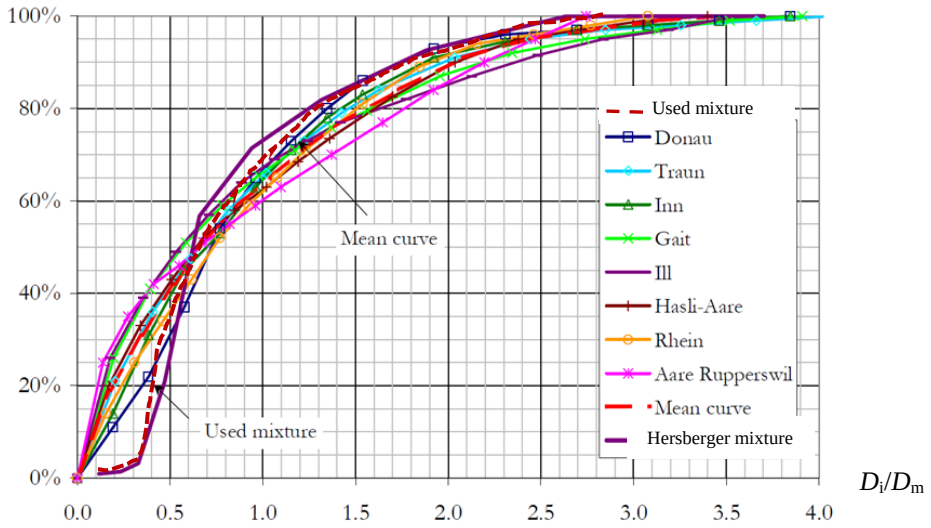

Figure 3.8 Grain size distributions used for filter beneath riprap some mountain rivers (from Hersberger, 2002)

The characterization of the grain size distribution of the supplied sediments, which are shown in Figure 3.8, is given in Table 3.3, where D_m = 8.5 mm is the mean diameter, corresponding to D_{65} and D_x is the grain size diameter for which x% by weight of the amount of sediments which have smaller diameters. The density of the sediment measured as ρ_s = 2650 kgm^{-3}.

Table 3.3 Characteristics of the granular material underneath the riprap (filter) and glued to the channel bed (in mm)

D_m	D_{10}	D_{35}	D_{50}	D_{75}	D_{90}	D_{max}
8.5	3.2	4.4	5.3	9.1	14.8	32

3.2.4 Channel slope

Three different slopes as S = 0.015, 0.030 and 0.055 are tested in the tilting flume. The main longitudinal channel slope is taken as S = 0.030 and most of the configurations are done on this slope.

3.2.5 Bank slope

Three different bank slopes are also chosen to define the effect of bank slope on the stability of riprap protection. β is the angle of bank slope to the bed and is chosen as 27°, 31°, 35° which are the ratio of 2.5V-5H, 3V-5H and 3.5V- 5H. The angle of repose for the blocks is used based on the study of Froehlich (2011).

3.2.6 Thickness

The thickness shows effect on the stability of riprap in literature review. To define this effect on the stability of packed blocks, a series of two layer tests also is performed in various configurations with the block size of D = 0.037 m.

3.2.7 Time to failure

Failure criterion on these series of tests is defined when the blocks are eroded in a way that whole blanket of riprap in one section slides down and the section becomes stable. Dumped blocks faced with this failure as soon as the direct block erosion occurs. However, in packed riprap, an extra support and interlocking forces doesn't let the section become unstable as soon as the blocks start to move. Then the time that the bank begins to become unstable by sliding the blocks is defined as the time to failure in packed riprap. Test duration is recorded by camera and exact time of failure can be obtained by video recorded.

3.2.8 Transitional discharge (critical discharge)

The tests run with a given discharge which remained constant during the experiment and increased for the next experiment. The first experiment which the failure occurs in it defined as the transitional test and the corresponding discharge named transitional discharge. This discharge has a role to define the boundary between failed and stable tests.

3.2.9 Erosion rate

The number of blocks which are eroded during the test and move from their place to the downstream are counted in frequency of one minute. In this way the erosion rate of blocks in a packed riprap can be obtained.

3.2.10 Velocity profile in a section

For some tests the velocity profile has been measured by using UVP. The variation of velocity profiles over the riprap and bed are obtained and roughness of the fixed bed and bank for three different sizes are analysed.

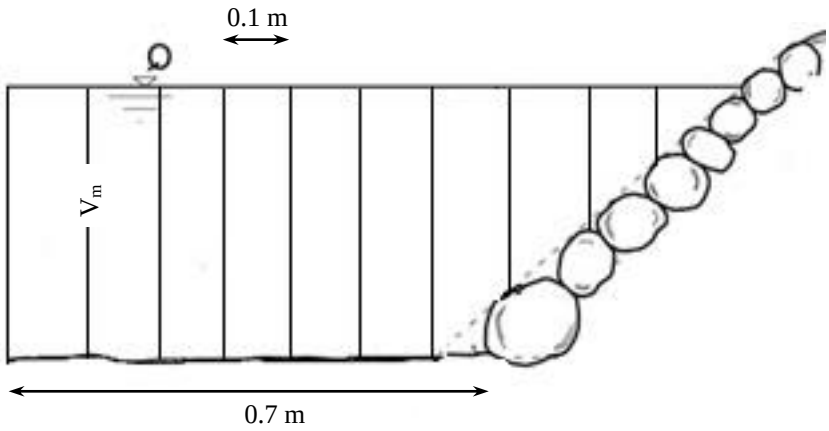

Figure 3.9 The positions of velocity measurements in a section

3.3 Experimental procedures

3.3.1 Dumped test

After installation the set-up explained in section 3.1.2.1 the tests start with a constant discharge (Table 3.4, Table 3.5). The maximum time to stop the test is 30 minutes in which no failure will be observed. This experiments are designed to calibrate the model and the results are compared with existing formulae. This also provide a chance to compare the result with the packed block tests. The number of eroded blocks are counted. Then all blocks which are eroded and accumulated in a basket at downstream of the channel are weighted and controlled with the weight of counted blocks.

3.3.2 Packed test

Packed riprap is supposed to be more stable. After installation explained in section 3.1.2.2 the given discharge will flow in the channel and time-based measurement of the erosion is performed. The tests are performed in one and two layers in order to define the effect of thickness on stability of packed riprap.

3.3.3 List of experiments

Table 3.4 and 3.5 presents the dumped tests with two different block sizes. Table 3.6 and Table 3.7 show the experiments of packed riprap on one layer and two layers respectively.

Table 3.4 Dumped test of blocks $D = 0.037$m, $S = 0.03$, $\alpha = 35°$

Test Series	q (m^2s^{-1})	h (m)	A (m^2)	R (m)	S (-)	V (ms^{-1})	Fr (-)
D1.1	0.0114	0.018	0.02	0.017	0.03	0.63	1.49
D1.2	0.0211	0.028	0.03	0.027	0.03	0.74	1.41
D1.3	0.0560	0.050	0.05	0.046	0.03	1.08	1.55
D1.4	0.0728	0.057	0.06	0.051	0.03	1.23	1.64
D1.5	0.0868	0.064	0.07	0.057	0.03	1.30	1.64
D1.6	0.0999	0.072	0.08	0.063	0.03	1.32	1.57
D1.7	0.1310	0.095	0.10	0.080	0.03	1.29	1.34
D1.8	0.1460	0.100	0.11	0.084	0.03	1.36	1.38
D1.9	0.1620	0.105	0.11	0.088	0.03	1.44	1.41
D1.10	0.1763	0.109	0.12	0.090	0.03	1.50	1.45
D1.11	0.1913	0.113	0.12	0.093	0.03	1.57	1.49
D1.12	0.2027	0.116	0.13	0.095	0.03	1.61	1.51
D1.13	0.2147	0.118	0.13	0.097	0.03	1.68	1.56
D1.14	0.2281	0.126	0.14	0.102	0.03	1.66	1.49
D1.15	0.2442	0.126	0.14	0.102	0.03	1.78	1.60
D1.16	0.2908	0.152	0.17	0.119	0.03	1.73	1.41
D1.17	0.3305	0.170	0.19	0.130	0.03	1.73	1.34

Table 3.5 Dumped test of blocks $D = 0.042$ m, $S = 0.03$, $\alpha = 35°$

Test Series	q (m^2s^{-1})	h (m)	A (m^2)	R (m)	S (-)	V (ms^{-1})	Fr (-)
D2.1	0.006	0.012	0.012	0.012	0.03	0.48	1.41
D2.2	0.021	0.026	0.026	0.025	0.03	0.79	1.56
D2.3	0.050	0.045	0.046	0.041	0.03	1.08	1.62
D2.4	0.065	0.053	0.055	0.048	0.03	1.17	1.63
D2.5	0.082	0.062	0.065	0.055	0.03	1.27	1.63
D2.6	0.103	0.072	0.076	0.063	0.03	1.37	1.62
D2.7	0.134	0.086	0.091	0.074	0.03	1.47	1.60
D2.8	0.145	0.091	0.097	0.078	0.03	1.50	1.58
D2.9	0.161	0.098	0.105	0.083	0.03	1.54	1.57
D2.10	0.175	0.104	0.112	0.087	0.03	1.57	1.55
D2.11	0.192	0.111	0.120	0.092	0.03	1.60	1.53
D2.12	0.206	0.117	0.127	0.096	0.03	1.62	1.51
D2.13	0.215	0.121	0.131	0.099	0.03	1.63	1.50
D2.14	0.229	0.127	0.139	0.103	0.03	1.65	1.48
D2.15	0.229	0.127	0.139	0.103	0.03	1.65	1.48
D2.16	0.293	0.154	0.171	0.120	0.03	1.71	1.39
D2.17	0.334	0.172	0.193	0.131	0.03	1.73	1.33

Table 3.6 Test program for packed riprap

Test Series	S (-)	Side slope (°)	D (m)	h (m)	Q (l/s)	V (ms^{-1})	Fr (-)	τ (Nm^{-2})	Failed or Stable
1	0.015	35	0.047	0.240	350	1.673	1.09	24.96	S
2	0.015	35	0.047	0.252	380	1.714	1.09	25.91	S
3	0.015	35	0.047	0.290	400	1.520	0.90	28.80	F
4	0.015	35	0.047	0.295	420	1.563	0.92	29.17	F
5	0.015	35	0.047	0.310	498	1.743	1.00	30.27	F
6	0.015	35	0.037	0.180	230	1.542	1.16	19.96	S
7	0.015	35	0.037	0.187	240	1.540	1.14	20.57	S
8	0.015	35	0.037	0.197	255	1.540	1.11	21.43	F
9	0.015	35	0.037	0.202	265	1.554	1.10	21.85	F
10	0.015	35	0.037	0.209	280	1.582	1.11	22.40	F
11	0.015	35	0.037	0.215	295	1.607	1.11	22.94	F
12	0.015	35	0.042	0.222	330	1.731	1.17	23.51	S
13	0.015	35	0.042	0.230	340	1.710	1.14	24.16	S
14	0.015	35	0.042	0.239	350	1.682	1.10	24.88	F
15	0.015	35	0.042	0.246	370	1.718	1.11	25.44	F
16	0.015	35	0.042	0.250	380	1.730	1.11	25.75	F
17	0.015	35	0.042	0.259	405	1.767	1.11	26.45	F
18	0.030	35	0.047	0.185	316	2.053	1.52	40.79	S
19	0.030	35	0.047	0.187	325	2.085	1.54	41.13	S
20	0.030	35	0.047	0.202	340	1.994	1.42	43.70	F
21	0.030	35	0.047	0.210	355	1.989	1.39	45.04	F
22	0.030	35	0.047	0.220	378	2.005	1.37	46.69	F
23	0.030	35	0.047	0.240	410	1.960	1.28	49.92	F
24	0.030	35	0.037	0.122	228	1.719	1.57	30.71	S
25	0.030	35	0.037	0.134	267	1.818	1.59	33.30	S
26	0.030	35	0.037	0.136	275	1.843	1.60	33.73	S
27	0.030	35	0.037	0.141	290	1.869	1.59	34.78	F
28	0.030	35	0.037	0.145	310	1.937	1.63	35.62	F
29	0.030	35	0.037	0.155	336	1.952	1.58	37.69	F
30	0.030	35	0.037	0.167	350	1.872	1.46	40.13	F
31	0.030	35	0.042	0.160	250	1.919	1.53	36.33	S
32	0.030	35	0.042	0.169	275	1.983	1.54	37.96	S
33	0.030	35	0.042	0.177	297	2.030	1.54	39.38	F
34	0.030	35	0.042	0.181	308	2.052	1.54	40.09	F
35	0.030	35	0.042	0.183	315	2.072	1.55	40.44	F
36	0.030	35	0.042	0.187	325	2.085	1.54	41.13	F
37	0.030	35	0.042	0.152	325	1.929	1.58	37.08	F
38	0.030	35	0.042	0.156	345	1.990	1.61	37.90	F
39	0.030	35	0.042	0.205	350	2.017	1.42	44.20	F
40	0.030	31	0.047	0.172	280	1.930	1.49	39.80	S
41	0.030	31	0.047	0.179	300	1.974	1.49	41.13	S
42	0.030	31	0.047	0.196	352	2.080	1.50	44.28	F
43	0.030	31	0.047	0.205	381	2.134	1.51	45.92	F
44	0.030	31	0.047	0.211	400	2.164	1.51	47.00	F
45	0.030	31	0.037	0.120	150	1.563	1.44	29.43	S
46	0.030	31	0.037	0.126	168	1.656	1.49	30.68	S
47	0.030	31	0.037	0.134	187	1.719	1.50	32.32	F
48	0.030	31	0.037	0.147	228	1.886	1.57	34.94	F
49	0.030	31	0.037	0.160	266	1.995	1.59	37.49	F
50	0.030	31	0.042	0.145	235	1.974	1.66	34.54	S
51	0.030	31	0.042	0.158	250	1.903	1.53	37.10	S
52	0.030	31	0.042	0.165	265	1.918	1.51	38.46	S
53	0.030	31	0.042	0.176	295	1.980	1.51	40.56	F
54	0.030	31	0.042	0.180	305	1.996	1.50	41.28	F

Test Series	S (-)	Side slope (°)	D (m)	h (m)	Q (l/s)	V (ms^{-1})	Fr (-)	τ (Nm^{-2})	Failed or Stable
55	0.030	31	0.042	0.181	310	2.013	1.51	41.50	F
56	0.030	27	0.037	0.118	152	1.575	1.46	29.90	S
57	0.030	27	0.037	0.129	176	1.646	1.46	32.34	S
58	0.030	27	0.037	0.137	195	1.701	1.47	34.08	S
59	0.030	27	0.037	0.142	208	1.740	1.47	35.16	S
60	0.030	27	0.037	0.146	218	1.765	1.48	36.02	F
61	0.030	27	0.037	0.150	228	1.788	1.47	36.87	F
62	0.030	27	0.037	0.157	228	1.695	1.37	38.35	F
63	0.030	27	0.037	0.170	265	1.792	1.39	41.06	F
64	0.030	27	0.042	0.140	200	1.701	1.45	34.73	S
65	0.030	27	0.042	0.150	226	1.773	1.46	36.87	S
66	0.030	27	0.042	0.150	227	1.780	1.47	36.87	S
67	0.030	27	0.042	0.155	240	1.811	1.47	37.93	F
68	0.030	27	0.042	0.165	267	1.871	1.47	40.02	F
69	0.030	27	0.042	0.165	268	1.878	1.48	40.02	F
70	0.030	27	0.042	0.185	325	1.985	1.47	44.13	F
71	0.030	27	0.042	0.185	325	1.985	1.47	44.13	F
72	0.030	27	0.042	0.202	378	2.075	1.47	47.54	F
73	0.030	27	0.042	0.206	390	2.090	1.47	48.34	F
74	0.030	27	0.042	0.208	398	2.107	1.48	48.73	F
75	0.030	27	0.042	0.209	400	2.105	1.47	48.93	F
76	0.030	27	0.042	0.211	405	2.107	1.47	49.32	F
77	0.030	27	0.042	0.211	410	2.133	1.48	49.32	F
78	0.030	27	0.042	0.180	423	2.670	2.01	43.11	F
79	0.030	27	0.042	0.217	430	2.161	1.48	50.50	F
80	0.030	27	0.042	0.223	445	2.162	1.46	51.67	F
81	0.055	35	0.047	0.122	230	2.395	2.19	53.37	S
82	0.055	35	0.047	0.132	255	2.432	2.14	56.96	S
83	0.055	35	0.047	0.145	270	2.317	1.94	61.51	F
84	0.055	35	0.047	0.148	278	2.331	1.94	62.55	F
85	0.055	35	0.047	0.164	296	2.209	1.74	67.94	F
86	0.055	35	0.047	0.175	308	2.133	1.63	71.56	F
87	0.055	35	0.037	0.095	135	1.851	1.92	43.21	S
88	0.055	35	0.037	0.099	145	1.900	1.93	44.76	S
89	0.055	35	0.037	0.100	156	2.022	2.04	45.14	S
90	0.055	35	0.037	0.109	180	2.123	2.05	48.56	F
91	0.055	35	0.037	0.113	200	2.267	2.15	50.06	F
92	0.055	35	0.037	0.118	215	2.323	2.16	51.90	F
93	0.055	35	0.042	0.115	230	2.557	2.41	50.80	S
94	0.055	35	0.042	0.119	240	2.569	2.38	52.27	S
95	0.055	35	0.042	0.123	250	2.580	2.35	53.73	F
96	0.055	35	0.042	0.139	265	2.385	2.04	59.43	F
97	0.055	35	0.042	0.145	285	2.446	2.05	61.51	F
98	0.055	35	0.042	0.153	304	2.455	2.01	64.25	F

Table 3.7 Test with two layers for $D = 0.037$ m

Test Series	Channel Slope (%)	Bank slope (°)	Q (l/s)	h (m)	V (ms–1)	Fr (-)	τ (Nm-2)	Failed or Stable
Double 1	0.015	35	340	0.233	1.684	1.11	24.40	S
Double 2	0.015	35	347	0.235	1.701	1.12	24.56	F
Double 3	0.015	35	355	0.239	1.706	1.11	24.88	F
Double 4	0.015	35	380	0.248	1.747	1.12	25.59	F
Double 5	0.030	35	310	0.150	1.867	1.54	36.66	S
Double 6	0.030	35	333	0.163	1.830	1.45	39.32	F
Double 7	0.030	35	350	0.168	1.860	1.45	40.33	F
Double 8	0.030	35	375	0.182	1.823	1.37	43.10	F
Double 9	0.030	31	188	0.132	1.758	1.55	31.92	S
Double 10	0.030	31	200	0.140	1.749	1.49	33.54	F
Double 11	0.030	31	228	0.151	1.842	1.52	35.53	F
Double 12	0.030	31	255	0.167	1.820	1.42	38.84	F
Double 13	0.030	27	218	0.145	1.779	1.49	35.80	S
Double 14	0.030	27	228	0.157	1.695	1.37	38.35	F
Double 15	0.030	27	240	0.162	1.719	1.36	39.40	F
Double 16	0.030	27	265	0.170	1.792	1.39	41.06	F
Double 17	0.055	35	180	0.109	2.123	2.05	48.56	S
Double 18	0.055	35	200	0.117	2.182	2.04	51.54	F
Double 19	0.055	35	215	0.122	2.239	2.05	53.37	F
Double 20	0.055	35	230	0.127	2.290	2.05	55.17	F
Double 21	0.055	35	245	0.138	2.223	1.91	59.08	F

3.4 Dimensional analysis

Dimensional analysis is used to define the dimensionless variables based on the selection of all relevant parameters. The dimensional analysis performed here is similar to that proposed by Neill (1967) and Maynord (1988) in which mean velocity is used instead of the critical tractive force approach. The relevant parameters governing the stability of riprap in open channels are:

Hydraulic parameters:

h = Flow depth, L

V = Mean velocity, L/T

μ = Viscosity, M/LT

ρ = Fluid density M/L^3

Riprap parameters:

$\gamma_S^{'}$ = Submerged specific weight of the riprap f (g, ρ_s)

D = Block size, L

N = $\frac{Thickness}{D_{100}}$

Channel geometry:

S = Channel slope

A = Bank slope

By applying Buckingham P Theorem three non-dimensional parameter are defined as:

$$Modified\ Froude\ number = \frac{V}{\sqrt{(S_B - 1)gh}}$$

$$Reynolds\ number = \frac{Vh}{\nu}$$

$$Relative\ roughness = \frac{D}{h}$$

The Reynold's number term is indicating the viscous effects which are not important in prototypes and in the model sizes used in this investigation. Thus the non-dimensional parameters of modified Froude number and relative roughness are the main results of dimensional analysis.

Chapter 4

Design of Riverbank Riprap Using Large Individually Placed and Packed Blocks

This chapter analyses the influence of packing blocks on the stability of river bank riprap. A riprap design formula for large individually placed blocks is proposed based on the data collected during the present research. Results of the experiments are also compared to existing formulae.

Abstract

The study which is framing this chapter is addressing the design of large block riprap built in mountain rivers with individually placed blocks, having relatively small spacing between them. The failure criterion opted in this case corresponds to when the blocks on the bank totally slide and make the section unstable. Since the interlocking forces are higher and blocks are in more support in packed riprap, the block size of the riprap can be decreased when compared with simply dumped protections. A specific relation for packed riprap design was developed based on 98 experiments performed in a trapezoidal section shape, using three different blocks gradations with the characteristic sizes of D_{50} = 0.037 m, 0.042 m, 0.047 m. The longitudinal channel slopes of 1.5%, 3% and 5.5% and the riprap bank slopes of 35°, 31° and 27° are tested. 34 dumped riprap laboratory tests are added and compared with existing methods of riprap design. The status of occurrence of failure or remaining stable for dumped and packed riprap tests are compared, and the extra strength is observed while the riprap is packed. The minimum size of the packed blocks to design stable riprap is defined by a functional relation taking into account the relative roughness and a modified Froude number. This proposed relationship can be applied to re-evaluate the stability of existing packed riprap bank protections.

4.1 Introduction

The erodible banks of mountain rivers need to be protected against the possible erosion and scouring. Among other flood protection measures that can ensure river bank safety against lateral erosion, riprap revetment is one of the most commonly used. Riprap is a flexible protection with self-healing capacity. It has affordable installation cost, and also is long lasting and easy to repair. Several methods of riprap design exist which have been mostly developed for dumped median size blocks. However, in mountain rivers and steep channels, the extra stability has to be provided by using the large blocks, which have to be placed individually due to their weight. Thus, the blocks are better packed and interlocked compared to dumped riprap. Nevertheless, the additional stability of such a packed/compressed riprap is not known. Several equations were developed to predict the riprap stability if exposed to the flow, considering the block size, the gradation and the

thickness as geometrical parameters, as well as the characteristics of an underneath filter (Stevens et al., 1976; Maynord et al., 1989; Escarameia and May, 1995).

The base for most of riprap design methods applied to define the block sizes go back to the classic work of Shields (1936) and Isbash (1936), who performed tests on the entrainment of particles subject to changing shear stress and velocity. Shields (1936) performed a series of tests in which he bordered the threshold for the movement of quite uniform grains as a function of the critical dimensionless shear stress. Lane (1953) later used the shear stress method for stable canal design in the noncohesive material. Anderson et al. (1968) developed this method which includes the effects of bank slopes and channel bends. Their work is used as the basis for riprap design by the US Department of Transportation (1975). Li et al. (1976) and Stevens and Simons (1971) developed tractive force methods which incorporate probability and safety factors into the design method.

Velocity based technics developed based on Isbash (1936) study. He analysed the stability of blocks and rocks eroded into the flow, framed as a critical flow velocity V that will move a rock of diameter D. The first purpose of the tests was to develop criteria for the stability of dams; however, the equation was later used in the riprap design (U.S. Army Corps of Engineers (USACE), 1991).

A probabilistic approach for the design of riprap against currents was studied by Li et al. (1996), PIANC (1987) and Froehlich and Benson (1996). Uncertainties in risk-based design procedures are resulting mostly from hydraulic forces, estimation of stone size, stone density, and channel depth and so on.

Stability of loosed (dumped) rock riprap was also studied by Froehlich (2011) regarding the protection of stream banks from erosive forces due to flowing water. This evaluation is based on the ratio of static moments resisting overturning. The ratio of moments in his research defined a safety factor which indicates the potential for riprap failure. Abt et al. (2008) studied the round-shaped riprap stabilization in overtopping flow as well.

Safety factor also is a considerable parameter to design riprap. Stevens et al. (1976) presented his safety factor based method by taking into account the stability of individual block in riprap. It was based on that each block is stable if the amount of the moments

causing the possible displacement of a block is less than the moment of submerged weight. Froehlich (2011), Ulrich (1987) and Stevens et al. (1984) also considered the weight of the submerged rock as the only resisting force. Wittler and Abt (1988) modified Stevens' analysis adding a contact and frictional forces from nearby blocks.

Froehlich and Benson (1996) also worked on wide angle of repose to refer the slope of embankment impact on the stability of riprap. They proposed a "particle angle of initial yield." Escarameia and May (1992) presented the general equation for design riverbank ripraps and gabion mattresses. At the same time, Brown and Clyde (1989) used both the Manning-Strickler equation with the Shields relation to make a combined formula for the size of stable blocks. Straub (1953), Grace et al. (1973) and Reese (1984) applied similar approach earlier.

The aim of this research is to investigate the behavior of large blocks individually placed as riprap bank protection and to develop a specific relation for packed riprap design. This chapter is based experiments performed in an open-channel with three different longitudinal channel slopes of 1.5%, 3% and 5.5% and three riprap bank slopes of 35°, 31° and 27°. 98 experiments were performed with packe riprap whereas 34 dumped riprap laboratory tests were made to compare with existing methods of riprap design. Next the experimental setup and the experimental procedure are shown, followed by the presentation and discussion of results and finally by the conclusions.

4.2 Experimental set-up and procedure

Ninety-eight experiments were conducted varying the block size and streamwise channel slope to analyze the effect of the packed block arrangement of the riprap on the stability of riprap bank protections. Thirty four tests also were performed with dumped blocks to compare the results with packed riprap.

The laboratory tests were carried out on a straight 10 m long, 1.5 m wide tilting flume. The longitudinal slope of the flume was set to S =1.5%, 3% and 5.5%. The transversal riprap bank slope was fixed at 3.5V-5H (35°), 3V-5H (31°) and 2.5V-5H (27°). Blocks were categorized in three groups based on their weight (50gr to 90 gr, 90gr to 130gr, and 130gr to 170gr). Then the apparent diameter spherically calculated based on the limestone block specific gravity equal to 2.66. Each group included a specific

block size (D_{50} = 0.037, 0.042 and 0.047 m, respectively). The riprap consisted of one single layer, and its thickness is accordingly D_{50}. The details of block gradations are explained in chapter 3.

Three different equivalent average block sizes D_{50} of 0.037, 0.042 and 0.047 m were tested individually. Ahmed (1987) and Wittler and Abt (1990) reported that a riprap with a uniform gradation (when expecting similar D_{50}) tends to be globally more stable, as compared to wide distribution of block sizes. The blocks were then uniformly selected and applied in the experiments. Froehlich (2011) conducted tests with various block sizes (including those used herein), considering crushed material. Thus, the angle of repose of blocks of 40 to 41 degrees can be assumed as based on Froehlich experiments (Froehlich, 2011). Tests were run until total failure occurred but with a maximum duration of 180 minutes.

Blocks were packed and placed on a wide grain size distribution representing the filter and river bank material. In order to simulate natural hydraulic roughness conditions, the roughness of the channel bed was imposed using the same material glued to the channel bed as for the filter (Table 3.3).

The distinction between dumped and packed set-up was based on porosity measurements. Preliminary tests were performed to obtain the air volume in a defined dumped or riprap volume. Table 3.2 shows the porosity (n_p) of these tests, as well as the averaged values per block size and construction type. Packed porosity reduced by 2% for D_{50} = 0.037 m, by 5% for D_{50} = 0.042 m, and by 10% for D_{50} = 0.047 m when compared with dumped riprap.

Based on preliminary tests and typical flood peak durations in mountain rivers the maximum duration of the experiments was set to 180 minutes. The corresponding prototype time is important for the analysis of the results since it represents the expected maximum duration of the flood peak assuming a constant mean discharge, which may cause the riprap failure. The time scale of a physical model based on the Froude similarity is given as:

$$\lambda_T = \frac{T_p}{T_m} = \sqrt{\frac{L_p}{L_m}} \tag{4.1}$$

where T represents a duration, L a length, and subscripts p and m stand for prototype and model, respectively. Considering a geometrical scale of the experimental set-up for typical alpine mountain rivers of $L_P/L_m = 25$, then a time scale λ_T of five results. Experimental tests lasting 180 minutes are thus roughly equivalent to prototype flood peak durations of 15 hours, which largely covers the flood observed durations in typical alpine mountain rivers.

The experimental program was defined in order to identify the stability condition of packed riprap during the test and the transitional unit discharge causing failure. Lower discharges could cause direct block erosion during the tests but not lead to full failure of the riprap. For the fixed channel slopes, supercritical flow conditions ($1.09 < Fr < 1.89$) occurred for all discharges (except four tests of flatter channel slope). The discharge was increased subsequently (for subsequent test) until failure occurred, providing the failure discharge. Flow depths were measured by ultrasonic probes with a precision of ±0.5 mm at four different positions located at each 2 m along the channel axis. They were all transversally located at the center. For the first 6 m upstream, the riprap protection was fixed on mortar, keeping, however, the same roughness, to avoid an influence of the model inlet.

The analysis of the block erosion were thus limited to the part of the flume between 6.5 m and 9.5 m where constant flow depth (roughly uniform flow) occurred. Erosion occurring outside that zone were excluded.

The detailed parameters of the experiments are shown in Tables 3.4 and 3.5 for dumped tests and 3.6 for all packed riprap. In Table 3.6 the occurrence of failure is indicated in the last column.

4.3 Results and discussion

4.3.1 Comparative analysis of the basic form of riprap design equations

This section is developed based on dimensional analysis performed in section 3.4. Riprap protection is endangered by the erosive effects of drag and lift forces resulting from the velocity distribution near particles. Considering riprap stability, different sizing methods were developed. The basic form of many sizing equation is given by Maynord and Neill (2008):

$$\frac{V_C}{[g(S_B-1)D]^{\frac{1}{2}}} = C_{ref}\left(\frac{h}{D_c}\right)^{P_{ref}} \quad (4.2)$$

Where V_c is characteristic velocity, g is acceleration of gravity S_B is specific gravity of stone, $S_B = \rho_s/\rho$, ρ_s is stone density, ρ is water density, D define as characteristic particle size, C_{ref} is a numerical coefficient, usually based on empirical data, h is the local water depth, P_{ref} is an exponent dependent on the hydraulic environment and the way the characteristic velocity V_c is defined.

Among the equations explained in Chapter 2, seven of them are found to be the most frequently used ones in literature: HEC-11 (Brown and Clyde, 1989), Escarameia and May (1992), Pilarczyk (1990), EM 1601 (USACE, 1994) supplemented by Maynord et al. (1989) and Maynord (1990), Isbash (1935, 1936), CABS (Racin et al., 2000), and HDS 6 (Richardson et al., 2001).

Two of the equations (Pilarczyk and HDS 6) require iterative solutions because a specific flow velocity can produce a range of shear stresses (tractive force) depending on the size of the riprap (roughness of the surface) (Lagasse et al., 2006).

There is a detailed comparison of these seven equations with data for three sites studied by Blodgett and McConaughy (1986) in the report of Lagasse et al. (2006). After all of the comparisons, four equations for further analyses were selected: CABS (equation (4.3)) for being representative to Isbash equation and supported by detailed design, EM-1601 (equation (4.4)) for being the most comprehensive one, HEC-11 (equation (4.5)) for being most frequently used and HDS 6 (equation (4.5)) for being representative for factor of safety approach.

Each of the equations (CABS, EM 1601 [Maynord], HEC-11, and HDS 6) was reduced to its basic form by removing correction factors related to bank bank slope, bend radius, and safety/stability and by converting each equation into a consistent dimensionless form. Each of the equations includes the dimensionless parameter of block size divided by flow depth as the dependent variable and the independent variable is the dimensionless parameter $V/[(S_B\text{-}1)gh]^{0.5}$, which is the Froude number divided by the square root of the submerged particle specific gravity. The resulting equations are valid for computing riprap size on a flat channel bed in a straight channel for incipient motion conditions. For two of the equations the consideration of the bank slope of 35° is included.

The riprap equations differ only in the coefficient and exponent applied to the independent variable, except that the HDS 6 equation includes a log term representing the effect of the relative roughness of the riprap surface. Because this term is related to the ratio of riprap size to flow depth, it is part of the dependent variable. The details of each equation are explained as follow:

- CABS Equation

Safety factor is assumed to be 1, the shape midway between a sphere and a cube is used to convert weight to nominal diameter, it is solved for a bank angle of zero degrees (Lagasse et al., 2006). Then equation becomes,

$$\frac{D_n}{h} = 0.263 \left[\frac{V}{\sqrt{(S_B\text{-}1)gh}}\right]^2 \tag{4.3}$$

- EM-1601 Equation

All the correction factors, bank angle factor and a channel bend correction factor are taken as 1 (cf. Chapter 2) (Maynord et al., 1989). Then the equation becomes,

$$\frac{D_{30}}{h} = 0.30 \left[\frac{V}{\sqrt{(S_B\text{-}1)gh}}\right]^{2.5} \tag{4.4}$$

- HEC-11 Equation

All correction factors including safety factor (C_{SF}) and bank angle factor is taken as 1 (Lagasse et al., 2006). Then the equation becomes,

$$\frac{D_{50}}{h} = 0.295 \left[\frac{V}{\sqrt{(S_B\text{-}1)gh}}\right]^3 \tag{4.5}$$

- HDS 6 Equation

It is converted to its basic form by setting the bank angle at zero and the stability factor as 1.

$$\frac{D_{50}}{h}\left[ln\left(\frac{12.3h}{D_{50}}\right)\right]^2 = 3.48 \left[\frac{V}{\sqrt{(S_B\text{-}1)gh}}\right]^2 \tag{4.6}$$

Comparison between the several design formulae can be seen in Figure 4.1 for the range of flows and riprap protections of the present research.

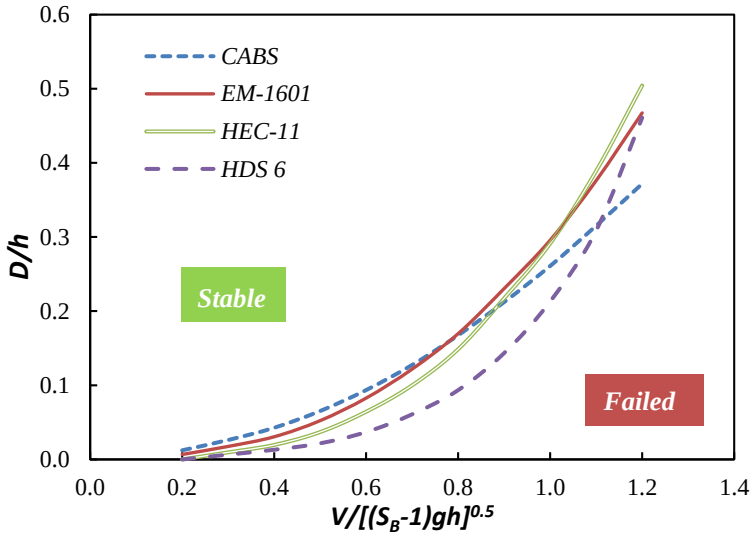

Figure 4.1 Comparison of four basic riprap size equations (adopted from Lagasse et al., 2006). The lines mean the boundary between stable and unstable flow conditions.

The four equations include the same dependent and independent variables. The differences are the coefficient and exponent applied to the independent variable. Figure 4.1 shows these four equations plotted for comparison. The HEC-11 and HDS 6 equations yield the smallest size, especially considering that they compute a D_{50} size as compared with EM 1601 (Maynord, 1989), which computes a D_{30} size. For typical design conditions, where a natural channel Froude number ranges from 0.5 to 0.9, the CABS, and EM 1601 (Maynord) equations are the most conservative (Lagasse et al., 2006).

4.3.2 Comparison of the laboratory dumped and packed riprap experiments with existing riprap sizing equations

Series of 17 tests of the dumped blocks with the size of D = 0.042 m are performed to compare to the equations developed by CABS (equation (4.3)), EM-1601 (equation (4.4)), HEC-11 (equation (4.5)), and HDS 6 (equation (4.6)). In Figure 4.2 relative roughness as a function of modified Froude number is presented for the test explained in Table 3.5. The block erosion occurs both for the blocks placed on the bed as well as on the bank slope. Therefore, the comparison shown in Figure 4.2 was done specifically for the bank slope of 0° and 35°.

In Figure 4.2, the equations of HEC-11 and EM-1601 are calculated for both plain bed (continuous lines) and with bank slope of 35° (dashed lines) in order to have a better comparison. The empirical results obtained in the present research for D = 0.042 m, and divided between occurrence of failure or stable conditions, are shown as well. The results show that the blocks of three tests remained stable even if they are in the area of failure for HEC-11 (with a bank slope of 35°).

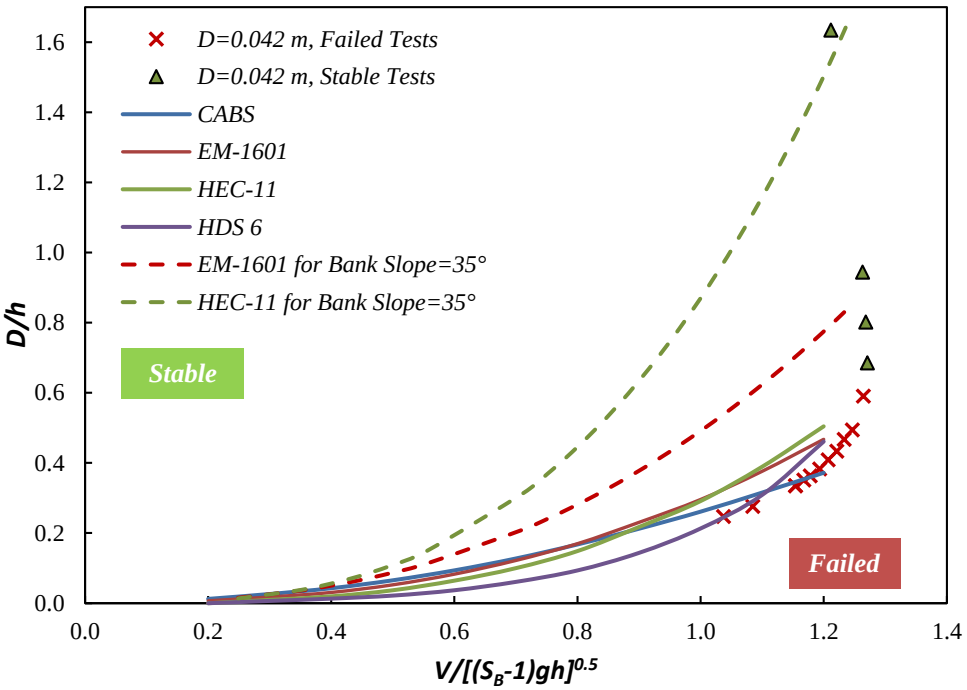

Figure 4.2 Relative roughness as a function of modified Froude number and comparison the dumped blocks size D = 0.042 tests in the bank slope of 0° and 35° with existing riprap design formulae.

The EM-1601 equation predicted better for both bed and bank, although, two of tests which had no block movement resulted in the area proposed for failure. The rest of experiments show good agreements with the existing equations for riprap design in the area of supercritical flow.

In order to see the differences in behaviour of dumped and packed blocks, 32 series of experiments, including failed and stable tests, with the same blocks size of D = 0.425 m and higher velocity (cf. Table 3.6) in packed placement is added to the same graph (The tests run only for channel slope of 3% are presented here). A significant shift of stable tests from dumped ones can be seen in Figure 4.3. All the equations (equations (4.3) to

(4.6)) display an overestimating the size of blocks against failure occurrence in this graph for packed blocks.

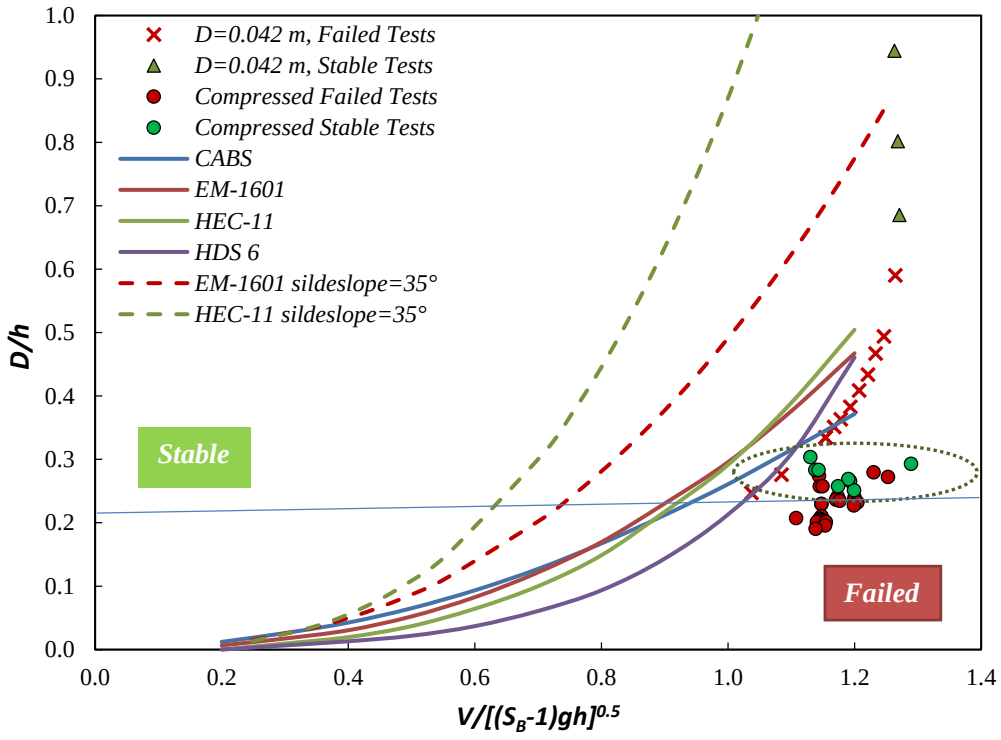

.

Figure 4.3 Relative roughness as a function of modified Froude number and comparison of the dumped and packed blocks size *D*= 0.042 tests in the bank slope of 0° and 35° with existing riprap design formulae

The reason of this difference is that the failure mechanisms of these two types of the tests are different. Thus, some limited erosion of the packed blocks is observed at the time that section remains stable. By this point of view, the equations could be valid for only the dumped median size of the blocks on the plain bed.

The same comparison is done for the block sizes of D = 0.037 m in Figure 4.4. Relative roughness plotted versus the modified Froude number shows the stability border of riprap in different design equations. The stability of blocks is evaluated by the result of dumped tests (cf. Table 3.4). Figure 4.4 shows that two tests resulted in failure within the safe area of plotted equations for bank slope of 0°. However, the equations plotted for the bank slope equals to 35°, overestimated the block sizes at least in four of the tests that remained stable but are nevertheless in the failed area of the graphic.

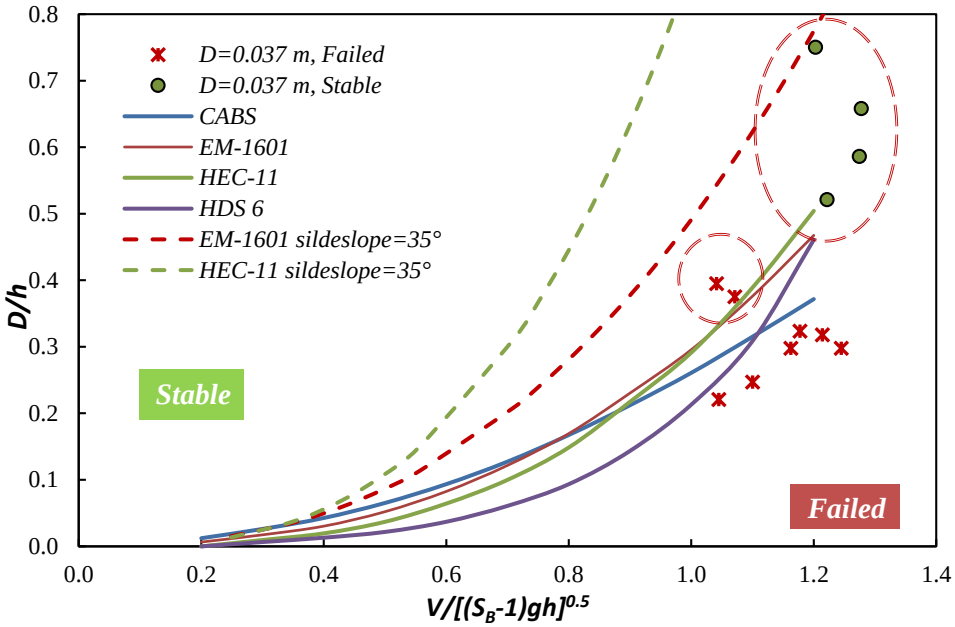

Figure 4.4 Relative roughness as a function of modified Froude number and comparison the dumped blocks size D = 0.037 tests in the bank slope of 35° with existing riprap design formulae

In Figure 4.5, the relative roughness of twenty-three tests performed with packed riprap versus the modified Froude number is plotted. Comparison with the existing equations shoes the extra stability of riprap with smaller block size.

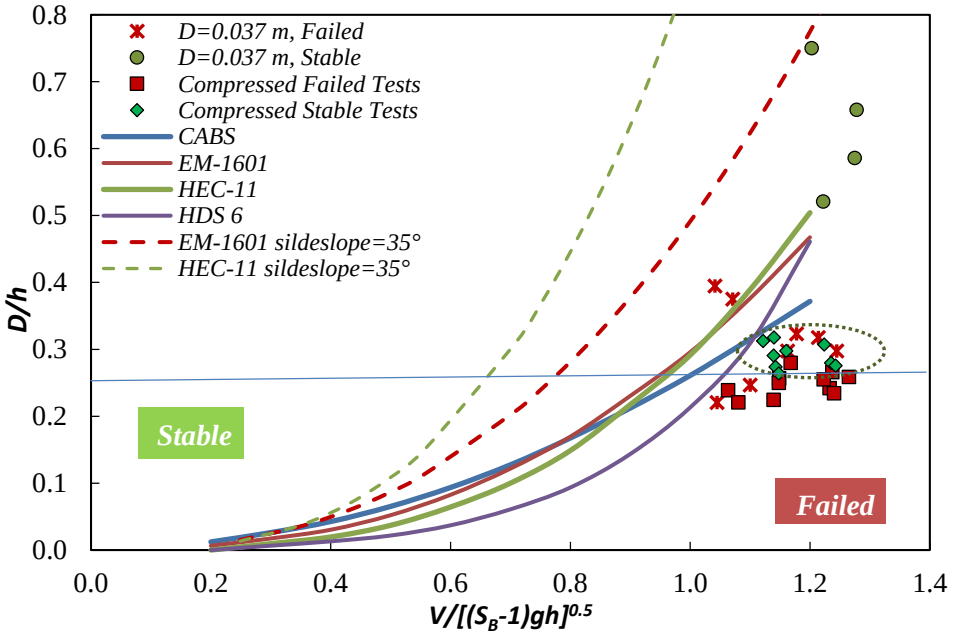

Figure 4.5 Relative roughness as a function of modified Froude number and comparison the dumped and packed blocks size D = 0.037 tests in the bank slope of 35° with existing riprap design formulae

4.3.3 Block erosion differences in packed and dumped tests

The block erosion rate q_s as a function of unit discharge q for dumped and packed riprap tests is plotted in Figure 4.6. In all experiments, the rate of erosion was measured by counting the number of eroded blocks in the frequency of one minute by video analysis.

In dumped experiments, the start of block erosion was taken as the failure, and the total bank failure always occurs quite fast as the blocks are less supported by each other. However, the packed tests remained stable for a longer time. The discharge for beginning of motion slightly increases from dumped tests to packed block tests. The rate of erosion also increased when the unit discharge increased. The more interlocking forces among blocks due to the compression, the less block erosion is observed. During the tests it is shown that the larger block size starts to move later than the smaller ones, but higher mass movement occurs with the same unit discharge.

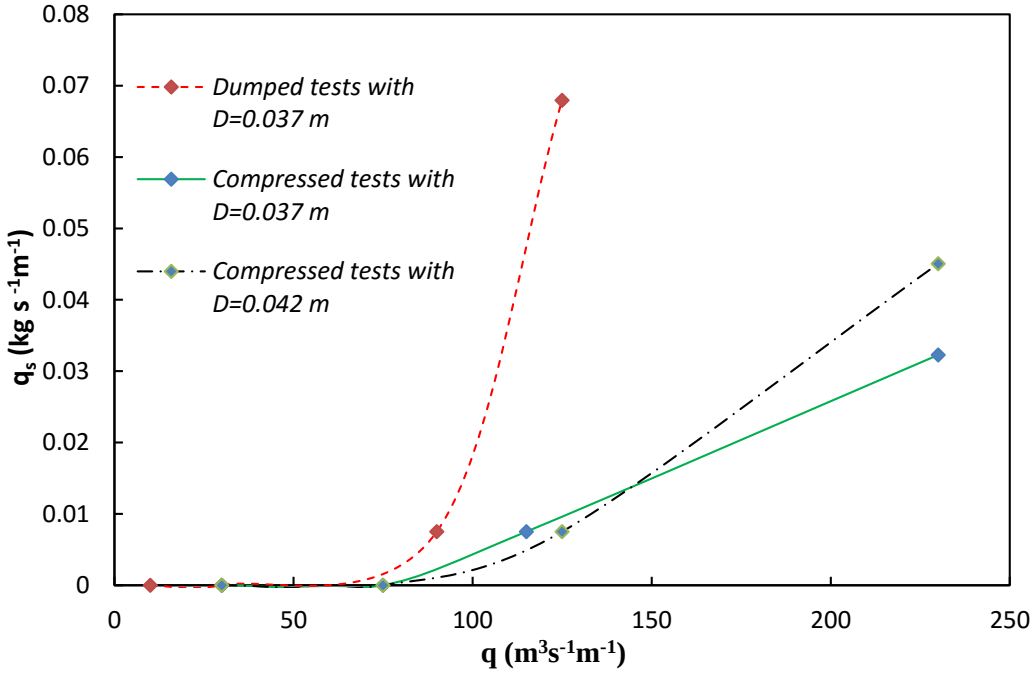

Figure 4.6 Block erosion rate q_s (kgs^{-1}m^{-1}) as a function of water unit discharge q (m^{3}s $^{-1}$m^{-1}) for the block sizes of D = 0.037 (dumped and compressed) and D = 0.042 (compressed)

4.3.4 Effect of channel longitudinal slope on block erosion rate

The block erosion transport rate was measured for 32 packed block tests which remained stable for the first one hour of testing. These tests include the three block sizes in three different channel slope and bank slope of 35° (cf. Table 4.5). Figure 4.7 shows the

influence of the longitudinal channel slope on block erosion transport rate q_s (kgh^{-1}) as a function of water unit discharge q (m^{3}s $^{-1}$m^{-1}). For a given unit discharge, higher block erosion transport occurs at steeper slopes (Figure 4.7). Data are grouped by channel slope, and power low trend lines are given for each slope (Figure 4.7). The three group of results based on channel slope (S) show that the correlation between unit discharge and block transport rate is probably not linear and increases exponentially. The same amount of blocks required higher discharge to move in lower longitudinal channel slope (S). Therefore, the slope has a dominant role on the erosion rate of large packed blocks.

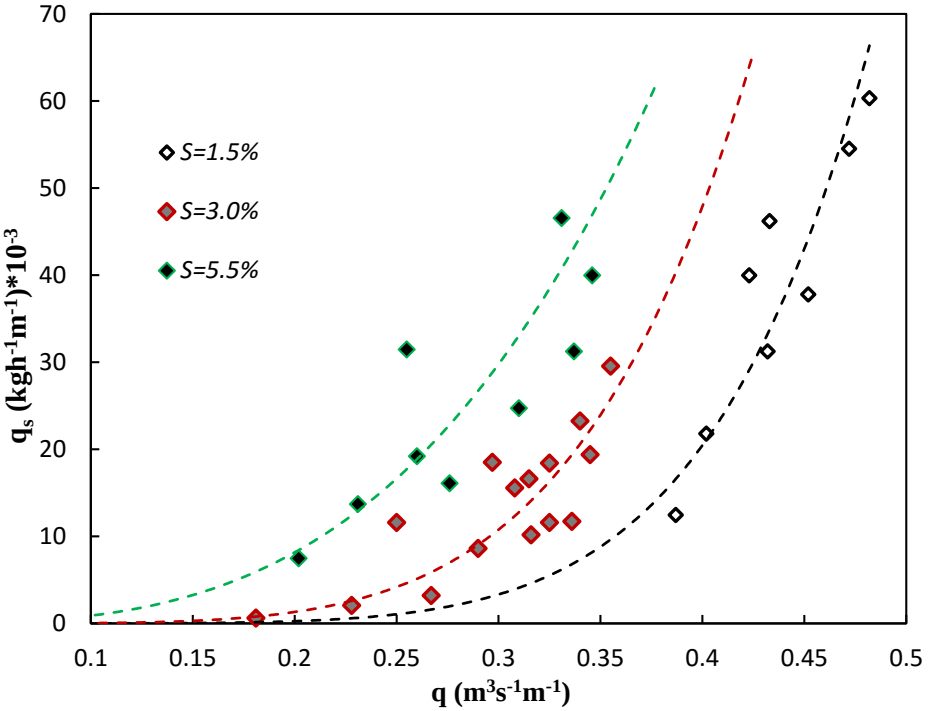

Figure 4.7 Block erosion rate q_s (kgh^{-1}m^{-1}) as a function of water unit discharge q (m^{3}s $^{-1}$m^{-1}). Data are grouped by channel slope, and power low trend lines are given for each slope, in three different sizes

One of the main problems of shear stress calculations is the need of a precise knowledge of the channel hydraulics, which typically has a high local variability in mountain rivers. On the other hand, stream power per unit width can be approximated from channel properties, such as width and slope, combined with the discharge of the river, as follows:

$$\omega = \rho\, gqS = \tau\, V \tag{4.7}$$

where ρ (1000 kgm^{-3}) is the fluid density, g (9.81 ms^{-2}) is the acceleration due to gravity, q (m^{3}s^{-1}m^{-1}) is the specific discharge, S (-) is the channel slope, τ (Nm^{-2}) is the

total bed shear stress, and V (ms^{-1}) is the average flow velocity. The stream power quantifies the rate of loss of energy as water flows downstream; it can also be seen as the flow power available to perform geomorphic work in the river bed (Ghilardi et al., 2014). Therefore, the block erosion rate in the channel is tentatively evaluated by the stream power produced in the channel as plotted in the Figure 4.8.

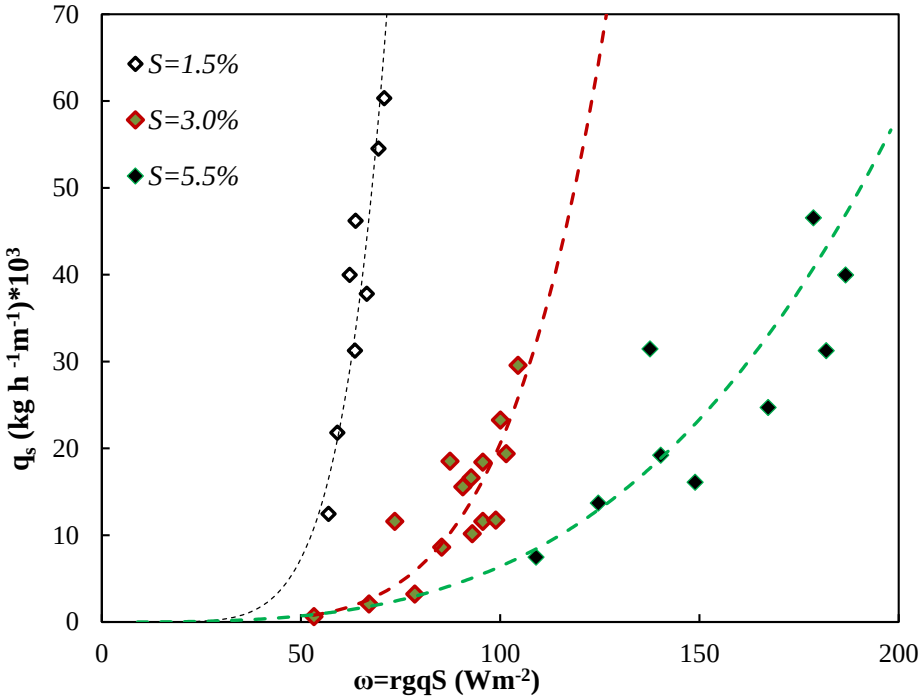

Figure 4.8 Block erosion transport rate q_s ($kgh^{-1}m^{-1}$) as a function of stream power (Wm^{-2}) Data are grouped by channel slope. Power low trend lines are given for each slope, in three different sizes

In Figure 4.8, as expected, the tests are clearly grouped by the slope. This graph indicates that the block erosion rate is clearly a function of both, unit discharge, and channel slope. These two parameters are both used in the stream power calculation. The lower channel slope S= 0.015 provides less stream power for a given block erosion rate. The stream power in this slope is more sensitive than other slopes and with small changes result in large differences in the block erosion rate. The effect of channel slope increases on stream power causing the block erosion rate is considerable (trend line slope smaller for longitudinal inclination of S = 0.055 than for the others). Considering shear stress (dimensional and dimensionless), the same pattern of results grouping by longitudinal slope can be seen in Figure 4.9 and 4.10.

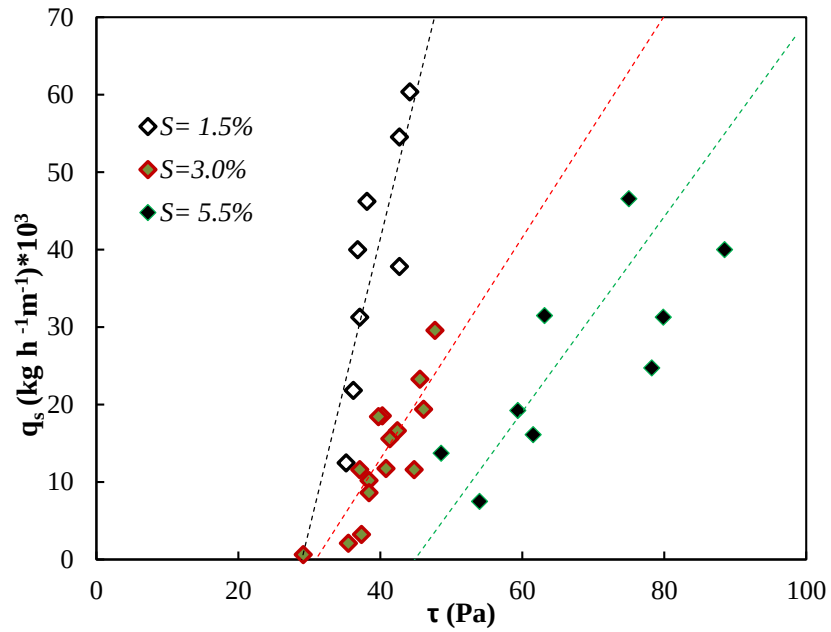

Figure 4.9 Block erosion transport rate q_s (kgh^{-1}m^{-1}) as a function of shear stress τ (Nm^{-2}) Data are grouped by channel slope and linear trend lines are given for each slope, in three different sizes

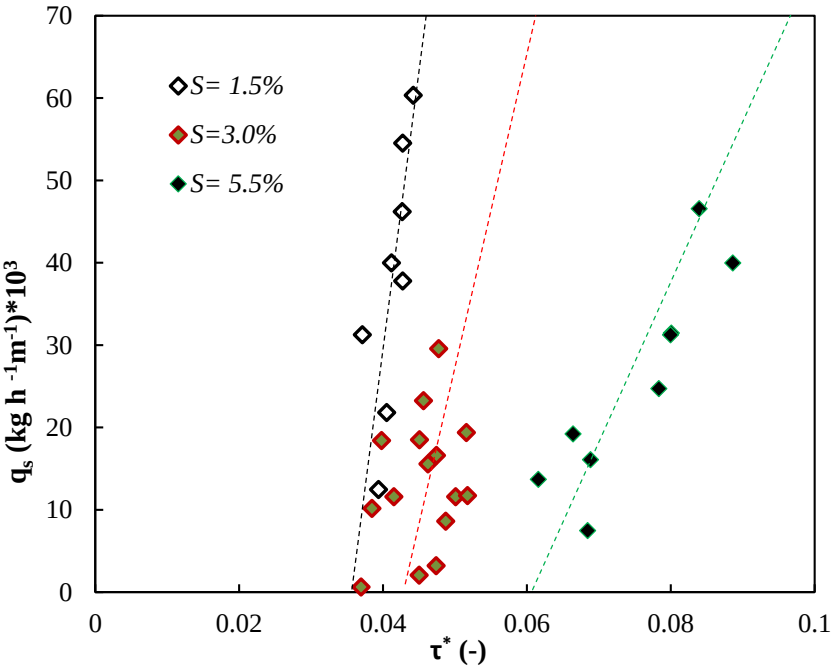

Figure 4.10 Block erosion transport capacity q_s (kgh^{-1}m^{-1}) as a function of dimensionless shear stress τ^* (-). Data are grouped by channel slope are given for each slope, in three different sizes

Figure 4.7 to Figure 4.10 illustrates the effect of channel slope on block erosion in packed riprap revetment. The block sizes did not have an influence on block erosion

transport whereas the channel slope has the dominant factor. Shear stress (τ) and dimensionless shear stress (τ^*) are plotted with the block erosion rate and the tests are clearly grouped and well aligned by slopes. Both parameters are higher on steeper channel slope as expected.

4.3.5 Riprap design equation considering large blocks individually placed

The review of previous works presented in 4.3.1 and 4.3.2 and a dimensional analysis indicate that numerous investigations have proposed a relation between a modified Froude number and the relative roughness to define the boundary between stable and unstable riprap bank protections.

The results of all 98 packed tests are used to evaluate relative roughness as a function of modified Froude number as:

$$Fr^* = \frac{V}{\sqrt{(S_B - 1)gh}} \tag{4.8}$$

Where V is velocity, S_B is specific gravity of the blocks, h is flow depth and g is gravitational acceleration. Results are grouped in two categories of stable and failed tests.

To define the best-fit line separating two categories of failed and stable tests, *transitional tests* were used from data set. Transitional tests are the ones that show the limit between stable and failed riprap and are empirically based. The discharge performed for a transitional test corresponds to the first discharge where total riprap failure occurs. This group of results acts as an envelope to show the boundary between failed and stable tests result.

Figure 4.11 presents the relative roughness as a function of modified Froude number (Fr^*) for failed, stable and transitional runs. The results are grouped well in three different channel slopes. The best-fit for these transitional tests with a linear least square algorithm are represented to separate failure runs from stable runs and present a very good agreement (R^2 = 0.92). The predictor, a confidence interval of 95% upper and lower limits and the prediction interval for the same limits are represented in Figure 4.11 as well.

The functional relation based on linear regression is defined as:

(4.9)

$$\frac{D_{50}}{h} = 0.18\frac{V}{\sqrt{((S_B - 1)gh)}} + 0.04$$

By applying equation (4.9), the mean size of riprap can be estimated for the range of application defined by the experimental setup and procedure herein presented. This equation is only valid for supercritical flow as all the tests were performed in a supercritical flow condition (only 4 tests of 98 experiments were in critical discharge with Froude number around 1 and for the lower channel slope).

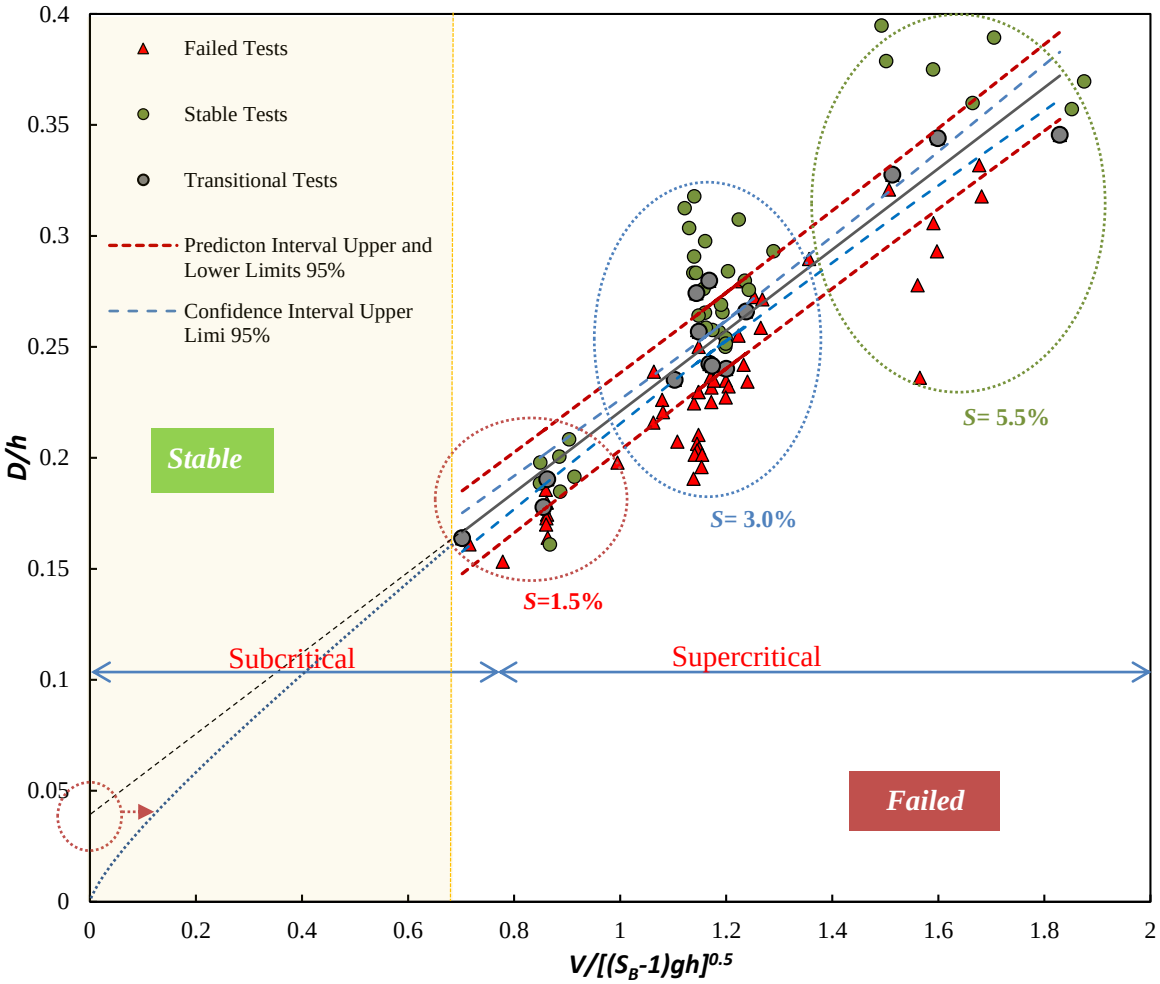

Figure 4.11 Relative roughness as a function of modified Froude number. Comparison of failed, stable and transitional tests in all sizes channel slopes and riprap bank slopes

The lack of data in the subcritical area does not let to generalize this linear relationship for the lower right hand side corner of the graphic in Figure 4.11. The analysis can be simplified since V becomes equal to zero, the modified Froude number limit goes

to zero and the limit of relative roughness gets close to zero. Therefore, the constant value of equation (4.9) could be eliminated and trend line changes to equation (4.10) with $R^2 = 0.88$.

$$\frac{D_{50}}{h} = 0.21 \frac{V}{\sqrt{((S_B - 1)gh)}} \tag{4.10}$$

4.3.5.1 Validation of equation by Logistic Classification

In statistics, logistic regression is a regression model while the dependent variable can be classified. The logistic classification model is used to predict a binary answer founded on one or more forecaster, making it a probabilistic categorization model in the frame of machine learning.

Logistic regression calculates the relationship between the dependent variable and one or more independent variables by approximating probabilities by means of a logistic function. The predicted values are probabilities and are therefore restricted to [0,1] by the logistic distribution function since logistic regression foresees the probability of particular results.

This logistic classification applied to the data set to validate the linear relation of transitional tests. The result is presented in Figure 4.12 the relative roughness as a function of modified Froude number by logistic classification of failed and stable tests. The equation given by this model is very close to regression achieved in equation (4.9). Figure 4.12 illustrates the probability of failure based on classifying the failed and stable test. Using this application has the advantage of obtaining the failure probability as a confident probabilistic approach.

Other machine learning method for classification such as Supervised Vector Machine (SVM) are applied. However, the results were not applicable because the lack of data. Logistic classification algorithm had accurate result, though.

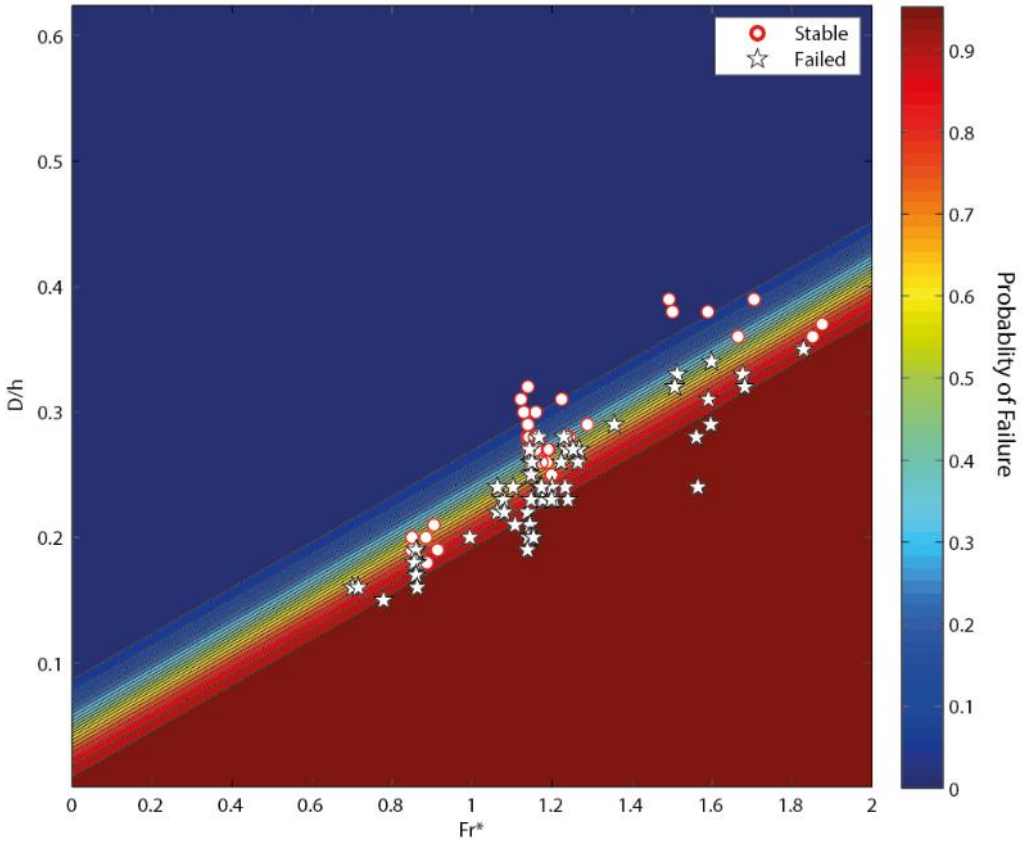

Figure 4.12 Relative roughness as a function of modified Froude number using a logistic classification of failed and stable tests

4.3.5.2 Confusion matrix

In the field of machine learning a confusion matrix, also known as an error matrix, is a explicit table design that gives a visualization of an algorithm performance, classically a supervised learning one. Each column of the matrix signifies the values in a predicted class while each row represents the instances in measured class.

In predictive analytics, a table of confusion is a table with two rows and two columns that reports the number of false positives, false negatives, true positives, and true negatives. This gives more detailed assessment than the ordinary quantity of correct deductions (accuracy).

By applying the confusion matrix for the result of logistic classification presented in Figure 4.12 a good agreement of 79% of accepted and correct classification is found.

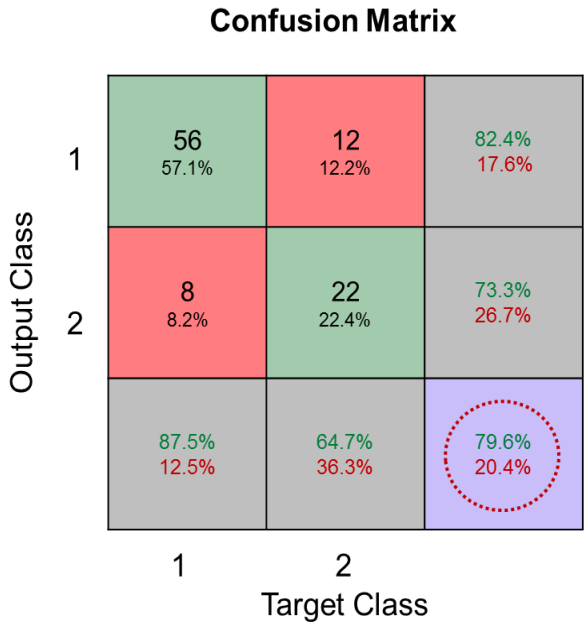

Figure 4.13 Confusion matrixes of logistic classification in relative roughness as a function of modified Froude Number

4.3.6 Comparison with existing formula

In Figure 4.11 relative roughness defined as a function of modified Froude number and a linear least square solver gave a relationship to predict the best size of riprap. Herein, the comparison of the 98 tests with four existing formula of riprap design as HDS 6, CABS, HEC-11 and EM-1601 can be seen in Figure 4.14. It is shown that the grouped data related to lower slope of S = 0.015 are relatively close to the existing formula. However, as far as the channel slope increases, the results show higher discrepancies between the existing relationships and the empirical results of this study. Therefore, the effect of compression is more obvious for the steeper channel, while, in less inclined channels, the results are adapted mostly to HEC-11, CABS, and EM-1601.

Two different equations for classifying failed and packed are defined from Figure 4.14; one is the linear presented before, and the other corresponds to a power law regression. Both equations are plotted and compared. The power law regression used to predict the boundary between stable and non-stable conditions, with R^2 = 0.93 is presented below:

$$\frac{D_{50}}{h} = 0.22 \left(\frac{V}{\sqrt{\left((S_B - 1)gh\right)}}\right)^{0.88} \tag{4.11}$$

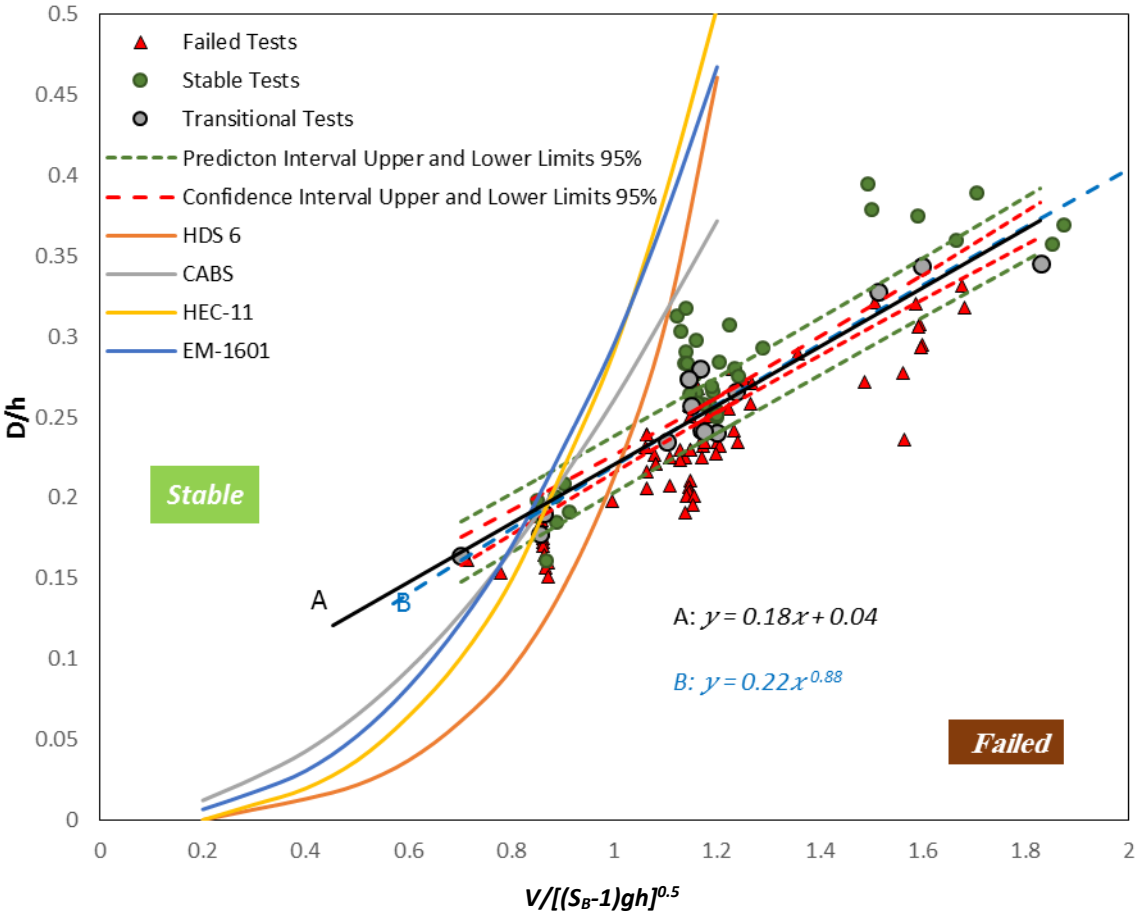

Figure 4.14 Comparison of existing formulae and the packed tests

This power law equation exhibits the same pattern of the existing formulae resulted in equations 4.3 to 4.6.

For the transitional test, the estimation results based on equation 4.9 and 4.12 are compared to the measured data in Figure 4.15 based on linear and power law regression respectively. The scatter shows quite the same for both regressions.

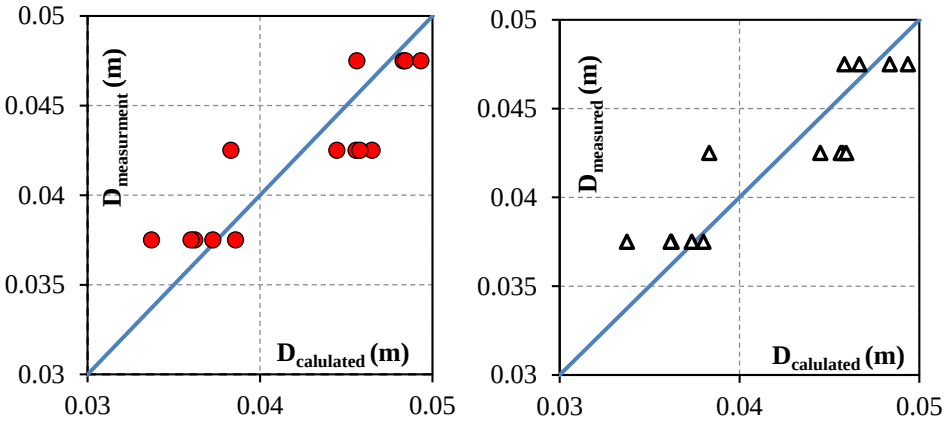

Figure 4.15 Block size measurement versus calculated in a linear (left) and power law (right) regression

4.3.7 Bank slope effect

As explained in detail in chapter 2, the bank slope of riprap has a significant effect on the stability.

$$D_{50} = 0.22 C_f \, h\left(\frac{V}{\sqrt{((S_B - 1)gh)}}\right)^{0.88} \tag{4.12}$$

$$C = 0.236 \left[\frac{tan(\alpha)}{tan(\varphi)}\right]^{0.2}, R^2 = 0.94 \tag{4.13}$$

$$C_f = \frac{C}{0.22} \tag{4.14}$$

Table 4.1 Bank slope coefficient description

Bank Slope (α)	C	C_f	R^2	Exponent	C (K1) (HEC11)	C (K2) (Maynord)
40°	0.236	1.07	-	0.89	0.296	0.30
35°	0.228	1.04	0.94	0.88	0.2601	0.28
31°	0.217	0.99	0.91	0.88	0.2322	0.26
27°	0.215	0.97	0.97	0.88	0.2022	0.23

To define this effect as a coefficient, the results of experiments in different block sizes and angle of repose analysed and presented in equations (4.12) to (4.14); were α is the riprap bank slope and φ (= 40°) is the angle of repose of the blocks. Table 4.1 presents the calculated bank slope coefficients on the experiments results and comparison with these coefficients in HEC-11 and Maynord's equations. The results revealed that by increasing the bank slope the C_f increases and the size of the blocks should be greater to be resistant against the flood.

4.4 Conclusion

This study addresses the sizing of large block riprap built in mountain rivers with the minimum possible spaces among the blocks. It specifically deals with the diameter of the riprap blocks *D*, longitudinal channel slope *S*, bank slope of the riprap and hydraulic conditions. The stability of packed riprap is evaluated and analyzed through a dataset of 98 experiments carried out with varying flume slopes, bank slope and size of the blocks. Thirty-four dumped riprap laboratory tests are also performed and compared with existing methods of riprap design.

By comparing the dumped riprap tests with existing methods the results showed agreements with equations of HEC-11 and EM-1601 considering the bank slope effect presented correctly regarding the boundary between stable or failed condition. However, the literature equations overestimated the size of blocks in some of the tests performed for dumped riprap.

Regarding the erosion rate, under the same hydraulic conditions, the packed block tests showed more stability, less block transport, remaining in the stable condition or showing a delay in failure. The channel slope *S* as a design parameter showed the strongest impact on the block erosion rate. However, it is also clearly shown that the block erosion decreases by compressing riprap according to the extra support among the blocks when they are packed.

A functional relation of the relative roughness and the modified Froude number is proposed to define the boundary between stability and failure providing the minimum size of the stable blocks. This relationship suggests smaller block sizes for the stable condition in packed block riprap, when comparing with dumped material, and can be applied to re-evaluate the stability of existing packed riprap facings.

Another functional relation is also analyzed to define the block size based on dimensionless shear stress, channel slope and modified Froude number. These equations which are developed to calculate the minimum block size for a stable riverbank riprap are validated by logistic classification model comparing to the experimental transition condition.

Chapter 5

Time-based Failure Analysis of Packed Riverbank Riprap

This chapter is based on a time dependent failure analysis of the packed riprap experiments. A characteristic time to failure is defined for prediction of the time of riprap failure as a function of several variables. The prediction model applied for the stable tests as examples.

Abstract

Riprap is frequently used as riverbank protection against lateral erosion. Several methods are developed for riprap design. However, they usually refer to dumped medium size blocks. Large blocks are used when more stability is required, being placed individually by a machine instead of simply dumped. Such arrangement generates additional resistance against flow erosion since the space between the blocks is minimized, and the interlocking is increased. The behavior of the latter protection was rarely studied for alpine river conditions. Therefore, an experimental investigation was carried out focusing on the stability of such packed riprap as river bank protection using a 10 m long and 1.5 m wide flume with a rough fixed bed. Riprap was reproduced with uniform crushed stones with three block sizes namely D_{50} = 0.037, 0.042 and 0.047 m. The tests were conducted on streamwise bed slopes of S = 0.015, 0.03 and 0.055, under supercritical flow conditions. Riprap stability was studied for a constant bank slope of 3.5V-5H (35°). A time-based analysis of failure was carried out where relationships among time to failure, shear velocity, and dimensionless bed shear stress were established. The result of 45 tests reveals that, for a given unit discharge, the rate of block erosion is significantly reduced if increasing the block size of the riprap. The time to failure also depends strongly on the longitudinal slope and the size of the blocks. An empirical prediction of riprap failure time was developed for a certain flood, which allows estimating the riprap failure time under specific conditions.

5.1 Introduction

Riprap is the most widely applied measure to protect river banks because it is flexible, long-lasting, easily constructed and natural in appearance (Schleiss, 1998). The stability of riprap is mainly determined by a combination of the submerged weight and the interlocking forces between adjacent blocks. Several equations were developed to predict the riprap stability considering the block size and the gradation, the thickness and the characteristics of an underneath filter (Stevens et al., 1976; Maynord et al., 1989; Escarameia and May, 1995).

There are two main approaches to design riprap (Recking and Pitlick, 2013); one is taking shear stress into account, and the other is defining a permissible velocity. Both are

based on Shields and Isbash equations respectively. Both approaches predict the behavior of blocks being exposed to turbulent flow. They used either critical shear stress or critical velocity, which has been referenced widely despite differences in the experimental methods (Maynord et al., 1989; Maynord and Neil, 2008).

Stevens et al. (1976) introduced a method based on a safety factor related to the stability of individual blocks in the riprap. They assumed that one block is stable if the different forces causing a possible displacement are below the reaction force resulting from the submerged weight. Wittler and Abt (1988) completed the study of Stevens et al. (1976), adding frictional and contact forces from adjacent blocks. Froehlich and Benson (1996) worked on different angles of repose in order to show the role of the bank slope effect on riprap stability. They proposed a "particle angle of initial yield" which was introduced earlier by Straub (1953), Grace et al. (1973), and Reese (1984). Brown and Clyde (1989) used the Manning-Strickler equation combined with the Shields relation to develop an equation for sizing stable blocks. Escarameia and May (1992) presented an equation for the design of riverbank ripraps and gabion mattresses. Stability of dumped riprap was also studied by Froehlich (2011) regarding the protection of banks from erosive forces. This evaluation was based on the ratio of static moments of resisting and provoking overturning. This ratio results in a safety factor of block overturning that indicates the potential for riprap failure. Stevens et al. (1984), Ulrich (1987) and Froehlich (2011) all considered the submerged weight of the blocks as the only resisting force. Abt et al. (2008) studied the effect of round-shaped riprap stability subjected to overtopping flow. Probabilistic procedures for the design of riverbank riprap were developed by Li et al. (1976), PIANC (1987), and later by Froehlich and Benson (1996). They describe the combination of different mechanisms including the persistence of hydrodynamic actions, which represents one of the advantages of these methods in the risk-based design procedure.

Several manuals give guidelines for the general application of dumped block riprap. The latter manual of Centre for Civil Engineering Research and Code (CUR, 1995) includes an equation developed by Pilarczyk (1990) for the riprap stability, which considers strengthening and destabilizing forces. The U.S. Army Corps of Engineers Manual (USACE, 1994) showed a method for design riprap in channels and rivers based on different coefficients concerning vertical velocity distribution, incipient failure, and

riprap thickness. This method was mostly based on Maynord's formula proposed in 1989 (USACE, 1994).

Most of these design methods are limited to dumped and medium size blocks. The incipient motion of particles is used as the failure criterion (De Almeida and Martin-Vide, 2009). However, if large and heavy blocks are required for stability reasons, they have to be placed individually by machines because of their weight. Consequently, for such construction method the design used for a dumped riprap become conservative.

Riprap failure occurs through different mechanisms. According to Lagasse et al. (2006), riprap failure modes are identified as (1) direct block erosion, (2) translational slide, (3) slump failure, and (4) side-slope failure. Direct block erosion started by flowing water is the most common mechanism. Most of the riprap design methods have been developed based on the failure criterion that considers the first movement of an individual block. Some other authors, such as Maynord (1989), proposed the start of the exposure of the filter underneath the riprap to the flow as failure criteria. This may cause other mechanism called translational slide or slump in the presence of multi-layers riprap (Jafarnejad et al., 2012).

In the present study, the temporal evolution of the riprap protection failure with well-positioned blocks was investigated. Particular attention was given to the influence of time or flood duration, during which blocks remain still stable. One approach to consider the time is to treat riprap behavior as a transport problem by defining maximum allowable transport rates. This approach is acceptable if multiple layers of material are considered (Maynord et al., 1987). If riprap is built with one single layer, the use of this approach may be questionable.

The erosion of one single block is hardly the reason for a total failure of a riprap with large and packed blocks placed individually by machines, mainly due to the interaction and support of packed and restablished blocks. Failure happens if a group of blocks slides and provokes an instability of the river banks. In the present study, the total collapse of all blocks in a section over the whole bank height is considered as failure. This failure is because of slumping or sliding down of riprap from toe of the embankment and full exposure of the filter to the flowing water. This situation causes bank instability and

consequently a downstream or upstream continuation of the riprap failure and the collapse of the bank.

Herein, the effect of the large block arrangement (with varying block sizes) on the stability of riverbanks is analyzed. The blocks are individually placed as riprap for various streamwise channel slopes. The present work includes 45 experiments. The analysis focused mainly on the characteristic time to failure and relevant hydraulic parameters for failure.

5.2 Experimental procedures

The goal of this part of study is to evaluate the resistance of a river bank riprap, consisting of individually placed and packed large blocks, subjected to hydrodynamic forces. By varying the block size and streamwise channel slope, 45 experiments were conducted to analyze the effect of the block size of the riprap on its stability. As explained in chapter 3, the laboratory tests were carried out in a tilting flume with a trapezoidal section. The setup of the flume is shown in Figure 5.1.

The longitudinal slopes of flume for these series of tests were set to S = 1.5%, 3% and 5.5%. The transversal riprap bank slope was fixed at 3.5V-5H (35°). The used riprap blocks used consisted of uniform crushed limestones, with a specific density of S_B =2.65. Three different equivalent average block sizes D = 0.037, 0.042 and 0.047 m were tested individually. Ahmed (1987) and Wittler and Abt (1990) reported that a riprap with a uniform gradation (when expecting similar D_{50}) tends to be globally more stable. The blocks were then uniformly selected and applied in the experiments. Froehlich (2011) conducted tests with various block sizes (including those used herein), considering crushed material. Thus, the angle of repose of blocks of 40 to 41 degrees can be assumed as based on Froehlich experiments (Froehlich, 2011).

Figure 5.1 Photo of the experimental flume, streamwise view

Blocks were packed and placed on a wide grain size distribution representing the filter and river bank material. In order to simulate natural hydraulic roughness conditions, the roughness of the channel bed was imposed using the same material glued to the channel bed as for the filter (Table 3.3).

The distinction between dumped and packed set-up was based on porosity measurements. Preliminary tests were performed to obtain the air volume in a defined dumped or packed riprap volume. Table 3.2 shows the porosity (n_p) of these tests, as well as the averaged values per block size and construction type. When packed porosity reduced by 2% for D_{50} = 0.037 m, by 5% for D_{50} = 0.042 m, and by 10% for D_{50} = 0.047 m when compared dumped riprap. The interlocking forces increase as the air volume between blocks reduces since the blocks have a closer arrangement. The porosity of the riprap in the experiments by Maynord and Abt (Maynord et al., 1989 and Abt et al., 1998) was 44% to 46%, with limestones blocks D_{50} = 0.025 m and D_{50} = 0.051 m similar to the present blocks if dumped.

Based on preliminary tests and typical flood peak durations in mountain rivers the maximum duration of the experiments was set to 180 minutes. The corresponding prototype time is important for the analysis of the results since it represents the expected maximum duration of the flood peak assuming a constant mean discharge, which may

cause the riprap failure. The time scale of a physical model based on the Froude similarity is given as:

$$\lambda_T = \sqrt{\frac{L_p}{L_m}} = \frac{T_p}{T_m} \tag{5.1}$$

where T represents the time, L a length, and p and m are prototype and model, respectively. Considering a geometrical scale of the experimental set-up for typical alpine mountain rivers (for example Kleine Emme, Switzerland) of $L_P/L_m = 25$, and then a time scale, $\lambda_T = 5$, is achieved. Experimental tests lasting three hours are thus roughly equivalent to prototype flood peak durations of 15 hours, which largely covers the flood observed durations.

The experimental program was defined in order to identify the time to failure and the limiting unit discharge causing failure. Lower discharges could cause direct block erosion during the tests but not lead to full failure of the riprap. For the fixed channel slopes, supercritical flow conditions ($1.09 < Fr < 1.89$) occurred for all discharges. The discharge was increased subsequently (for subsequent test) until failure occurred, providing the failure discharge (Table 5.1). Flow depths were measured by ultrasonic probes with a precision of ±0.5 mm at four different positions located at each 2 m along the channel axis. They were all transversally located at the center. The first 6 m of the riprap from upstream was fixed on mortar, keeping, however, the same roughness, to avoid an influence of the model inlet.

The riprap erosion rate was measured with a one-minute frequency by tracking and counting the number of eroded blocks, observed by three cameras. Furthermore, the eroded blocks were collected and weighed in a sediment trap at the downstream channel end to validate the total erosion. Single blocks eroded during the start of the tests (< 2 min) were not considered for the calculation of the erosion rate. Moreover, the results are grounded on the part of the flume between 6.5 m and 9.5 m where constant flow depth (roughly uniform flow) occurred. Blocks being eroded outside of that zone were excluded.

The detailed parameters of the experiments are listed in Tables 5.1. Experiments were divided into three groups I to III. Each group includes a different block size

(D_{50} = 0.037, 0.042 and 0.047 m, respectively). The riprap consisted of one single layer, and its thickness is accordingly D_{50}. Tests were run until total failure occurred but with a maximum duration of 180 minutes. Figure 5.2 shows the set-up before and after three different tests. Eroded parts of the riprap and the failed area after the experiment are illustrated in figure 5.2b. In Figure 5.2b, direct block erosion is visible along the toe of the riprap. At the model end, total riprap failure over the whole bank height can be seen.

5.3 Results and discussion

The tests were divided into three groups, I, II and III corresponding to the block sizes used for the riprap (see Table 5.1). For each group, several unit discharges were tested. Some of them initiated failure while for other discharges no failure occurred during the maximum test duration of 180 minutes.

Protection for the channel bank was materialized with one layer of riprap blocks. Table 3 summarizes the hydraulic parameters of all 45 tests under analysis for the three different channel slopes, including unit discharge (q), water depth (h), size of the blocks (D_{50}), mean velocity (V_m, based on continuity), Froude number (Fr) and bed shear stress (τ) estimated considering uniform flow conditions. The time to failure (t_f) and the riprap condition after the end of the test (failed, *Yes*, or remained stable, *No*) are given as well.

Three examples of tests with an identical channel slope of S = 3% but different block sizes are shown in Figure 5.2, (tests 2, 10 and 17). During the test number 2, with the smallest size of the blocks (D_{50} = 0.037 m) and a unit discharge of q = 0.262 m^2s^{-1}, direct block erosion started right after launching the test. However, the total bank failure occurred only after 94 minutes. For the test 10 with a block size of D_{50} = 0.042 m and a unit discharge of q = 0.421 m^2s^{-1}, the total failure occurred after 121 minutes. It can be observed that the filter was fully exposed over the bank height in the failed sections, whereas the riprap remained stable upstream and downstream. For the test 12, with a block size of D_{50} = 0.042 m and a unit discharge of q = 0.442 m^2s^{-1}, the total failure occurred after only 14 minutes. A significant erosion at the toe of the riprap protection is observed in this case.

The time evolution of the cumulated number of eroded blocks for the different groups of experiments and a longitudinal slope of S = 3% is shown in Figure 5.3 (a to c)

(see Table 5.1). The total failure of a riprap that occurs at any channel section is indicated by an abrupt rise of the cumulative curve (inclination = ∞) corresponding to a sudden increase of the eroded block number.

Figure 5.3a shows the tests of the smallest blocks (group I) for six different discharges. It is observed, as expected, that the time to failure increases when the discharge decreases. Two of the tests in this group had a total failure and the failure discharge for this block size is between $q = 0.249$ m^2s^{-1} and $q = 0.262$ m^2s^{-1}, depending on the flood peak duration. The complete failure occurred after 94 minutes for $q = 0.262$ m^2s^{-1} and already after 62 minutes for the unit discharge of $q = 0.301$ m^2s^{-1}.

For medium size blocks (group II), the data of seven different tests is given in Figure 5.3b. The significant influence of increasing discharge at the time of total failure and the number of eroded blocks is evident. The first complete failure was observed for a discharge $q = 0.407$ m^2s^{-1} after 162 minutes. By increasing the unit discharge, total failure occurs much earlier.

For the largest blocks (group III, Figure 5.3c), the failure condition was reached only for the test with a discharge $q = 0.480$ m^2s^{-1}. Figure 5.3c indicates that larger blocks increase not only the failure discharge but also the time to failure. Thus, for similar unit discharge, the rate of block erosion reduces if the blocks become larger.

Table 5.2 represents the water level measurements in 3 different positions in the distance of 4, 6 and 8 meters from upstream of the channel. The error calculation with the average of 0.002 shows that the flow is quasi-uniform and velocity could be calculated based on continuity.

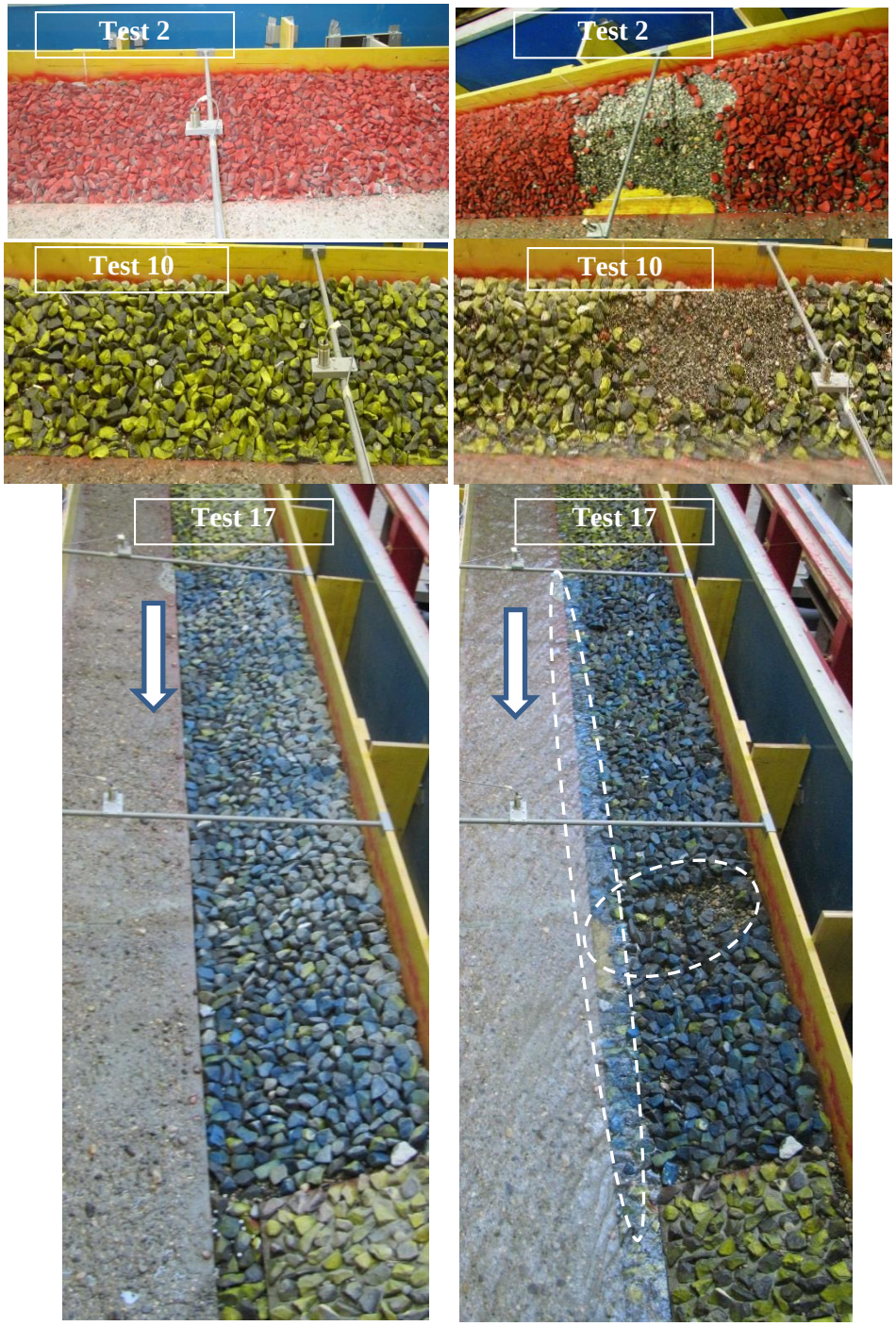

Figure 5.2 Riprap (a) before, and (b) after failure for tests 2 and 10 and 17 (according to Table 5.1)

Table 5.1 Characteristics and main results of the tests with three different longitudinal slopes

Test	Channel Slope	Group	D_{50} (m)	q (m^2s^{-1})	h (m)	v_m (m)	Fr (-)	τ (Pa)	t_f (min)	Failure (-)
1	3%	I	0.037	0.166	0.121	1.59	1.46	35.61	-	No
2				0.208	0.131	1.84	1.62	38.55	-	No
3				0.242	0.143	1.97	1.66	42.08	-	No
4				0.249	0.145	1.99	1.67	42.67	-	No
5				0.262	0.150	2.03	1.67	44.15	94	Yes
6				0.301	0.165	2.13	1.67	48.56	62	Yes
7		II	0.042	0.348	0.167	2.27	1.78	49.15	-	No
8				0.380	0.175	2.38	1.81	51.50	-	No
9				0.407	0.183	2.44	1.83	53.86	162	Yes
10				0.421	0.186	2.49	1.84	54.74	121	Yes
11				0.430	0.188	2.52	1.85	55.33	68	Yes
12				0.442	0.193	2.52	1.83	56.80	14	Yes
13				0.473	0.200	2.61	1.87	58.86	6	Yes
14		III	0.047	0.432	0.188	2.53	1.85	55.92	-	No
15				0.443	0.191	2.55	1.87	56.21	-	No
16				0.461	0.196	2.59	1.87	57.68	-	No
17				0.480	0.210	2.65	1.89	58.86	160	Yes
18	1.5%	I	0.037	0.287	0.181	1.510	1.10	21.22	-	No
19				0.303	0.197	1.540	1.11	21.43	172	Yes
20				0.314	0.202	1.554	1.10	21.85	87	Yes
21				0.330	0.209	1.582	1.11	22.40	43	Yes
22				0.346	0.215	1.607	1.11	22.94	9	Yes
23		II	0.042	0.387	0.220	1.580	1.09	23.67	-	No
24				0.402	0.239	1.682	1.10	24.88	143	Yes
25				0.423	0.246	1.718	1.11	25.44	123	Yes
26				0.433	0.250	1.730	1.11	25.75	63	Yes
27				0.458	0.259	1.767	1.11	26.45	6	Yes
28		III	0.047	0.432	0.252	1.714	1.09	25.91	-	No
29				0.452	0.259	1.745	1.10	26.45	134	Yes
30				0.472	0.266	1.774	1.10	26.99	95	Yes
31				0.482	0.270	1.784	1.10	27.30	71	Yes
32	5.5%	I	0.037	0.2022	0.100	2.391	2.03	60.13	-	No
33				0.2314	0.109	2.424	2.05	60.82	120	Yes
34				0.2552	0.117	2.463	2.04	62.89	42	Yes
35				0.2731	0.122	2.506	2.05	63.91	4	Yes
36		II	0.042	0.2602	0.121	2.15	2.00	51.71	-	No
37				0.2767	0.123	2.250	2.05	53.73	151	Yes
38				0.3315	0.139	2.385	2.04	59.43	55	Yes
39				0.3547	0.145	2.446	2.05	61.51	8	Yes
40				0.4287	0.163	2.630	2.08	67.61	2	Yes
41		III	0.047	0.310	0.135	2.53	1.85	55.92	-	No
42				0.3372	0.141	2.55	1.87	57.68	135	Yes
43				0.3466	0.143	2.59	1.87	58.86	111	Yes
44				0.3671	0.149	2.65	1.89	59.71	50	Yes
45				0.3809	0.152	2.68	1.9	55.92	5	Yes

Unit discharge q,, water depth h, diameter of blocks D, time of total failure t_f, mean velocity v_m, Froude number Fr and bed shear stress τ.

Table 5.2 Water level slope calculations and slope errors

Test	Channel slope	Group	D_{50} (m)	q (m^2s^{-1})	h at 4 m (m)	h at 6 m (m)	h at 8 m (m)	Water level slope *(-)*	Error *(-)*
1	3%	I	0.037	0.166	0.122	0.121	0.118	0.0310	0.001
2				0.208	0.131	0.131	0.128	0.0308	0.001
3				0.242	0.143	0.143	0.14	0.0308	0.001
4				0.249	0.145	0.145	0.141	0.0310	0.001
5				0.262	0.151	0.150	0.145	0.0315	0.002
6				0.301	0.166	0.165	0.16	0.0315	0.002
7		II	0.042	0.348	0.168	0.167	0.16	0.0320	0.002
8				0.380	0.176	0.175	0.168	0.0320	0.002
9				0.407	0.182	0.183	0.177	0.0313	0.001
10				0.421	0.187	0.186	0.179	0.0320	0.002
11				0.430	0.188	0.188	0.18	0.0320	0.002
12				0.442	0.195	0.193	0.186	0.0323	0.002
13				0.473	0.201	0.200	0.194	0.0318	0.002
14		III	0.047	0.432	0.189	0.188	0.183	0.0315	0.002
15				0.443	0.191	0.191	0.186	0.0313	0.001
16				0.461	0.197	0.196	0.19	0.0318	0.002
17				0.480	0.212	0.210	0.198	0.0335	0.004
18	1.5%	I	0.037	0.287	0.182	0.181	0.179	0.0158	0.001
19				0.303	0.197	0.197	0.195	0.0155	0.001
20				0.314	0.203	0.202	0.2	0.0158	0.001
21				0.330	0.21	0.209	0.206	0.0160	0.001
22				0.346	0.217	0.215	0.211	0.0165	0.002
23		II	0.042	0.387	0.22	0.220	0.218	0.0155	0.001
24				0.402	0.24	0.239	0.236	0.0160	0.001
25				0.423	0.246	0.246	0.243	0.0158	0.001
26				0.433	0.25	0.250	0.246	0.0160	0.001
27				0.458	0.26	0.259	0.255	0.0163	0.001
28		III	0.047	0.432	0.254	0.252	0.25	0.0160	0.001
29				0.452	0.261	0.259	0.253	0.0170	0.002
30				0.472	0.268	0.266	0.261	0.0168	0.002
31				0.482	0.273	0.270	0.267	0.0165	0.002
32	5.5%	I	0.037	0.2022	0.105	0.100	0.092	0.0583	0.003
33				0.2314	0.111	0.109	0.103	0.0570	0.002
34				0.2552	0.119	0.117	0.109	0.0575	0.003
35				0.2731	0.123	0.122	0.118	0.0563	0.001
36		II	0.042	0.2602	0.124	0.121	0.117	0.0568	0.002
37				0.2767	0.126	0.123	0.119	0.0568	0.002
38				0.3315	0.143	0.139	0.134	0.0573	0.002
39				0.3547	0.149	0.145	0.141	0.0570	0.002
40				0.4287	0.168	0.163	0.157	0.0578	0.003
41		III	0.047	0.310	0.138	0.135	0.131	0.0568	0.002
42				0.3372	0.142	0.141	0.136	0.0565	0.001
43				0.3466	0.146	0.143	0.139	0.0568	0.002
44				0.3671	0.151	0.149	0.144	0.0568	0.002
45				0.3809	0.155	0.152	0.148	0.0568	0.002

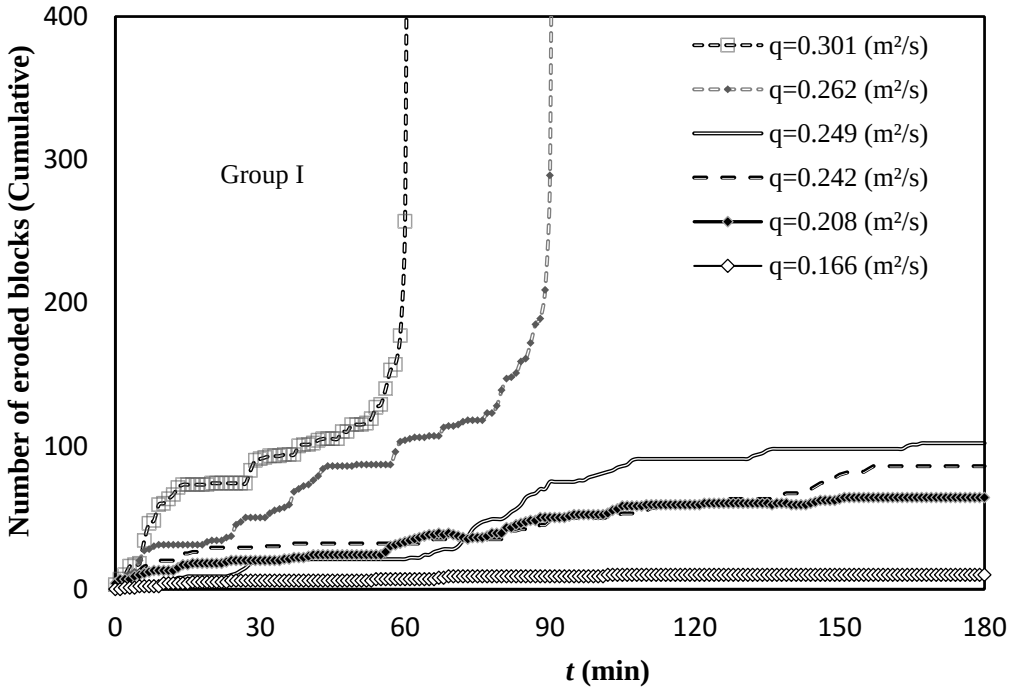
Number of eroded blocks (Cumulative)
400
300
200
100
0
Group I
q=0.301 (m²/s)
q=0.262 (m²/s)
q=0.249 (m²/s)
q=0.242 (m²/s)
q=0.208 (m²/s)
q=0.166 (m²/s)
0
30
60
90
120
150
180
t (min)

(a)

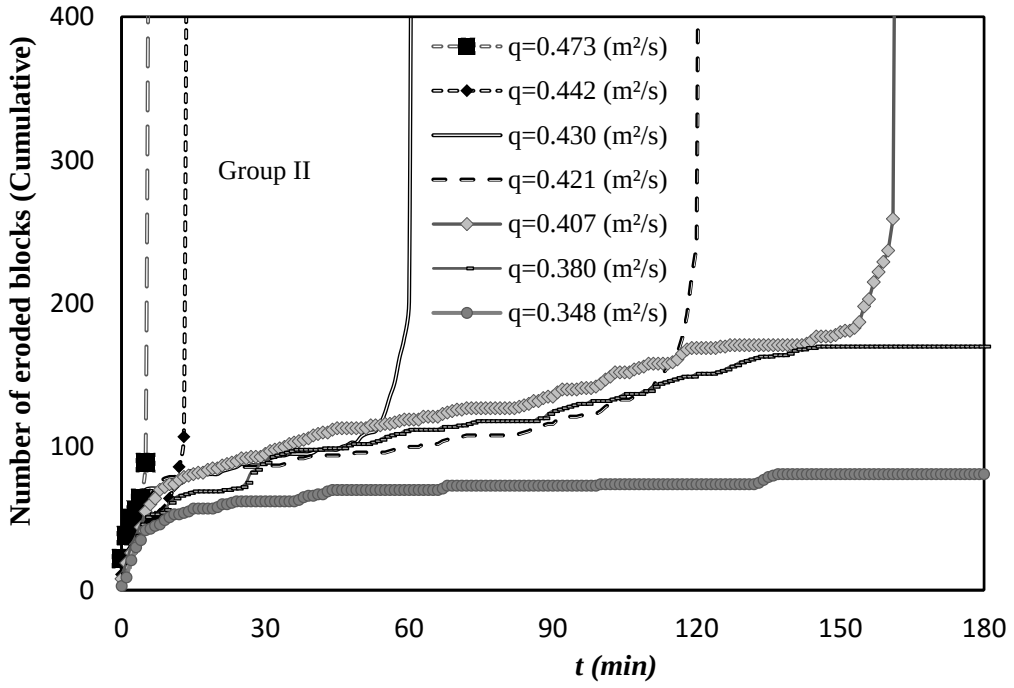
Number of eroded blocks (Cumulative)
400
300
200
100
0
Group II
q=0.473 (m²/s)
q=0.442 (m²/s)
q=0.430 (m²/s)
q=0.421 (m²/s)
q=0.407 (m²/s)
q=0.380 (m²/s)
q=0.348 (m²/s)
0
30
60
90
120
150
180
t (min)

(b)

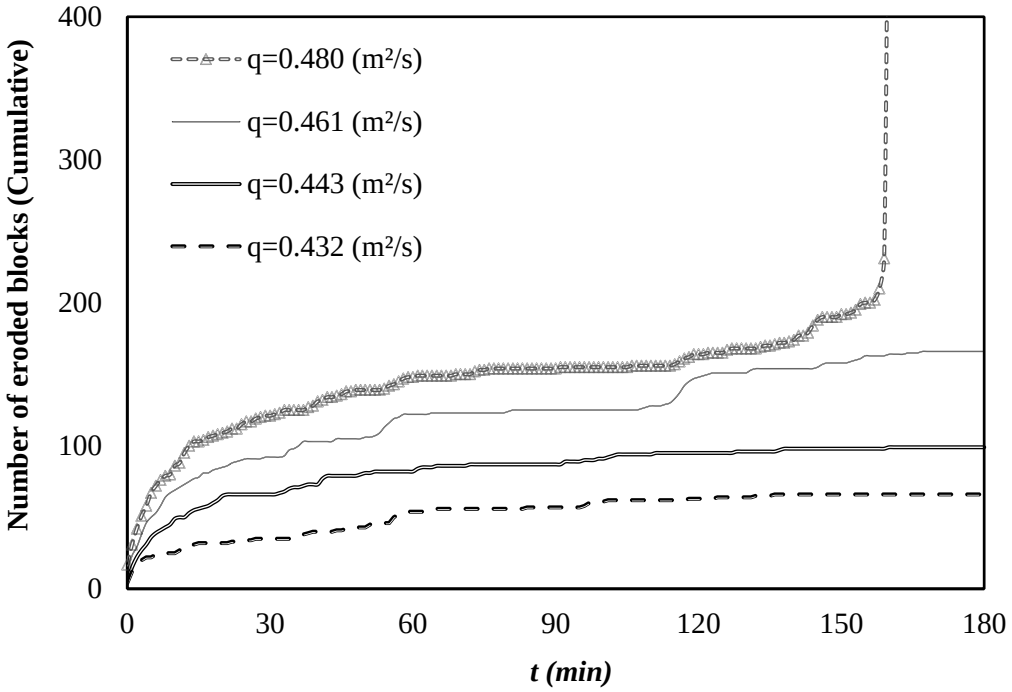

(c)

Figure 5.3 Time evolution of cumulative block erosion rate for different tests for a longitudinal channel slope of 3% with (a) D = 0.037 m (Group I), (b) D = 0.042 m (Group II) and (c) D = 0.047 m (Group III)

The dimensionless bed shear stress represents the balance of hydrodynamic forces acting on the riprap and the submerged weight of the blocks as:

$$\tau^* = \frac{\tau}{(S_B - 1)g\rho D} \tag{5.2}$$

where S_B is the specific gravity of blocks, g is the gravitational acceleration, D_{50} is the size of blocks, and ρ is water density. Bed shear stress, τ was calculated as:

$$\tau = \rho g R_h S \tag{5.3}$$

where R_h is the hydraulic radius and S is the channel slope.

In Figure 5.4, the dimensionless bed shear stress (Shields parameter) calculated according to relation (5.2) is compared with the time to failure which is normalized with the total time of the experiment, which is 180 minutes. The value of $t^* = \frac{t}{180} = 1.00$ corresponds to tests where failure was not observed within the experiments time framework. The results in Figure 5.4 show an overlap in terms of failure time for the slope

of S = 3%. It can be observed as well that a limit of the Shields parameter of 0.7 seems to exist after which the failure occurs.

In relation to the characteristic block diameter, a dimensionless time to failure T_D^* can be defined with the block size as length scale as follows:

$$T_D^* = \frac{t_f u^*}{D} \tag{5.4}$$

where u^* is:

$$u^* = \sqrt{\frac{\tau}{\rho}} \tag{5.5}$$

The friction velocity (shear velocity), considered as a velocity scale representative of the shear causing erosion and acting on the blocks of size D. In order to understand what influences the time to failure, the dimensionless bed shear stress was compared to the dimensionless time to failure T_D^* (Figure5.4).

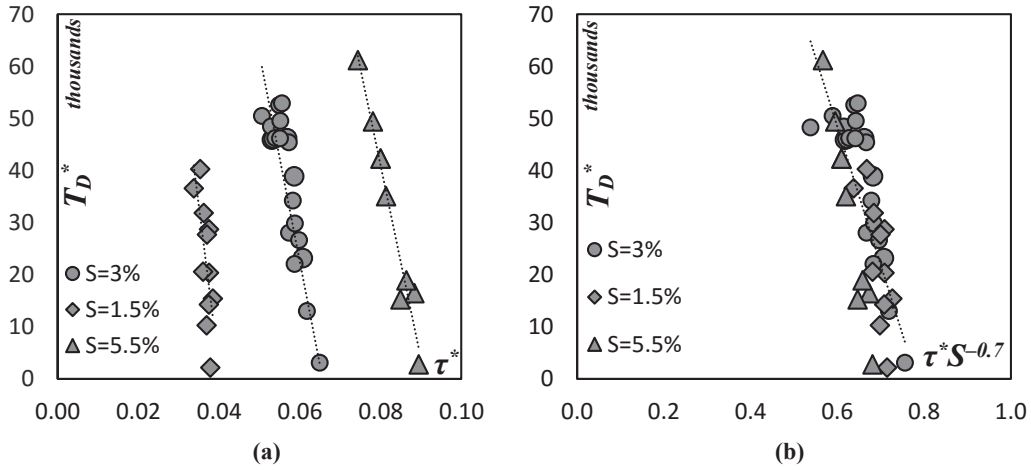

Figure 5.4 (a) Dimensionless failure time T_D^* as a function of dimensionless bed shear stress τ^*, grouped by slopes S = 1.5%, 3% and 5.5% for the tests encounter the failure. The dotted lines represent linear regressions made within the same slope. (b) Dimensionless failure time T_D^* as a function of the dimensionless bed shear stress ($\tau^* S^{-0.7}$). The dotted line corresponds to a linear regression of the data.

It can be seen in Figure 5.4 a that for a certain channel slope, the relationship between T_D^* and τ^* is linear with good agreement: $R^2 \approx 0.94$, 0.83 and 0.90 for S = 1.5%, 3% and 5.5% respectively, with R^2 as coefficient of determination. Nevertheless a small change in τ^*has very high effect on T_D^*, which diminishes with increasing slope. For each

slope group, the relationship between T_D^* and τ^* seems to be linear. Figure 5.4 also shows that the inclination of the linear relation between T_D^* and τ^* changes with S. Results confirm, as expected, that a higher bed shear stress is needed to generate the same characteristic time to failure.

Figure 5.4b shows the relation between T_D^* and the Shields parameter multiplying by the term $S^{-0.7}$. The linear regression shown in Figure 5.4b has a significant correlation coefficient of 0.60. In Figure 5.4 only the block size D was used as geometric scale to normalize the variables in the description of the time to failure. Dimensional analysis considerations indicate that, however, the time to failure may also be normalized using the flow depth h as geometric parameter:

$$T_h^* = \frac{t_f u^*}{h} \tag{5.6}$$

This normalization indicates that the flow depth scales with the shear stress action responsible for the block movement.

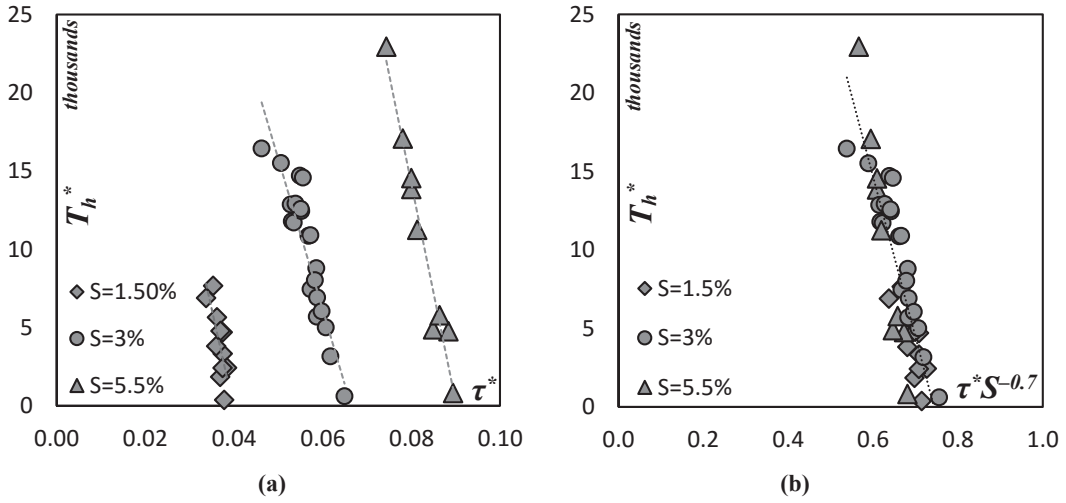

Figure 5.5 (a) Dimensionless failure time T_h^* as a function of dimensionless bed shear stress τ^*, grouped by slopes S = 1.5%, 3% and 5.5% for the tests encounter the failure. The dotted lines represent linear regressions made within the same slope.
(b) Dimensionless failure time (T_h^*) as a function of the dimensionless bed shear stress ($\tau^* S^{-0.7}$). The dotted line corresponds to a linear regression of the data.

Figure 5.5a shows the dimensionless time to failure T_h^* again as a function of τ^* for the three tested longitudinal slopes. There is still a good agreement for a linear relationship between T_h^* and τ^* ($R^2 \approx 0.85$, 0.83 and 0.96 S = 1.5%, 3% and 5.5%,

respectively). Figure 5.5b shows again that the time to failure normalized with the flow depth presents a good collapse as a function of Shields parameter multiplied by $S^{-0.7}$. Compared to the approach with T_h^*, this results in a better correlation coefficient of $R^2 = 0.78$ which indicates a stronger influence of the flow depth.

The time to failure (t_f) for tests which remained stable during the three hours tested is now predictable based on Figure 5.5b and on the parameters defined in relations (5.2) and (5.6). In Figure 5.6, the cumulative number of the eroded blocks is shown as a function of time normalized by the time to failure ($T^* = t/t_f$).

In the experiments where the failure occurred, the number of eroded blocks presents an asymptote for $T^* = 1$. In the stable experiments, data on the number of eroded blocks stop within the time range of $0 < T^* < 1$. For these experiments, the unit discharge is lower than the critical value for the occurrence of the failure. The range of block erosion in this figure shows that the number of eroded blocks are not increased drastically comparing to the predicted normalized time to failure. This means that total block erosion remains in a narrow range until the failure occurs, independent of the block size.

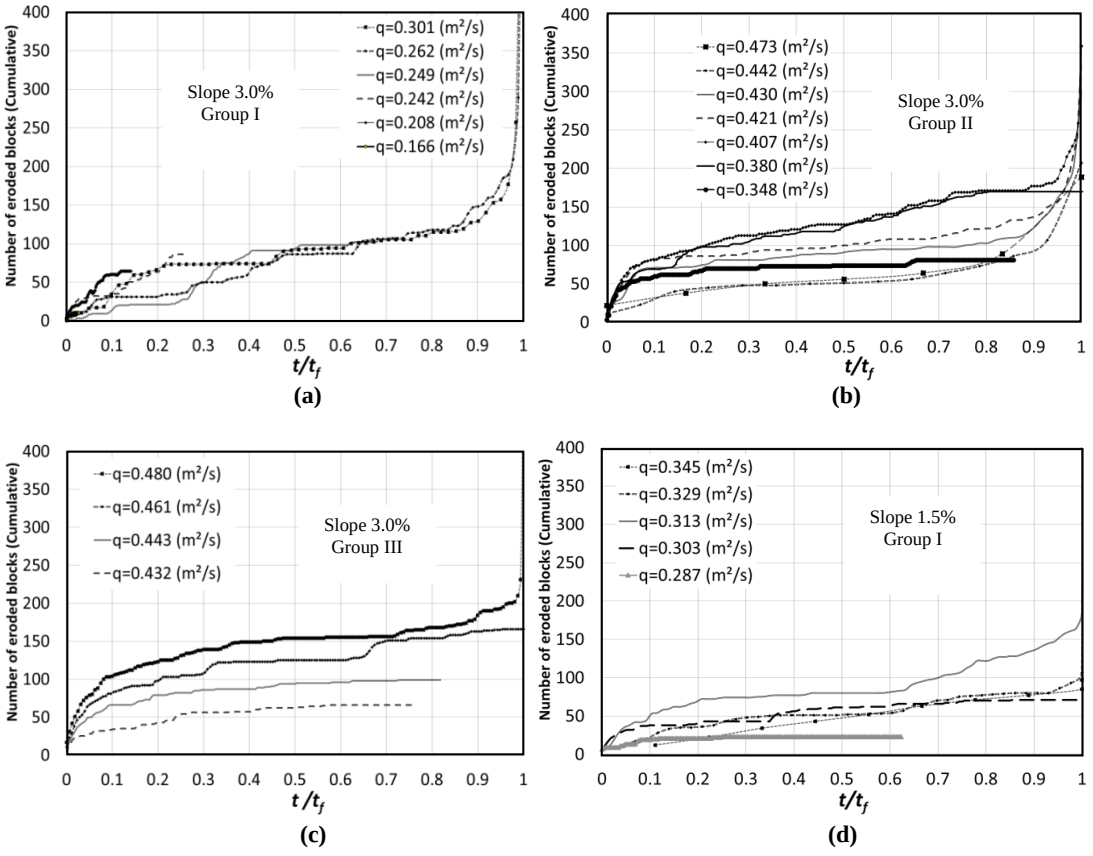

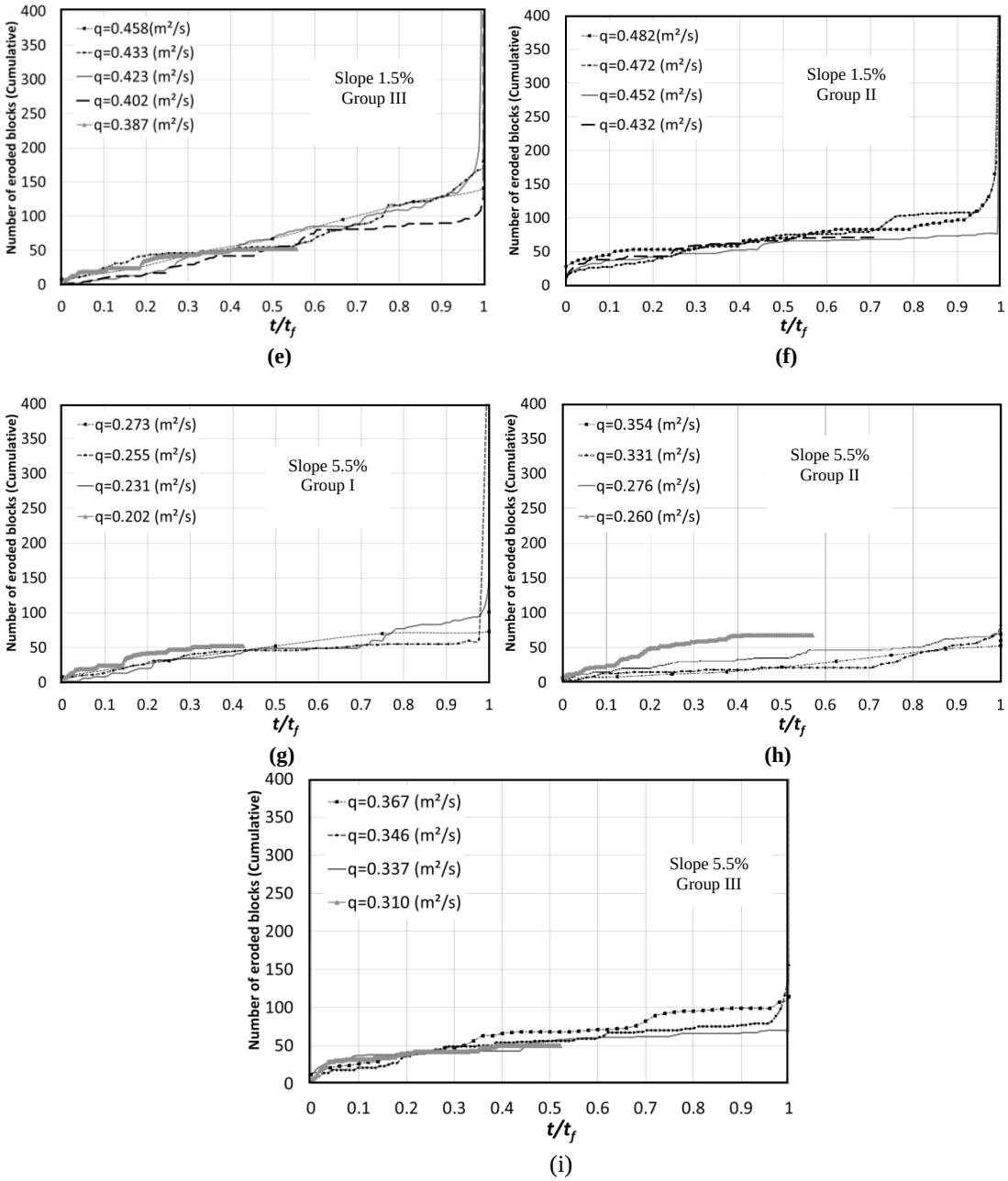

Figure 5.6 Relative failure time of cumulative block erosion rate for different tests: for the same longitudinal channel slope of 3% (a) with D = 0.037 m; (b) with D = 0.042 m; and (c) with D = 0.047 m, for the longitudinal channel slope of 1.5% (d) with D = 0.037 m; (e) with D = 0.042 m; and (f) with D=0.047 m and for the longitudinal channel slope of 5.5% (g) with D = 0.037 m; (h) with D = 0.042 m; and (i) with D = 0.047 m

The block erosion for the different experiments shown in Figure 5.6 remains in a similar pattern. An approximated model for the block erosion, bounded by the beginning of the hydrodynamics action and the failure of the riprap, may be established based on Figure 5.6. A fast erosion happens at the beginning of the experiment; then the rate of

erosion becomes roughly constant until near the failure time. The number of eroded blocks just before the time of failure increases asymptotically.

In Figure5.6a to 5.6c, the rate of time to failure is shown for the slope of 3% for three different block sizes. The cumulative number of eroded blocks for 90% of the normalized time are less than 200 for all block sizes. It can be seen that lower block sizes face to failure with lower unit discharges. Figure 5.6d to 5.6f also show the rate of time to failure for three different block sizes when the longitudinal channel slope is 1.5%. The cumulative number of eroded blocks for 90% of the normalized time are less than 150 for all block sizes. Figure 5.6g to 5.6i indicate the rate of time to failure for the slope of 5.5% also for three different block sizes. The cumulative number of eroded blocks for 90% of the normalized time are less than 100. The limits in the rate of erosion are higher for S=3% as compared to the other slopes. It should be noticed that the unit discharge in each group of tests increases with the larger block size.

5.4 Conclusion

The stability behavior of packed, well-positioned riverbank riprap consisting of one layer was experimentally analyzed herein, considering the influence of the block sizes, the specific discharge and river bed slope on the time to failure. Particular attention was given to the time of failure defined as the duration for which the riprap collapsed totally after beginning of the experiments. The experiments included three different longitudinal channel slopes of 1.5%, 3% and 5.5% and embankment slope of 3.5V-5H. The block sizes varied from 0.037 m to 0.047 m. A maximum three hours duration of the flume tests was established to cover roughly a 15 hours flood duration when taking into account a typical scale factor.

Classical stability criterion is typically limited to the steady boundary condition which means that the failure occurs at the time of the first movement as a direct block erosion. For packed riprap, the criterion of failure is linked to the time to failure. Sliding the riprap in a section and a complete failure occurs after a specific duration of block erosion. Thus, a time-dependent analysis of failure was implemented.

The results of this study indicates that the time to failure is dependent on the tested parameters as block size, channel slope, and specific discharge. The result also revealed

that the slope of the channel has a significant effect on the characteristic time to failure regardless the block size. In addition, not only the larger block sizes postponed the time to failure but also reduced the block erosion rate for a fixed longitudinal slope.

A clear relationship between the time to failure and the bed shear stress adimensionalized with the block size could be found. However, the best results were obtained using an approach of adimensionalizing the time to failure based on the flow depth. This empirical relationship gives the possibility of calculating the time to failure for the tests which remained stable. The results revealed that the range of erosion which is shown in the number of eroded blocks are not increased severely comparing to the predicted normalized time to failure. This means that total numbers of eroded block could be remained in a specific range until the failure occurs. The cumulative number of eroded blocks is distributed in a narrow band, independent from the block size.

This study can be utilized as a forecasting model for the time to failure of packed riprap used as river banks protection in the range of application corresponding to the experimental setup here described.

Chapter 6

Effect of a Second Layer on the Stability of Packed Riprap as Riverbank Protections

This Chapter analyses the effect of two layers of blocks on the stability of packed riprap comparing to one layer. A time based analysis is performed to clear this comparison and the results revealed that the second layer could reduce the size of the blocks up to 10%.

Abstract

This study addresses the effect of thickness on the stability of packed and compressed riprap as river bank protection. There are several methods to design riprap which are limited to dumped and medium size blocks. Nevertheless, an additional resistance against erosion can be achieved by individually placing blocks in one or several layers instead of dumping them arbitrarily. An experimental investigation has been performed to evaluate the stability of large blocks which are packed as a river bank protection in one and two layers. The influence of the riprap layering (e.g. riprap thickness) on the bank stability was thus studied by 49 series of tests. The investigation was performed in a 10 m long and 1.5 m wide tilting flume, with a rough fixed bed. Riprap median particle size was chosen as D_{50} = 0.037 m. Testing was conducted for longitudinal channel slopes 0.015, 0.030 and 0.055 and riprap side slopes of 27, 31, and 35 degrees. Supercritical flow conditions were considered, given the steep channel slope. The complete removal of the riprap in a section under a constant discharge was defined as the failure criterion. The results revealed that, in similar conditions, the second layer delays the time to failure. Nonetheless, block erosion rate was found to be increased in this latter situation. The analysis of riprap bank slope variation also indicated that in the same longitudinal channel slope, the second layer has more stabilizing role when the angle of the protection layer is closer to the angle of repose of the blocks.

6.1 Introduction

The existing studies mainly define the riprap sizing but rarely focus on the thickness of the riprap and the number of block layers respectively. Maynord (1988) performed a limited number of experiments to evaluate the thickness effect and reported it as stability criteria. For relatively low-turbulence applications such as riverbank protections USACE (1994) specifies a minimum thickness of D_{100} or 1.5 D_{50} whichever is greater. Stability tests of Abt et al. (1988) and Maynord (1988) revealed that any additional thickness above these minima results in rising the stability. Consequently, a larger thickness of a smaller gradation may sometimes provide equivalent stability. The increase in stability with thickness is more substantial and for very wide block gradations but relatively low for uniform gradations (Maynord and Neil, 2008). The improvement in stability with increasing thickness results can be explained by the fact that more material is available

which can move to damaged area and cover it again. Thus, more energy should be dissipated to expose the filter underlying the blocks (Simons, 1995).

Existing design methods are limited to dumped blocks, and the first movement of particles is used as failure criterion (De Almeida and Martín-Vide, 2009). However, if large and dense blocks are needed for stability reasons in mountain rivers, they must be positioned individually due to their high weight. Based on hydraulic model studies for several flood protection projects, Schleiss (1998) suggests to use a critical shear stress of $\theta_{cr} = 0.1$ instead of Shields critical shear stress usually taken as 0.047. Therefore, in large packed blocks as rock ripraps, the erosion of one single block may not cause a total failure due to the added support of packed blocks. Failure happens when a group of blocks slips and exposes a large of the river bank to the flow. This kind of failure included the observation of lateral breakdown of the blocks on the riverbank slope (as a slide or slump) is identified as failure criterion in this investigation.

Figure 6.1 shows a riprap under construction in two layers where large blocks are separately placed on a geo-textile. Furthermore, the toe blocks are lined together by cables. This research analysis the influence of a second layer of these large blocks individually placed as riprap. However, one of the issues which not yet fully known in the design of riprap protection is the influence of time (flow duration) on failure (Jafarnejad et al. 2013).

Figure 6.1 Riprap built of individually placed large blocks in two layers on Reuss river in Switzerland (by A.J. Schleiss, 1988)

Therefore, the effect of thickness on riprap installation on changing the time to failure is investigated herein through flume experiments by considering the dynamic behavior of packed large blocks. The study presented in this chapter is based on the result of forty-nine series of tests performed to evaluate the failure process. The analysis focuses mainly on the characteristic time to failure and on the critical hydraulic parameters for the occurrence of the complete failure. In the end, relative roughness as a function of modified Froude is analyzed and compared to the finding in chapter 6.4.

6.2 Experimental setup and procedure

The main goal of this study is to evaluate the role of the second layer in the resistance of river bank riprap protection, built by individually positioned large blocks, due to hydrodynamic forces. In this part the experimental setup, experimental design and procedure, the preliminary and systematic tests are explained.

Forty-nine systematic experiments were performed to analyze the impact of thickness on the stability of packed riprap. The tests were conducted in one layer, and two layers of the same block size. These laboratory tests were applied in a straight 10 m long, 1.5 m wide flume with a trapezoidal section. Water in the channel was supplied by the internal closed pumping circuit of the laboratory. A schematic sketch of the longitudinal side view and cross section of the setup can be seen in Figure 6.2.

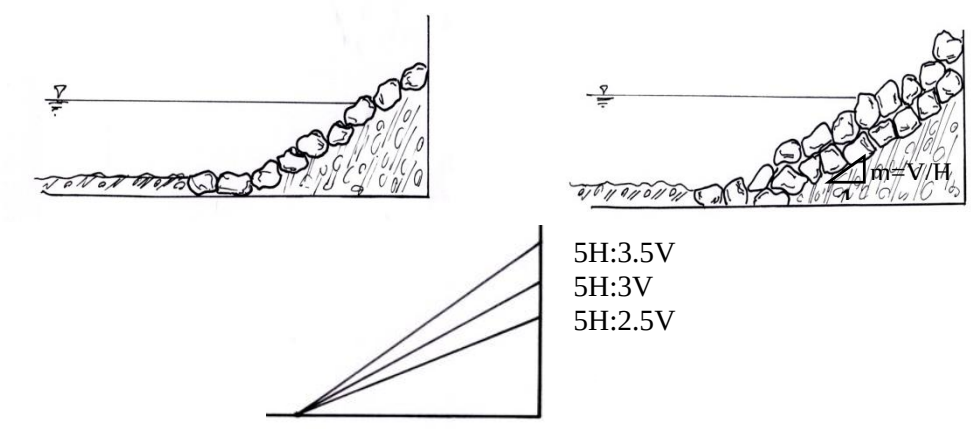

Figure 6.2 Sketch of cross-section view of the experimental flume with schematic one and two layers of blocks (units in mm)

The experiments were performed for a longitudinal slope of the flume as 1.5% and 3% and 5.5%. The transversal riprap bank slopes were varied as 2.5V-5H (27°), 3V-5H (31°), and 3.5V-5H (35°). Studied riprap material consists uniform crushed stones with block sizes of D_{50} = 0.37m. Blocks were placed individually in a packed way over a wide grain size distribution filter. In order to simulate natural hydraulic conditions, the roughness of the natural river bed was reproduced with the same material of the filter (cf. Table 3.3), fixed on the bed of the channel.

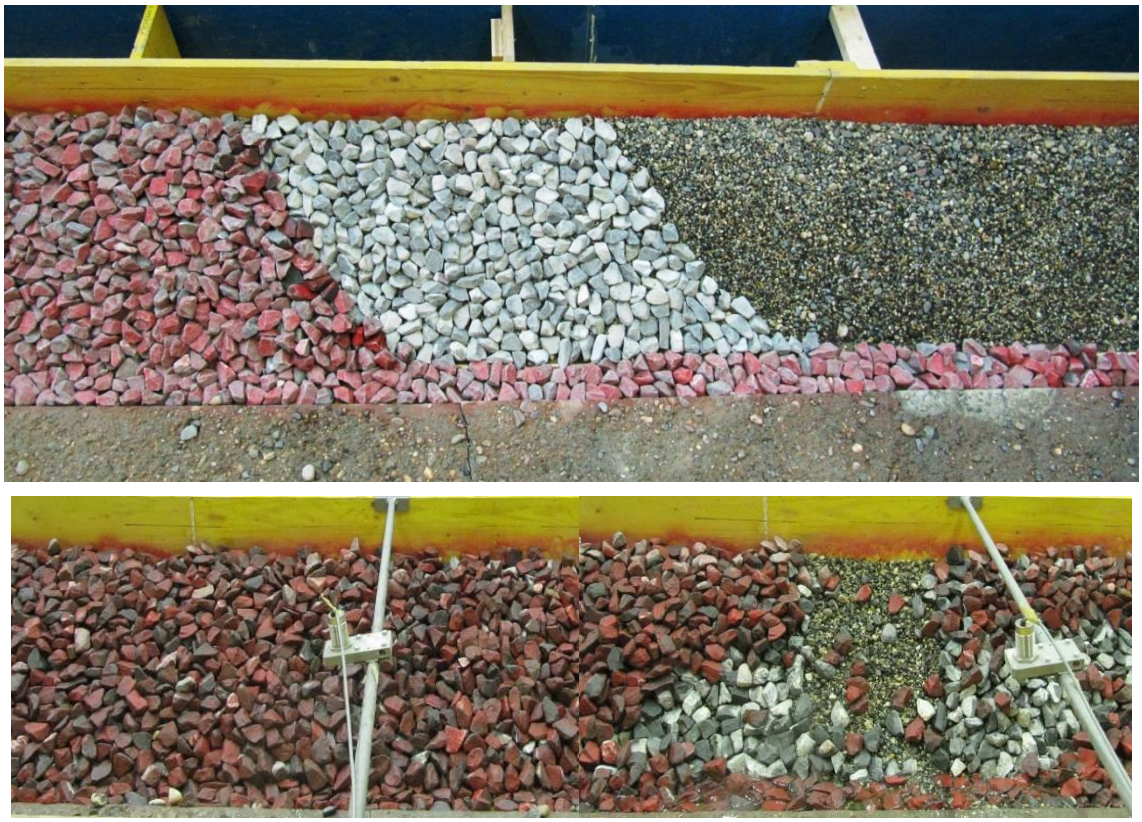

Figure 6.3 The experimental set up of test 8 before (left) and after (right) the test with the complete failure of the riprap protection (see Table 6.2 for tests numbering).

For the experiments the difference between dumped and packed riprap was assessed by means of porosity measurements. Tests (explained in Chapter 3) were performed to obtain the air volume within the dumped or packed riprap volume. Table 6.1 shows the porosity (n_p) of these tests, as well as the averaged values per construction type. The test results show that the porosity of packed blocks reduced in average by 2.2% (from 43.7% to 41.5%) for D_{50} = 0.037 m, when compared to the dumped ones. The interlocking forces increase as the air volume between blocks reduces since the blocks have a closer

arrangement. The porosity of the riprap in the experiments by Maynord and Abt (Maynord et al., 1989 and Abt et al., 1998) was equal to 44% with limestone blocks in size of D_{50} = 0.035 m, comparable to the blocks in the present study if they are dumped.

Table 6.1 Porosity (n_p) of dumped and packed riprap for the blocks corresponding to D_{50} = 0.037 *m*; results are shown for four porosity tests and the averaged values.

D_{50} (m)	Dumped n_p (%)	Average (%)	Packed n_p (%)	Average (%)
0.037	42.96	43.71	41.86	41.52
	43.05		42.02	
	44.62		41.00	
	44.20		41.22	

As shown in , forty-nine tests were run with the parameters including thickness (number of layers), slope of channel, riprap side slope, unit discharges (q), flow depth (h). The time to failure (t_f) considering uniform flow conditions is also given. From this forty-nine experiments, 28 tests were performed with one layer and 23 tests with two layers of riprap installations. The discharge was kept constant during maximum three hours of each experiment for both one and two layers. Thus, the delay of failure due to the changes of the thickness of the riprap is comparable. Lower discharges may cause direct block erosion during the experiments but not a full failure of the bank slope whereas higher discharges may cause very fast failure. Tests were carried out under supercritical flow conditions (Table 6.2). Water depth, block erosion rate and time to failure were measured during the tests. Channel was fed by two pumps, measured by electromagnetic flow meters with of ±2 l/s of precision. Furthermore, the eroded rocks were collected and weighed in a sediment trap at the downstream end of the channel. Each run of the tests had a constant specific discharge.

Tests were run during maximum three hours unless the total failure of the blocks occurred in a section. Failure criterion that causes the stop of the test in these series of experiments were the time that the total collapse or sliding of the blocks over bank slope occurs and the section became unstable. In Figure 6.3 an example of installation, the view before and after one test of two layers can be seen (the test 8 in this case, cf. Table 6.2).

Table 6.2 Tests Program

Series	Number of layers	Slope of Channel (%)	Slope of riprap (°)	q (m^2s^{-1})	h (m)	t_f (min)
1	one	0.015	35	0.287	0.187	-
2	one	0.015	35	0.303	0.197	172
3	one	0.015	35	0.314	0.202	87
4	one	0.015	35	0.330	0.209	43
5	one	0.015	35	0.36	0.190	9
6	two	0.015	35	0.392	0.233	-
7	two	0.015	35	0.400	0.235	165
8	two	0.015	35	0.408	0.239	73
9	two	0.015	35	0.433	0.248	10
10	one	0.030	35	0.210	0.122	-
11	one	0.030	35	0.244	0.134	-
12	one	0.030	35	0.251	0.136	-
13	one	0.030	35	0.263	0.141	94
14	one	0.030	35	0.281	0.145	73
15	one	0.030	35	0.301	0.165	62
16	one	0.030	35	0.313	0.167	12
17	two	0.030	35	0.280	0.150	-
18	two	0.030	35	0.299	0.163	161
19	two	0.030	35	0.313	0.168	102
20	two	0.030	35	0.332	0.182	23
21	one	0.030	31	0.209	0.126	-
22	one	0.030	31	0.230	0.134	143
23	one	0.030	31	0.314	0.147	27
24	one	0.030	31	0.345	0.170	3
25	two	0.030	31	0.239	0.132	-
26	two	0.030	31	0.245	0.140	137
27	two	0.030	31	0.316	0.151	78
28	two	0.030	31	0.359	0.167	14
29	one	0.030	27	0.186	0.118	-
30	one	0.030	27	0.212	0.129	-
31	one	0.030	27	0.233	0.137	-
32	one	0.030	27	0.247	0.142	-
33	one	0.030	27	0.258	0.146	172
34	one	0.030	27	0.268	0.150	44
35	one	0.030	27	0.301	0.157	33
36	one	0.030	27	0.344	0.170	17
37	two	0.030	27	0.258	0.145	-
38	two	0.030	27	0.301	0.157	92
39	two	0.030	27	0.320	0.162	44
40	two	0.030	27	0.344	0.170	21
41	one	0.055	35	0.202	0.100	-
42	one	0.055	35	0.235	0.109	120
43	one	0.055	35	0.255	0.117	42
44	one	0.055	35	0.273	0.122	4
45	two	0.055	35	0.231	0.109	-
46	two	0.055	35	0.255	0.117	146
47	two	0.055	35	0.273	0.122	101
48	two	0.055	35	0.291	0.127	62
49	two	0.055	35	0.307	0.138	11

6.3 Results and discussion

6.3.1 General observations

Figure 6.4 shows an example of the experiments, two instants of the test 8 (cf. Table 6.2 for tests numbering) where the riprap protection, before (left) and after (right) failure, is observed. In this experiment, with a channel slope of 1.5%, the external layer is covered with red blocks. Eroded parts of riprap in both layers, as well as the collapsed area, can be seen as red blocks in Figure 6.4 (right). The slope of the channel was 1.5% and a unit discharge of q = 0.408 (m^2s^{-1}), direct block erosion occurred at the beginning of the test. However, total failure was observed after 73 minutes. It can be witnessed that in the failed sections the filter and the second layer were fully visible while other areas were still stable.

Figure 6.4 The experimental set up before (left) and after (right) one test (the test 8, cf. Table 6.2)

6.3.2 Temporal analysis of failure

In chapter 5, a time-dependent analysis was performed where the time to total failure of the riprap was investigated based on the evolution of the sediment transport measured at the downstream section. Here a similar analysis is shown aiming at investigating the time delay caused by the existence of a second layer of riprap in the bank protections. The results are analysed and discussed taking into account the effect of the channel longitudinal slope and the riprap bank slopes on the time to failure.

Figures 6.5 to 6.8 show the time evolution transport rate of the blocks from the riprap protection that is measured at the downstream section of the channel. The time evolution allows identifying the total failure of a section bank corresponding to a sudden increase in the transport rate, where a vertical asymptote is observed (as in chapter 5). In this and the following figure, and for visualization purposes, the time is normalized by the maximum duration of the tests T_{max} =180 as follows:

$$t^* = \frac{t}{T_{max}} \tag{6.1}$$

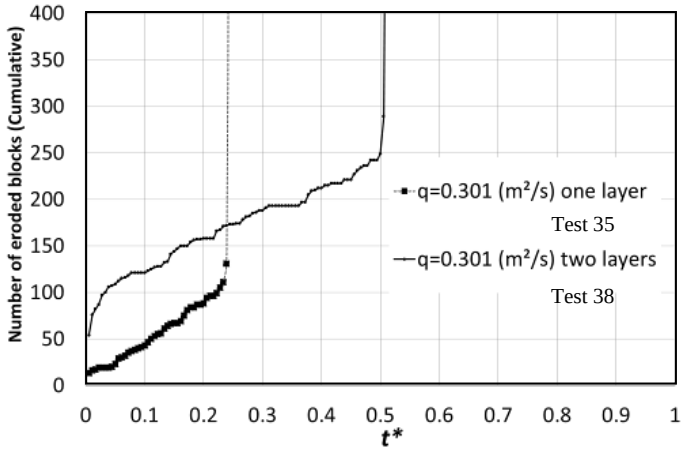

(a)

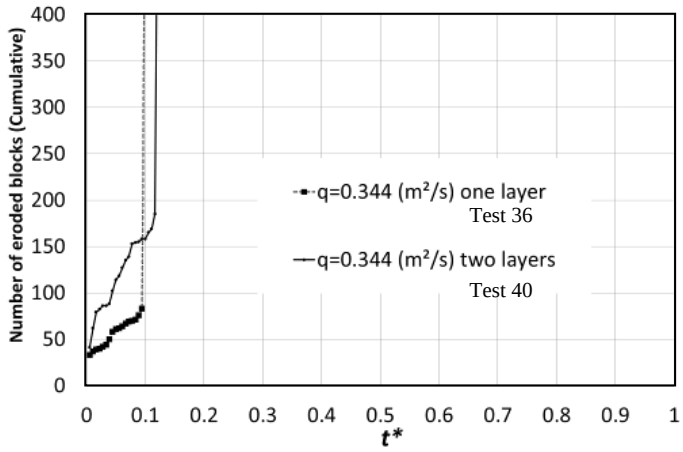

(b)

Figure 6.5 Time evolution of the cumulative block erosion rate for one layer and two layers with the same discharge for channel slope of 3% and riprap slope of 27° and for two different unit discharges provoking failure, a) q = 0.301 m^2s^{-1} and b) q = 0.344 m^2s^{-1}.

The results in Figures 6.5 to 6.8 generally illustrate that, although all the unit discharges shown provoke failure for single and double layered riprap protections, having two layers of riprap induces a delay on the failure time of the protection. In Figure 6.5a a significant delay of the time to failure is verified when using a double layer protection; however, by increasing the unit discharge to which the bank protection is exposed of about 12%, the effect of the second layer becomes minor. These results indicate thus that the use of two layer protection for high discharges became ineffective on the delay of structural failure in Figure 6.5b.

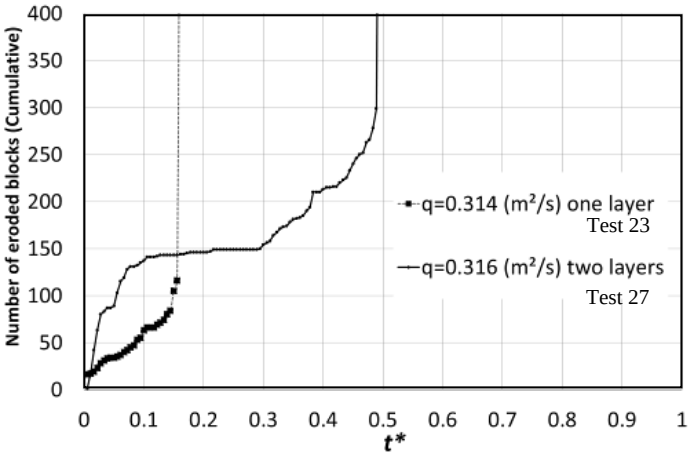

(a)

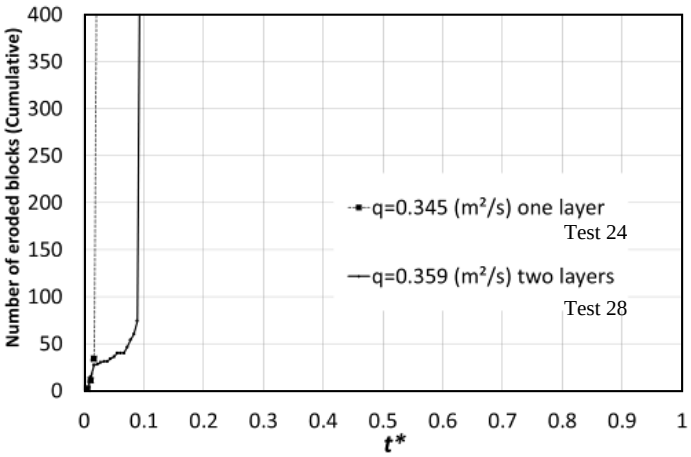

(b)

Figure 6.6 Time evolution of the cumulative block erosion rate for one layer and two layers with the same discharge for channel slope of 3% and riprap slope of 31° and for two different unit discharges provoking failure, (a) $q \approx 0.315$ m^{2}s^{-1} and (b) $q \approx 0.350$ m^{2}s^{-1}.

The effect of the increase in the unit discharge in a decrease of the time to failure is evident when comparing the results in.Figure 6.5 and Figure 6.6 However, for the case of one layer protection, the effect on the reduction of the time to failure is less (about 15% when compared to 38% in the two layers case), indicating that there is a limit to the advantage of the using two layers of riprap bank protections in postponing failure.

For different riprap side slopes with the same longitudinal channel slope (Figure 6.6 and Figure 6.7), the results in terms of time evolution of structural failure of the riprap, for the one layer and two layer situations, are similar to the comments above. Once again, results in Figure 6.6, for a different riprap side slope, display that the use of two layers of

the riprap as bank protection delays the failure time. The effectiveness of the delay of the failure time by the use of two layers is also reduced with the increase of the discharge acting on the bank protection, for lower riprap side slope. Comparing results of Figure 6.5 and Figure 6.6 reveals that the riprap side slope has a stabilizing effect. It can be observed that considering the same discharges in both side slopes, the time to failure reduced smoother in lower bank slope.

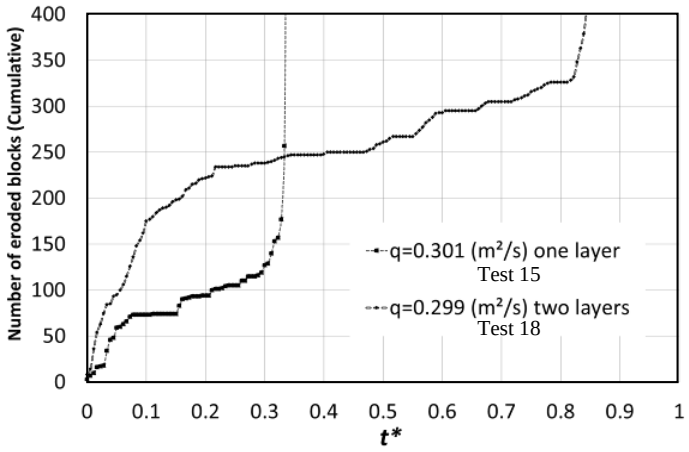

Figure 6.7 Time evolution of cumulative block erosion rate for one layer and two layers with the same discharge for channel slopes of 3% with riprap inclination of 35°

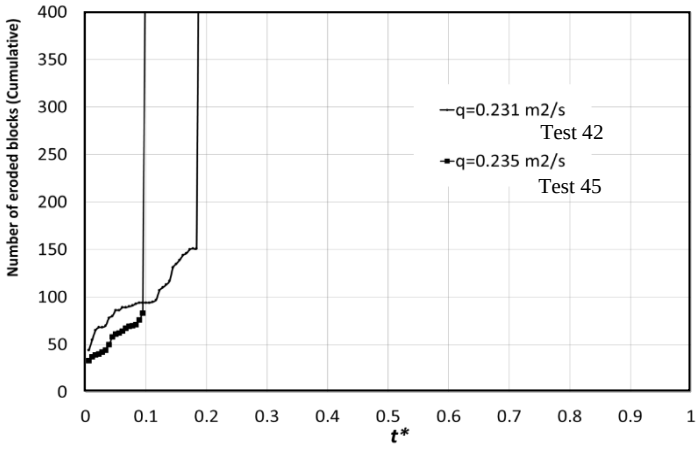

Figure 6.8 Time evolution of cumulative block erosion rate for one layer and two layers with the same discharge for channel slopes of 5.5% with riprap slope of 35°

In the case represented in Figure 6.7, a significant decrease in the time of occurrence of a total failure in one layer test is visible, which has been reduced by more than 50%. This shows that the use of two layers not only delayed considerably the time to failure

but also increased the resistance of the protection to the erosive action of the flow greatly. The comparison of the time to failure of riprap set up in one and two layer in highest longitudinal channel slope of 5.5% (Figure 6.8) shows a shift of 10% in a time to failure. However, the impact of thickness is reduced when compared to the lower longitudinal channel slope.

6.3.3 Parameterization of the time to failure

The influence of the second layer on the stability of riprap protections, namely on the delay to failure above observed is now investigated by means of normalization of the time to failure. The dimensionless bed shear stress which represents the balance of hydrodynamic forces acting on the riprap and the submerged weight of the blocks and is calculated as equation (5.2) and (5.3).

A dimensional analysis is applied based on the characteristic time to failure as a function of dimensionless bed shear stress as:

$$T^* \sim f(t_f, V, u^*, h, \rho, g, D, \gamma_w, \gamma_s) \tag{6.2}$$

A dimensionless parameter for the characteristic time to failure T_h^* can be defined with the flow depth as length scale and the friction velocity as kinematic scale as equation (5.6) and (5.7)

The friction velocity (shear velocity) is considered as a velocity scale (6.3) representative of the shear causing erosion and acting on the blocks of size *D*. In order to understand what is influencing the time to failure, the dimensionless bed shear stress was compared to the characteristic time to failure T_h^* (Figure 6.9).

Figure 6.9 shows the dimensionless time to failure T_h^* as a function of τ^* for the three tested longitudinal slopes. There are good agreements for a linear relationship between T_h^* and τ^* for one layer tests when the pairs of results are grouped by slope ($R^2 \approx 0.92$, 0.95 and 0.99 for S = 1.5%, 3% and 5.5%, respectively). The same condition is shown for the two layers tests with a shift of maximum 10% to higher dimensionless bed shear stress with a good agreement for a linear trend ($R^2 \approx 0.89$, 0.96 and 0.96 for S = 1.5%, 3% and 5.5%, respectively). This normalization, indicating that for each slope group the relationship between T_h^* and τ^* seems to be linear, suggests that the flow depth

combined with the bed shear stress is an appropriate scale to describe the block movement. Figure 6.9 also shows that the inclination of the linear relation between T_h^* and τ^* changes with *S*, which suggests that a relationship with the inclusion of a factor of this variable should be introduced to obtain similitude. Results confirm, as discussed above that at the same characteristic time to failure higher bed shear stress is needed for the steeper channel.

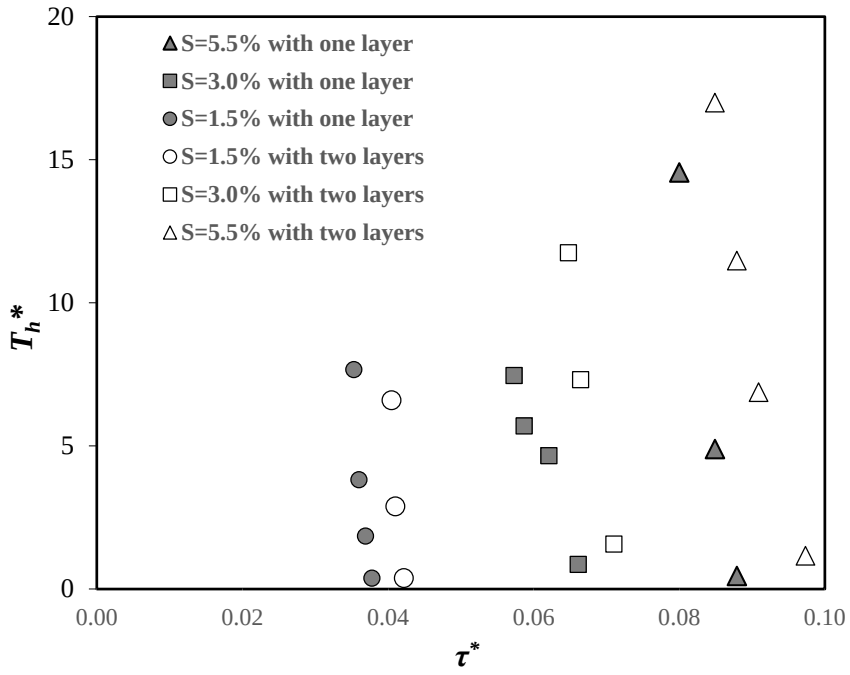

Figure 6.9 Dimensionless failure time T_h^* as a function of dimensionless bed shear stress τ^*, grouped by slopes S = 1.5%, 3% and 5.5% for the tests encounter the failure.

From the results above discussed, a functional relation of the characteristic time to failure with modified dimensionless parameters is proposed as made in chapter 5. Figure 6.10 displays that the time to failure normalized by the flow depth presents a good collapse with the Shields parameter multiplied by $S^{-0.7}$(Chapter 5). This normalization indicates the importance of the longitudinal slope and the flow depth scales for the block movement. The data groups now by the thickness of the layer instead of the longitudinal slope, thus Figure 6.10 provides the possibility of forecasting the delay in the time to failure provoked by the second layer or riprap protection. Figure 6.10 illustrates the improvement of the stability due to the presence of a second layer.

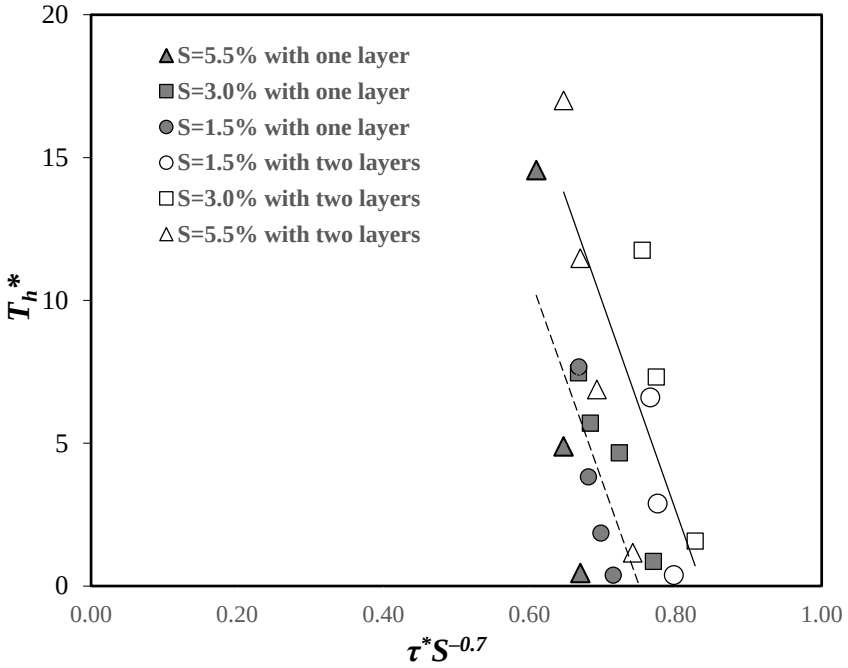

Figure 6.10 Dimensionless failure time (T_h^*) as a function of the dimensionless bed shear stress ($\tau^* S^{-0.7}$). The straight lines correspond to linear regressions applied to the results with single (dashed) and double (continuous) riprap layer.

The characteristic time to failure for a channel with a longitudinal slope of 3%, as a function of dimensionless shear stress, is shown in Figure 6.11 for three different riprap side slopes and considering single and double layered riprap bank protections. The range of τ^* varies from 0.055 to 0.072 for highest side slope in two layer tests. However, for other lower riprap side slopes the result shows the same ranges between 0.053 and 0.067 with the same pattern for the one layer and two layers. The results reveal a shift (dashed line) to higher dimensionless shear stress in the highest bank slope while this shift is less for the other tests. The difference in riprap side slope of 35° between two conditions is 10%. Since the angle of repose for the blocks in the size of 0.037 m is 41°, therefore, the analysis of the variation of riprap side slope specified that in the same channel slope, the second layer has more stabilizing role when the riprap side slope gets closer to the angle of repose of the blocks, which is 41° for the blocks of 0.037 m.

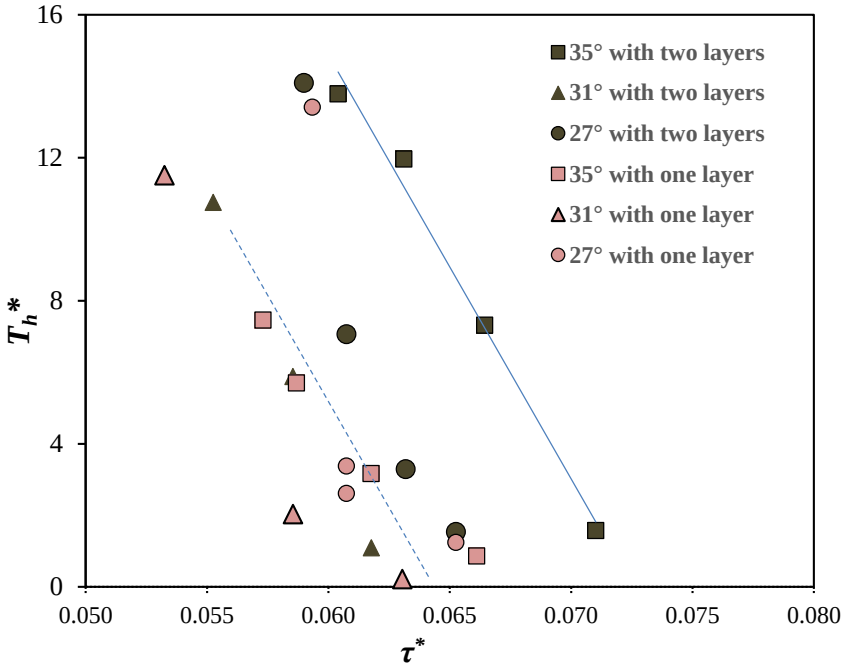

Figure 6.11 Characteristic time to failure T_h^* as a function of the dimensionless bed shear stress (τ^*) in three riprap side slopes of 27°, 31° and 35° and channel slope of 3%. The straight lines correspond to linear regressions applied to the results with single (dashed) and double (continuous) riprap layer.

6.3.4 Critical conditions for failure

By applying dimensional analysis, one can establish a relationship between the relative roughness and the following variables:

$$\frac{D}{h} = f\left[\left(\frac{\gamma_w}{\gamma_s - \gamma_w}\right)^{1/2} \frac{V}{\sqrt{gh}}\right] \tag{6.4}$$

The basic relationship between relative roughness (D/h) and depth average velocity (V), considering both the single and double layers of riprap is shown in Figure 6.12. The stable and failed tests are presented for both thicknesses with distinct symbols. So called limit conditions are also represented and correspond to the tests with specific discharges that have the first failure and the lower discharges remained stable in an equilibrium state, thus corresponding roughly to critical conditions of stability. These critical discharges are chosen as the envelope of both conditions. The full and dashed lines are the linear regressions of the critical condition in one layer and two layers tests respectively. The results show a slight shift representing that there is more stability in the application of a double layered riprap protection when compared to the single layer test, for the same

block size. This difference is about 2% which means roughly 10% reduction of the designed blocks' diameter when they are constructed in two layers. Also, the trend line related the critical discharges for two layer tests has better agreement with the equation (4.10) in chapter 4, which referred to all the experiments with different sizes, riprap, bank slopes and thicknesses. In developing a velocity based procedure of design, it is important to define a reference velocity to be evaluated which here corresponds to the mean velocity in the middle of the channel.

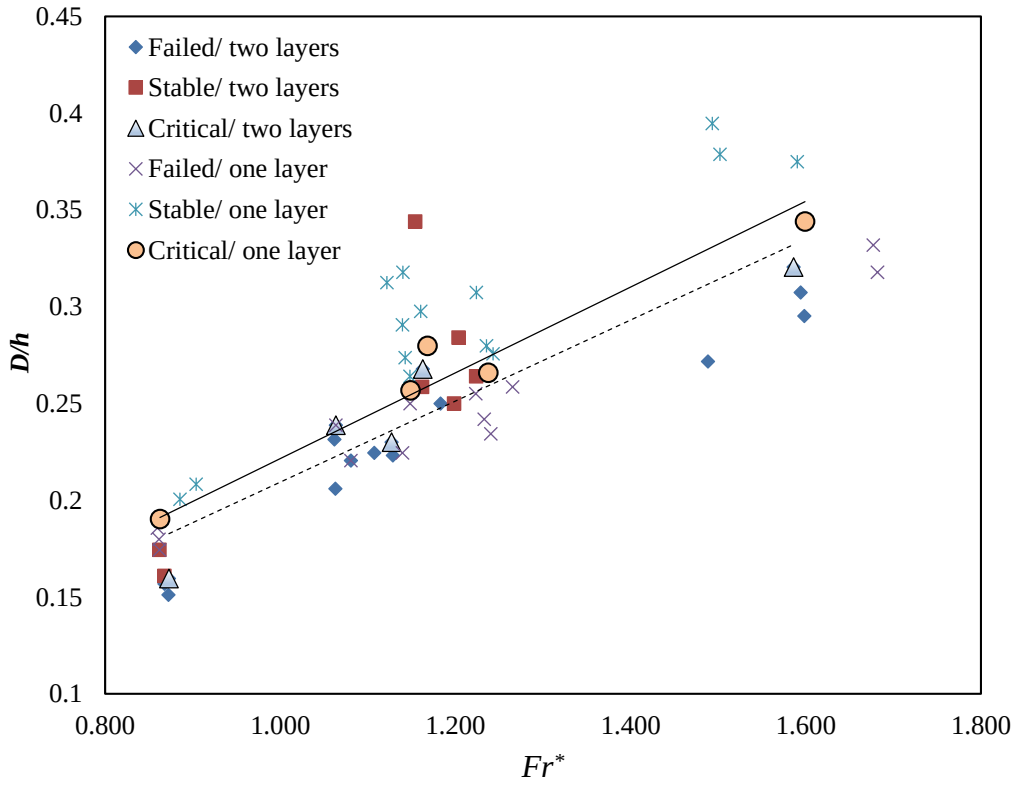

Figure 6.12 Relative roughness as a function of modified Froude number for Stable and Failed test in one and two layers

6.4 Conclusion

This research was performed to analyze the effect of thickness on the stability of packed and packed riprap as riverbank protections. Empirical results are shown in terms of channel longitudinal slope, riprap side slopes and thickness of the protection layer. The influence of a second layer of the riprap protection is considered on both the time to failure and sizing of riprap. In contrast to the dumped blocks, the failure criterion in the

packed riprap is defined at the time that the blocks slipped on the side slope, and the section became unstable. The observation of the experiments showed that:

- The results revealed that in the same longitudinal channel slope and side slope, the second layer stabilized the section and postponed the failure. However, the block erosion rate is increased significantly.
- The higher is the discharge that causes the failure; the less is the effect of the second layer on stabilizing the section. It means that in the lower discharges, the thickness has more influence on the stability of the riprap.
- Regarding the riprap side slope, double layer tests are more stable in higher inclinations (side slope) comparing to single layer.
- Results also show that longitudinal slope of the channel seems to be the most dominant parameter. Nevertheless, the impact of thickness in higher channel slope reduced comparing to the lower channel slope.
- A time-dependent analysis showed that the characteristic time to failure has a functional relationship with dimensionless shear stress (τ^*) and longitudinal slope.
- The analysis revealed that the two layer tests resist for higher τ^* at the same time to failure. In the other word, for the identical forces acting to move the blocks the characteristic time for failure is higher for double layer riprap.
- The thickness of the riprap has a more considerable influence to protect channel bank for higher riprap side slope than the flatter ones. It means that, by variation of riprap side slope, the second layer has a more stabilizing role when the riprap side slope gets closer to the angle of repose of the blocks.

In this study, tests with the occurrence of failure and tests that remained stable are compared. The limit between failed and stable tests is defined. Finally, as the second layer stabilizes the protection system considerably, in addition to delaying the failure time, in practical terms the blocks can be designed in a smaller size riprap, with higher thickness.

Chapter 7

Probabilistic Failure Analysis of Riprap as Riverbank protection under flood Uncertainties

In this chapter, the concept of a probabilistic assessment model based on Monte Carlo Simulation, Moment Analysis Methods, and Point Estimation Method are presented. The probability of failure in different mechanisms is defined. The failure probability of riprap is assessed by a probabilistic function in terms of the design safety factor.

Abstract

Existing riverbank riprap could face the risk of failure if the flood regime changes in future. Additionally, changed sediment transport in rivers, as a possible result of climate change, impacts the failure risk of flood protection measures. Evaluation of this potential failure is the primary issue of riprap stability and safety assessment. The consequences of the bank failure are probably uncontrolled erosion and flooding with disastrous consequences in residential areas or damage to infrastructures. Thus, a probabilistic analysis of riprap failure considering different mechanisms due to the flood and sediment transport uncertainties is required to assess embankment stability. In this chapter, the concept of a probabilistic assessment model based on Monte Carlo Simulation, Moment Analysis Methods, and Point Estimation Method are presented to define the failure risk of riprap bank protection. The probability of failure in different modes, namely direct block erosion, toe scouring and overtopping, has been defined by taking into account the bed level variation based on bedload transport described with a probabilistic function of the peak discharge.

7.1 Introduction

7.1.1 Failure risk of riprap

Changing atmospheric condition will influence the amount of precipitation and its regional distribution, thus possibly the frequency and the magnitude of extreme flood events and their time of occurrence will change respectively. The expectation is that climate change will impact flooding and sediment transport in mountain rivers and catchments of Switzerland in future (Köplin et al. 2012). This modified hydrological and hydraulic regime will further impact on sediment transport dynamics as well. Sediment yield in a catchment is dependent both on the transport capacity of the stream and availability of loose material. Therefore, sediment transport flow will be influenced by climate change (Turowski et al., 2009). These changes will affect the behaviour and performance of flood protection measures and may increase their risk of failure. Destruction or collapsing of flood protection measures will result in uncontrolled flooding and lateral erosion with a displacement of meanders and the formation of braided river patterns. These processes can have catastrophic consequences for urban areas and

infrastructures, especially along Alpine rivers. For this reason, flood protection strategies have to be adopted to cope with changing conditions due to climate change. Hence, probabilistic analysis of failure mechanisms of riprap due to flood events and sediment transport is necessary.

Figure 7.1 The view of riverbank riprap and residential area in the central part of Switzerland (Kander, Switzerland, 2012)

Riprap is one of the most commonly used protection measures to keep the stability of the riverbank. In this paper, a probabilistic assessment of riprap failure is assessed probabilistically for different mechanisms of failure and models of riprap design as well as risk analysis methods will be discussed in the following part. Then the probabilistic simulation methods and the results will be described and concluded.

7.1.2 Failure mechanisms of riprap

According to Blodgett and McConaughy (1986), riprap failure mechanisms are identified as direct block erosion, translational slide, slump, and side-slope failure. Direct block erosion by flow is the most often considered erosion mechanism. This mode of failure occurs when the resistance against the flow decreases if the blocks are not large enough. Blocks tend to be dislodged more by rolling rather than sliding (Stevens et al. 1976 and Froehlich 2011). Downslope of riprap material movement can cause a translational slide as a failure. The initial phases of a translational slide are shown by cracks in the upper part of the riprap blanket that extend parallel to the channel. Translational slides are initiated by the steep slope of the riverbank and excessive hydrostatic pore pressure. However, this failure process mostly occurs due to toe scouring and instability of the riprap caused by the weakness in the toe foundation. Modified slump failure of riprap is

the mass movement of material within only the riprap blanket, and the blocks seem to slide on each other. Probable causes of the modified slump are the steep slope of the embankment and lack of toe support. Slope instability of the riprap is causing mostly due to overtopping. It would be a rotation-gravitational movement of material along a surface of rupture. It relates to the shear failure of the underlying base material that supports the riprap. While overtopping occurs, the water saturates the riprap and the material behind it. Once the level of the water decreases the water in the saturated part tends to release faster, and the slide-slope in riverbank riprap takes place (Jafarnejad et al. 2012). To sum up, the main reasons for failure in riprap due to extra forces that overlap the resistance and stability could be categorized in three modes: Direct block erosion; Toe Scouring; Overtopping. Such failure occurs since the hydrodynamic forces are higher than designed resistance or sediment deposition or erosion changes the bed level. Consequently, the water depth (h) and the foundation depth of the riprap changes as the bed changes. This bed level variation (Δh_s) could cause toe scouring as soon as the erosion depth reaches the level of buried part of riprap (Figure 7.2).

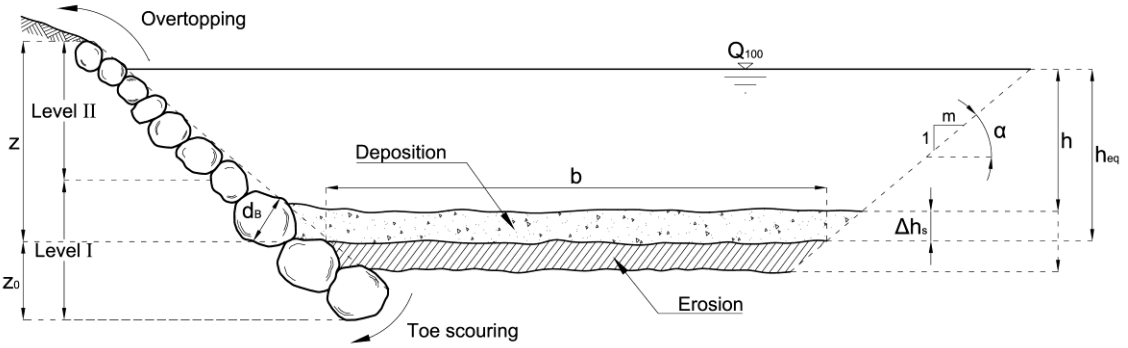

Figure 7.2 Selected trapezoidal section showing bed and water level variation due to change in sediment and different failure modes

7.1.3 Riprap design methods

Details of riprap design methods are explained in chapter 2 and in the introduction of chapter 4 and 5. However, this study focuses on the probabilistic simulation of the bank failure in a section protected by riprap by a Monte Carlo simulation method and defining the probability of failure in different mechanisms. This model mainly adopted Stevens et al. (1976) approach to define the riprap failure based on direct block erosion. Another failure mode is described as riprap sliding or slumping caused by toe scouring when the bed erosion continues until the whole riprap foundation exposes to the water. The

overtopping mode is also the condition that the water level is over the section height and causes the damage of riprap mostly based on slope instability. A Moment Analysis Method and Rosenblueth method are also applied to compare the results with Monte Carlo simulation to evaluate the accuracy of achieved probabilities of failure.

7.1.4 Probabilistic Simulation methods and risk analysis

Risk (R) is a joint measure of the probability and severity of an opposing effect. It is often estimated by the product of the probability of the adverse event occurring, also called failure probability (P_f), and the expected consequences or damage. In the case of flood protection measures, a contrary effect refers to a structural failure of them. Therefore, risk analysis necessitates first determination of failure probabilities and then the probabilistic estimation of consequences (Kassa, 2009).

The methods for conducting probabilistic risk analysis are classified differently. For instance, PIANC (1987b) categorized them into three classes based on the approach of conducting uncertainty. According to PIANC, the Joint Committee on Structural Safety distinguished three levels:

Deterministic approach (often called "quasi-probabilistic approach"): It presents constructional design methods with relevant safety factors. The approach simplifies the problem by assuming design parameters as primarily deterministic variables and uncertainty is accounted through the use of empirical safety factors. Safety factors are derived based on historical experiences.

Semi-probabilistic approach: This comprises some approximate methods in which normal distributions can often be assumed for both strength and loading. The reliability function is linearized at a specific point to determine the actual probability of failure. Point estimate methods, and Moment Analysis Methods are categorized in this group.

Full probabilistic approach: This method takes into account the exact probability distribution functions including correlations among the parameters. This approach gives the best-fit probability density functions of all related stochastic design parameters from both strength and load sides. The Monte Carlo Simulation Method can be categorized under this group. While the act of a designed system is a function of design parameters,

and design parameters are random variables, the performance of the systems is consequently a function of RV (Haldar and Mahadevan, 2000).

7.2 Set up of probabilistic simulations

The riverbank riprap model is developed by a probabilistic approach. Three different failure modes as direct block erosion, toe scouring and overtopping are simulated as the limit functions. The simulation code was set up with mathematical and statistical software based on Monte Carlo Simulation Method, Moment Analysis Method, and Rosenblueth Point Estimation Method. The hypothesis and sediment transport concept considered to compute the probability of failure.

7.2.1 The Monte Carlo Simulation Method (MCSM)

Monte Carlo Simulation Method is a statistical trial method. In MCSM design parameters (X_i's) are random variables by a certain probability density function. The simulation is run randomly to produce arrays of X_i's from the possibilities defined by the respective bounding pdf of the X_i's. It means that the generation of values is based on the corresponding probability. At each simulation step, a corresponding value of Y_i is calculated using functional relations in design equations. In this way, the simulation calculates many scenarios for outputs. Adequate number of simulations is taken to converge the solution. In MCSM, random design variables have to be described using continuous distributions (*pdf*'s). The technique has the advantage that it is relatively easy to implement and can deal with a wide range of multivariate functions (Haldar and Mahadevan, 2000; Ang and Tang, 2005; Kassa, 2009). This method has been applied in this research in order to define the best probability function of riprap failure.

The objective of the probabilistic simulation is to define the failure risk of riprap considering future changes in sediment transport and water discharge. The riprap failure modes can be categorized in direct block erosion, overtopping and toe scouring. Figure 7.3 illustrates the implication of the model of MCSM to define the probability of failure for the different failure mechanisms.

The Hypothesis is to study the stability of riprap by comparing the conditions before and after a flood. The initial condition will change until the section reaches its equilibrium

condition after a flood. In other words, at the end, the final sediment transport capacity of the section will be equal to the sediment supplied to the channel.

According Figure 7.3 the MCSM is implemented with the following steps of assumption:

(i) The procedure starts with a histogram of the predicted n-years flood (Q_n), for example 100 years flood, of a specific river. Next step is generating Q_n based on Monte Carlo Simulation technique.

(ii) Flow depth (h) corresponding to the generated Q_n is calculated by using uniform flow conditions according to Manning-Strickler:

$$Q = K_s A R_h^{\frac{2}{3}} J^{\frac{1}{2}} \tag{7.1}$$

which defines the discharge based on the initial slope (J), hydraulic radius (R_h), roughness coefficient (K_s), and cross section area (A).

(iii) A distribution of flow depth (h values) with their corresponding probabilities can then be obtained by this method. Sediment transport capacity of the section is estimated according Smart and Jäggi (1983) formula. Bedload discharge can be calculated as $Q_s = q_s b$ which b is bed width of the section and q_s is the bedload unit discharge; d_m is Mean diameter of bedload sediments; q corresponds to unit discharge.

$$q_s = 2.5 J^{0.6} q \left(J - \frac{d_m}{12.1h} \right) \tag{7.2}$$

Where m_s is a sediment transport rate coefficient that gives sediment transport supply from upstream compared to the transport capacity and indicated as:

$$m_s = \frac{Q_{b\ supply}}{Q_{b\ capacity}} \tag{7.3}$$

If the supply sediment ($Q_{b\ \text{supply}}$) is higher than the transport capacity of the reach ($Q_{b\ \text{capacity}}$), deposition on the channel bed occurs. On the contrary, erosion of the channel bed will take place. To reach the equilibrium condition in the section, the final capacity of the reach should be equal to the sediment

supply from upstream. In this case, there are two equations of hydraulics and sediment transport capacity of the section (Eqs. 1 and 2) with two variables. The variables are slope and water depth before and after the flood in an equilibrium condition. By considering a fixed point of the channel bed at the certain distance in downstream, end of the considered river reach, the bed level change (Δh_s) can be calculated.

(iv) Toe scouring happens if the bed erosion depth is below the level of the deepest block under the bed ($\Delta h_s > z_0$) (Figure 7.2).

(v) If the final computed water depth (h_{eq}) exceeds the height of riprap (z), overtopping failure occurs (Figure 7.2).

(vi) The safety factor of the riprap is computed according Stevens et al. (1976). Direct block erosion occurs when the safety factor is less than 1.0. According to Schleiss (1998), for large blocks in mountain river the modification of Stevens' safety factor can be explained as below:

$$\eta = \frac{\tau}{\tau^*} = \frac{7.7hJ}{(s-1)d_B} \tag{7.4}$$

Equations (7.5) to (7.7) describe the calculation of safety factor based on Stevens et al. (1976) based on parameters explained in Table 7.1.

$$\xi = \eta \frac{S_m}{\cos \alpha} \tag{7.5}$$

$$S_m = \frac{\tan \phi}{\tan \alpha} \tag{7.6}$$

$$SF = \frac{S_m}{2}\left(\sqrt{\xi^2 + 4} - \xi\right) \tag{7.7}$$

This safety factor just corresponds to the failure mechanism of direct block erosion and a confrontation of demand and capacity which means the values less than 1 show the failure occurrence.

(vii) NO Failure presented the condition that none of the failure modes as toe scouring and overtopping occur, and the calculated safety factor is more than 1.

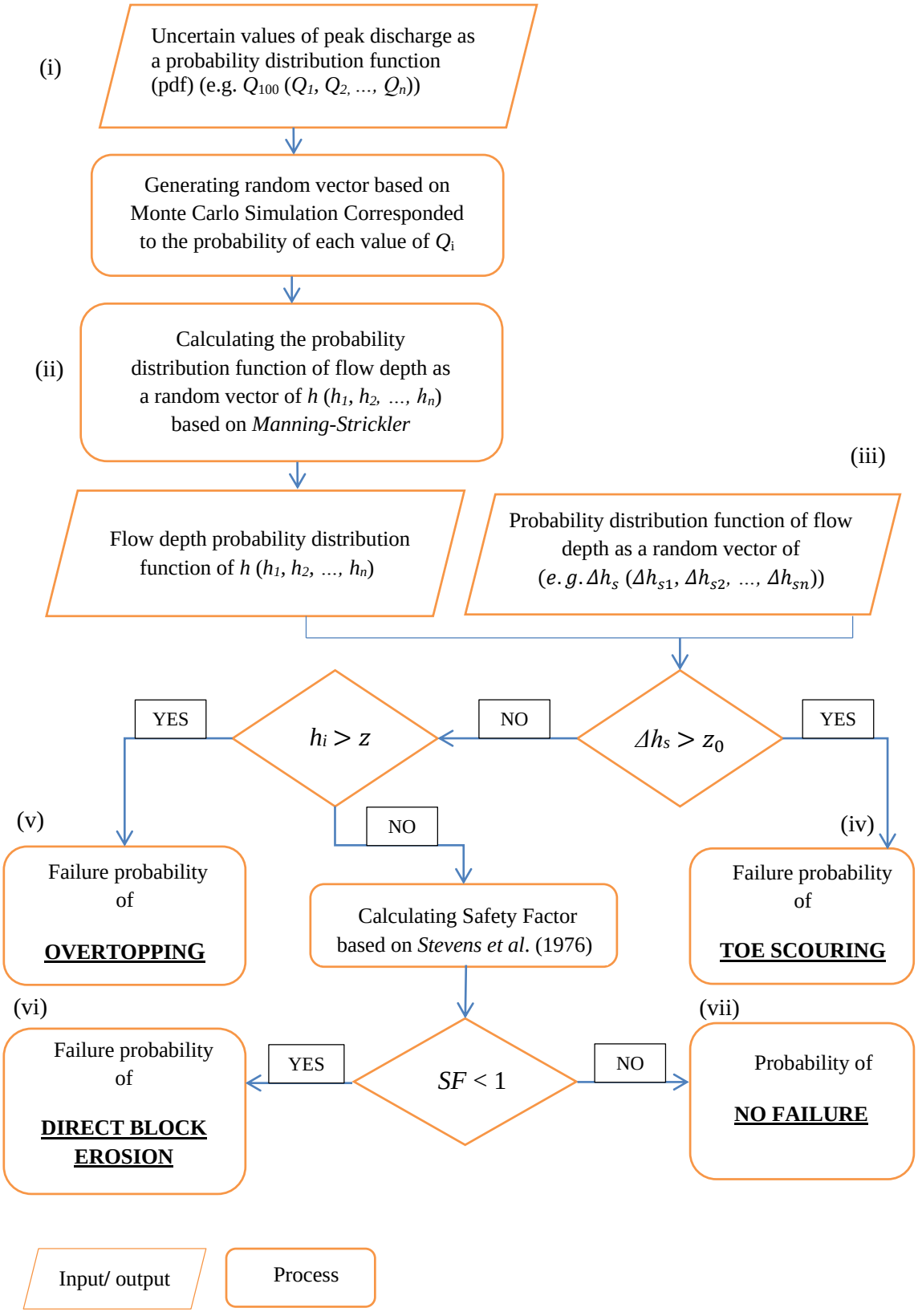

Figure 7.3 MCSM implementation for riprap safety assessment

The probabilistic function of the safety factor and the probability of the different failure mechanisms can be obtained by this simulation. In this study various probabilistic simulation and assessment models are applied in order to define the failure risk of river bank protection structures. These probabilistic simulations allow assessing the riprap safety regarding the changed flood and sediment transport in the future.

7.2.2 The Moment Analysis Methods (MAM)

Moments of distributions are used to summarize important characteristics of distributions as a single value. The first orders of moments as mean, variance, skew and kurtosis are the most important ones in probabilistic design. MAM are approximate ways of solving distribution problems involving Function of Random Variables (FRVs) (Haldar and Mahadevan, 2000).

The basic principle of MAM is specifying of randomness of uncertain variables that are arguments of a design equation by their moments- mean, variance, skew, and kurtosis, as μ_{Xi}, v_{Xi}, s_{Xi}, k_{Xi}, etc. Then the moments of the outputs of the design equations are available as a function of moments (Kassa, 2009). However, we cannot achieve a distribution of known standard type for the outputs. Nevertheless, the distributions of result (Y) can be approached using the derived moments μ_Y and v_Y. The most frequently used moment methods are first-order second moment (FOSM) and second order second-moment approximations (SOSM) which use Taylor's series expansion for the first and second orders. According to Hartford and Baecher (2004) in these methods the procedure for calculating the mean (μ_Y) for outputs involves expanding the FRV $Y = h(X)$ as Taylor series about mean values of the random variables in h and determining μ_Y by calculating the terms in the expansion. In many practical applications μ_Y is near $h(\mu_{Xi})$, so higher terms in the series become small and can be neglected. The FOSM is when the truncation is done after the first order term, and a better precision is achievable by second-order term called SOSM. Figure 4 presents the implementation architecture of these approximate methods.

There are several equivalent forms of writing Taylor's series for multiple variables. One of the commonly used versions, in general, is Equation (7.8).

$$Y = h(x_1, x_2, \cdots, x_n) = h(\mu_{x_1}, \mu_{x_2}, \cdots, \mu_{x_n}) + \frac{1}{1!}\sum_{i=1}^{n}(x_i - \mu_{x_i})\frac{\partial h}{\partial x_i} + \frac{1}{2!}\sum_{i=1}^{n}\sum_{j=1}^{n}(x_i - \mu_{x_i})(x_j - \mu_{x_j})\frac{\partial^2 h}{\partial x_i \partial x_j} + \frac{1}{3!}\sum_{i=1}^{n}\sum_{j=1}^{n}\sum_{k=1}^{n}(x_i - \mu_{x_i})(x_j - \mu_{x_j})(x_k - \mu_{x_k})\frac{\partial^3 h}{\partial x_i \partial x_j \partial x_k} + \cdots \quad (7.8)$$

This model cannot take all different mechanisms of failure into account. Direct block erosion is the only mechanism that can be taken in this case. Herein, for a condition with no failure in toe scouring and overtopping, *Y* can be substituted by Safety Factor as seen in (7.9):

$$Y = SF = h(Q_n,\ d_B,\ J,\ \cdots) \quad (7.9)$$

This *Y* function can be calculated by equations (7.4) to (7.7). Figure 7.4 illustrates the implementation of the model of moment analysis to define the probability of failure by describing the safety factor.

(i) First step defines the moments of random variables of discharge Q_n determined from variables of a probability density function of it for future.

(ii) Then the function of random variables which is Safety Factor could be defined as a function of water depth ($SF = h(h_i)$). This has to be expanded by Taylor series on the mean values μh_i of random variables and truncate it at appropriate order.

(iii) In the next step the nth central moment function of Safety factor ($\mu SF_i, \nu SF_i, sSF_i, kSF$) is obtained by calculating the expectation of terms in expansion and substitution μQ_n.

(iv) Finally the probability density function of the safety factor (SF) can be defined and analyzed.

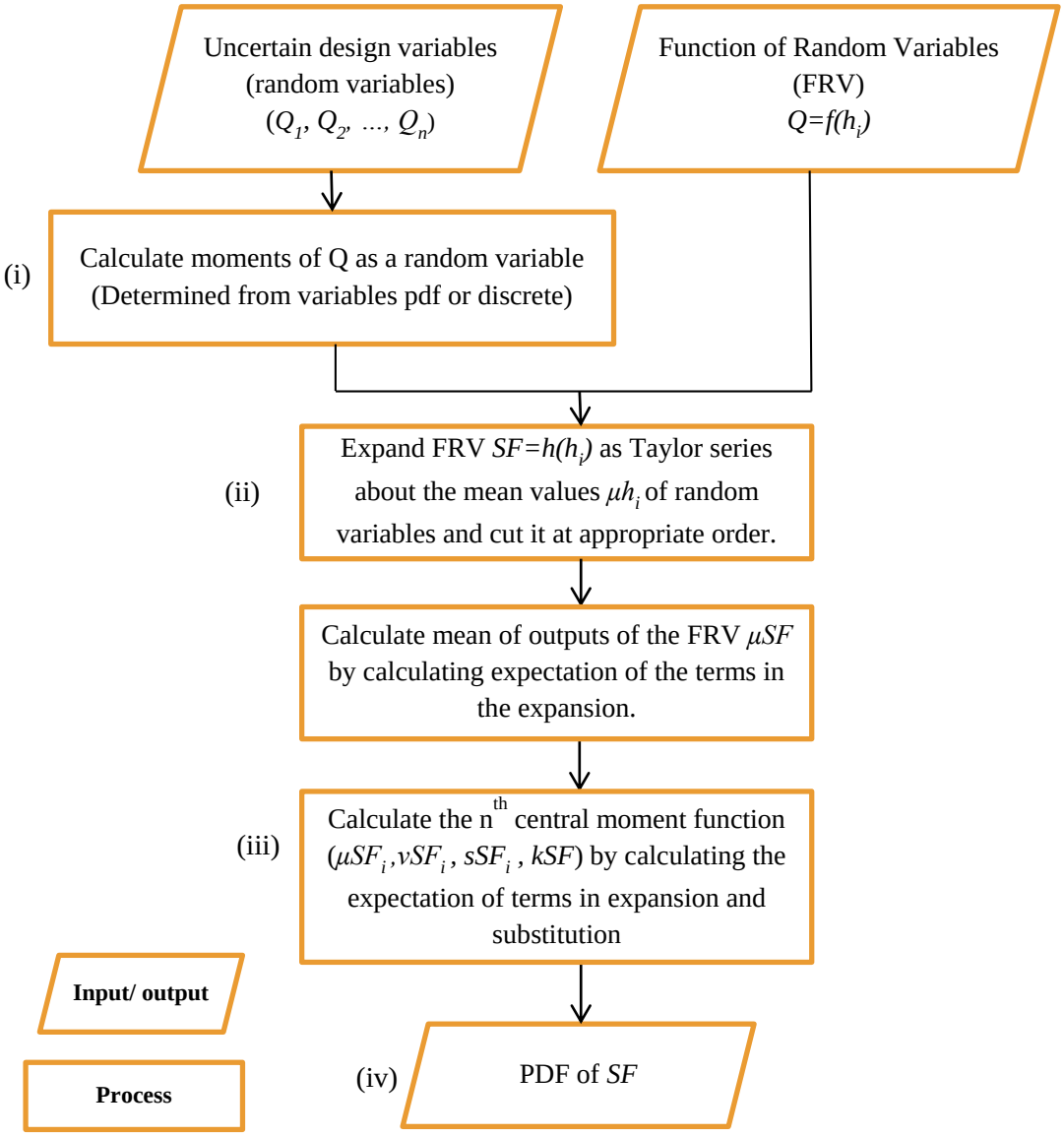

Figure 7.4 MAM implementation for safety riprap assessment

7.2.3 Rosenblueth Point Estimation Method (RPEM)

Point Estimation methods offer a direct procedure to obtain the moments (particularly mean and variance) from known moments of RV. Rosenblueth (1975) first proposed the model to solve the problems with symmetric, uncertain and correlated input factors. Then, the original method was modified to apply for asymmetric random variables. When the probability distribution function of the state variables is unknown, it is possible to obtain 1 order moment, 2 order center moment, and 3, 4 order center moment of the state function (safety factor). Thus, the reliability index of the assumed probability distribution can be achieved (Conciatori et al., 2009).

RPEM is based on the hypothesis that the area under the entire probability distribution of a chosen random variable X_i can be rearranged to a finite number of distinct points, which the first moments of the distribution are preserved.

7.3 Results and discussion

7.3.1 Monte Carlo Simulation results

7.3.1.1 Results for a straight channel

The riverbank riprap model on MCSM was mathematically set up as described under section 2.1. The parameters used in the simulation, such as the geometry of cross section, sediment transport, and hydraulic parameter are described in Table 7.1 with their reference values for a selected river cross section. The data was considered as an example, and the peak discharge is taken as a normal distribution.

In Table 7.2, the size of the blocks at different levels of the riprap is given. The goal of this example is to show the variation of the block sizes in one specific river section protected by riprap. In Table 3 the probability values for the different failure modes in this trapezoidal section are summarized. The presented model allows for taking the probabilistic values of any variables into account.

Figure 7.6 shows the probability of the safety factor for different failure mechanisms and stable conditions. First two columns are representing the probability of failure in toe scouring and overtopping. The next part shows the range of safety factors (*SF*) in the selected trapezoidal section. The values of safety factor for less than 1 express the probability of failure in direct block erosion for each calculated safety factor. The rest values regarding the frequency of occurrences belong to the stable condition.

Table 7.1 Description and reference values of parameters used in hydraulics and bedload transport calculations

Description	Variable	Value	Unit
Bed width of the section	b	55	m
Angle of riprap	α	30	°
Slope	J	3%	
Bed roughness	K_s	37	$m^{1/3}/s$
Density ratio	$s = \rho_s/\rho$	2.65	
Angle of repose	ϕ	60	°
Mean diameter of bedload sediments	d_m	0.014	m
Mean peak discharge of n-years flood (here is 100)	μQ_n	800	m^3/s
Standard deviation of peak discharge of n-years flood (here is 100)	σQn	180	m^3/s
Sediment transport rate	m_s	0.9	—
Distance between the considered section and the next fix point	L	1000	m
Depth of riprap protection from initial bed level	z	2.50	m
Depth of deepest riprap block below initial bed level	z_0	−1.90	m
Depth of deposit (+) or erosion (-) compared to initial bed (explained in Figure 7.5)	Δh_s	—	m

Table 7.2 Size of the blocks for the selected riprap at two different levels

Level	h_i (m)	d_B (m)
I	–1.00	0.80
	1.00	
II	2.80	0.40

Table 7.3 Probability of the safety factor (*SF)* and failure modes

Safety Factor Ranges / Failures	Frequency	Percent
Toe Scouring: $\Delta h_s > z_0$	50	5.0%
Overtopping: $h_{eq} > z$	147	14.7%
0 < SF < 1 (Direct Block Erosion)	315	31.5%
SF ≥ 1 (No Failure)	488	48.8%

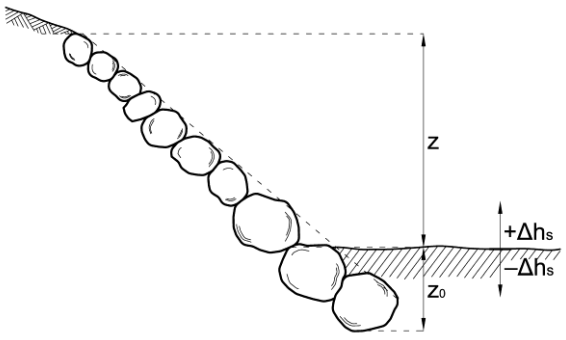

Figure 7.5 Deposition (+) and erosion (–) of sediment in a section due to flood

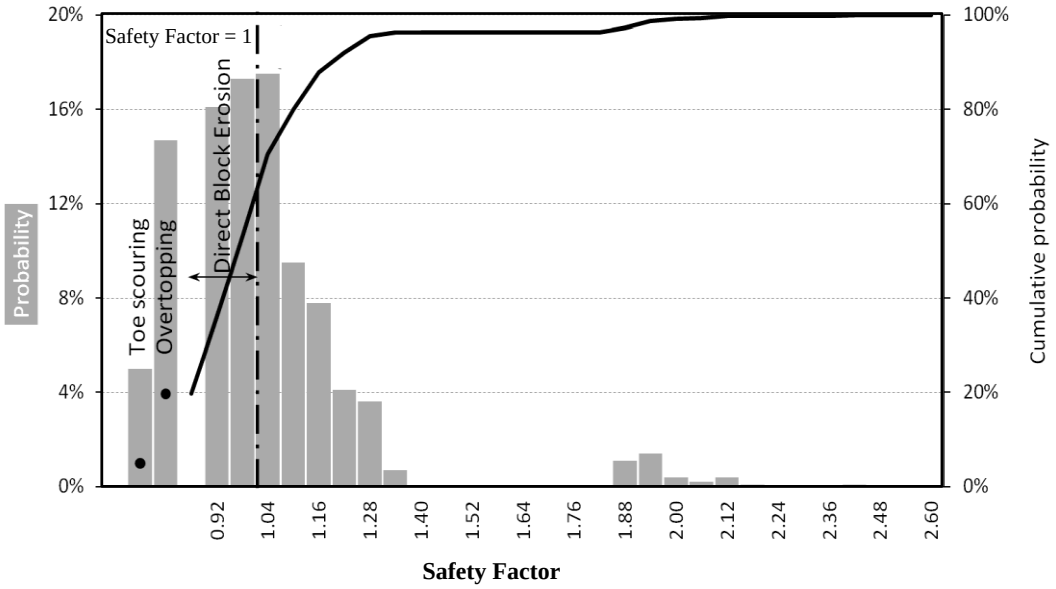

Figure 7.6 The probability of the safety factor in different failure modes of a selected trapezoidal section

7.3.1.2 Curved channel vs. straight channel

The model was also developed for a curved channel. In the bend, a secondary current occurs which consequences an outer bend scour. The transverse velocity profile has been investigated experimentally by Kikkawa et al. (1976). Their empirical equation has been chosen for this study. In order to obtain the bend scour with Kikkawa et al.'s equation, the inner and outer radius of the bend has to be given. Table 7.4 shows the data of specific river section in straight and curved channel with external radius of 2000m.

Table 7.4 Description and values of parameters using in hydraulics and bedload transport calculations in curved channel

Description	Variable	Value	Unit
Bed width of the section	b	55	m
Angle of riprap	α	30	°
Slope	J	1%	
Bed roughness	K_s	37	$m^{1/3}/s$
Density ratio	$s = \rho_s/\rho$	2.65	
Angle of repose	ϕ	60	°
Mean diameter of bedload sediments	d_m	0.014	m
Mean peak discharge of n-years flood (here is 100)	μQ_n	600	m^3/s
Standard deviation of peak discharge of n-years flood (here is 100)	σQn	150	m^3/s
Sediment transport rate	m_s	0.9	—
Distance between the considered section and the next fix point	L	1000	m
Depth of riprap protection from initial bed level	z	6.5	m
Depth of deepest riprap block below initial bed level	z_0	−2	m
Depth of deposit (+) or erosion (-) compared to initial bed (explained in Figure 7.5)	Δh_s	—	m

Figure 7.7 Failure probability distribution function of a riprap in a straight channel by Monte Carlo Simulation

In Figure 7.7 the probability of failure in a straight channel is shown. In the same condition, by adding a curve with an external radius of 2000 m in the channel the probability of failure changes to 100% as can be seen in Figure 7.8.

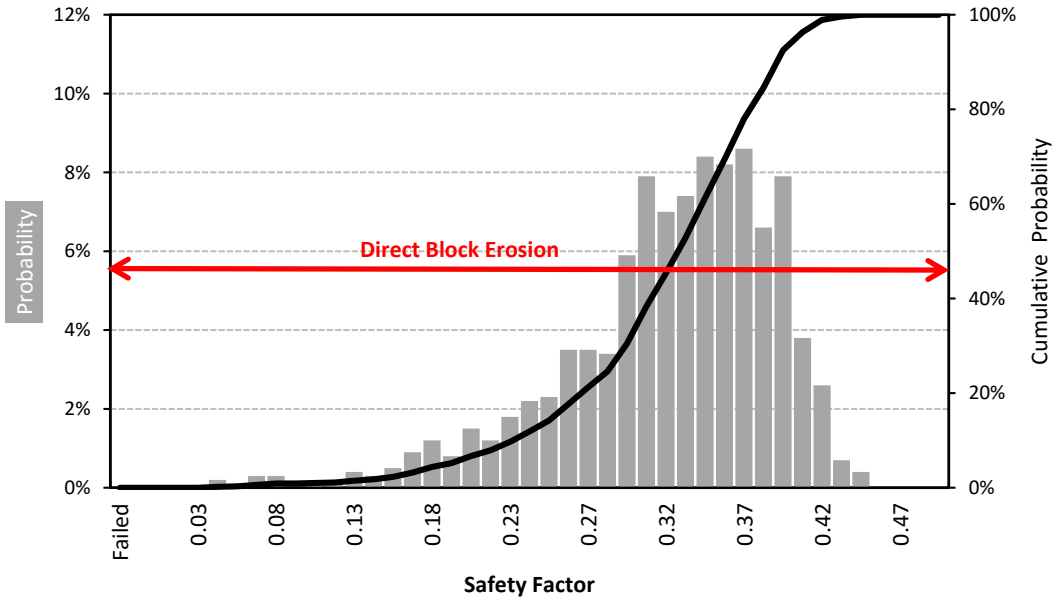

Figure 7.8 Failure probability distribution function of a riprap in a curved channel by Monte Carlo Simulation.

7.3.2 Results of MAM and comparison with MC

The MAM model as explained in part 7.2.2 was implemented for the example related to Table 4. In this especial case, safety factor of riprap design is $SF = h(X)$ with only one independent variable Q (uni-variate FRV's). When the value of h is given for some value of $Q = \mu Q$, then $SF = h(Q)$ can be found for any other values of Q in the neighborhood of μQ using Taylor's series as:

$$SF = h(Q) = h(\mu_{QX}) + \frac{1}{1!}(Q - \mu_Q)\frac{dh}{dQ} + \frac{1}{2!}(Q - \mu_Q)^2\frac{d^2h}{dQ^2} + \frac{1}{3!}(Q - \mu_Q)^3\frac{d^3h}{dQ^3} + \cdots \quad (7.10)$$

where derivatives are evaluated at the point $Q = \mu_Q$.

Figure 7.9 compares the results of MCSM and First Order Second Moment method for the example presented in Table 7.4. Mean values of both distributions are similar, and just one failure mechanism occurred in this example. The difference between the probabilities of safety factor of less than 1 in these two methods is less than 10% that could be seen in Figure 7.9.

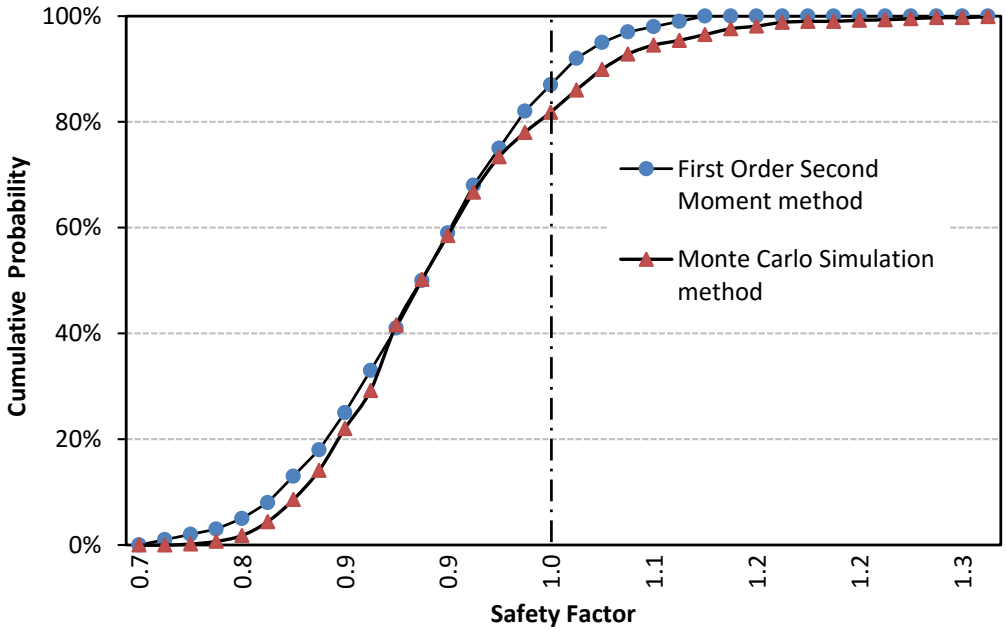

Figure 7.9 MCSM versus MAMs (MCSM, FOSM)

7.3.3 Results of Rosenblueth method and comparison with MAM and MC simulations

The Rosenblueth Point Estimation Method was applied in order to obtain the probability function of safety factor for the same example. As explained in section 2.3, this model can be used for two random variables or more. However, in following example only one variable was taken into account to make the comparison with the results of Monte Carlo Simulation and First Order Second Moment analysis. On the other hand, the variability of the other parameters could be smaller. The function of random variable Q_n can be defined as:

$$SF = h(x) = h(Q_n) \tag{7.11}$$

The average and variance of Q_n for the example of one variable according to Table 4 is taken as μQ_n= 600 m^3/s and σQ_n= 150 m^3/s.

$$h_1 = h(\mu Q_n + \sigma Q_n) = h(450) = 1.19$$
$$h_2 = h(\mu Q_n - \sigma Q_n) = h(750) = 1.04$$
$$P_j = \frac{1}{2}(j = 1,2)$$

$$\mu_{SF} = \sum_{1}^{2} P_j\, h_j = \frac{1.28 + 0.8}{2} = 1.11$$

$$\sigma_{SF}^2 = \left(\sum_{1}^{2} P_j\, h_j^2\right) - \mu_{SF}^2 = 1.7 - 1.23 = 0.00562$$

$$\sigma_{SF} = 0.075$$

It is assumed that $SF = h(Q_n)$ is normally distributed and $Z \sim N(\mu_{SF}, \mu_{SF}^2)$, Then the reliability index β is (G.B Baecher and J.T. Cristian 2003):

$$\beta = \frac{\mu_{SF} - 1}{\sigma_{SF}} = 1.53$$

Then, failure probability will become:

$$P_f = 1 - \Phi(\beta) = 1 - 0.068 = 93.2\%$$

In Figure 7.10 the results of the three methods are compared for the example in Table 4. A correlation among three methods can be observed. The functions provided by Monte Carlo Simulation and First Order Second Moment method have closer values as the means of the distributions are the same. Rosenblueth method gives a different mean value. The probability of failure ($SF < 1$) which represented the direct block erosion increases only around 5% from MCSM to FOSM and RPEM. The higher probability of failure is calculated by RPEM in this example.

The asymmetric result for the safety factor as a reliability function and the balance of the correlation coefficient causes the different mean. However, the standard deviation is similar.

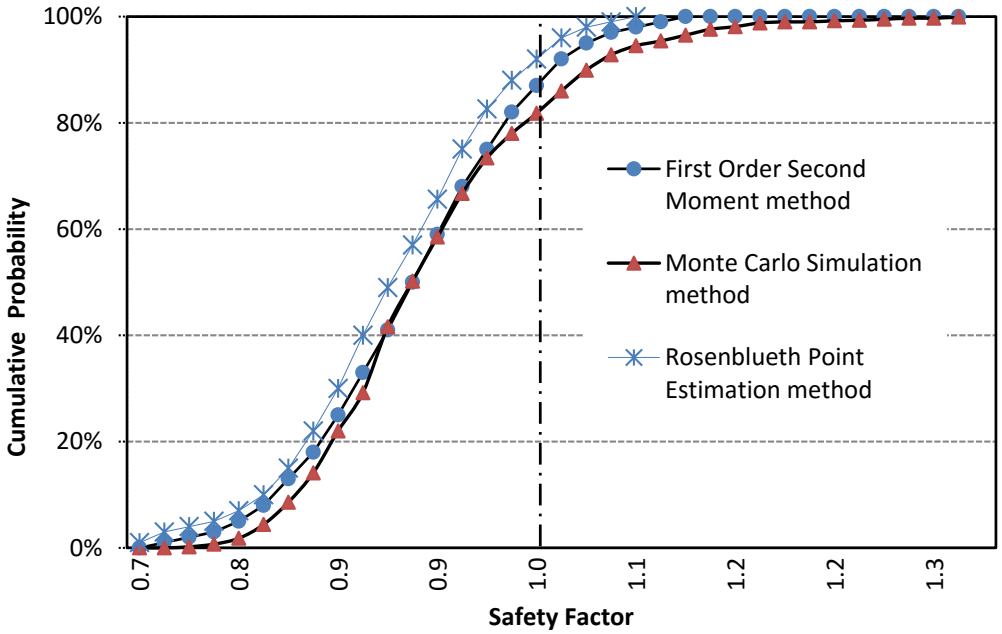

Figure 7.10 MCSM versus Moment Analysis and Point Estimation Methods (FOSM, MCSM, and RPEM)

The higher moments also were checked, and slight changes were shown in this example and can thus be neglected. Since we put other parameters as variables like block size (wide block size distribution) or the slope variation or bed level variation, the MAMs could not be accurate and Monte Carlo Simulation needs more runs. In this situation, the Rosenblueth point estimation could be a convenient model to reach the probability function of failure.

7.4 Conclusion

The potential failure probabilities of ripraps have been evaluated by using Monte Carlo Simulation and MAM as well as Rosenblueth Point Estimation Method. The advantages of the probabilistic model are the flexibilities on covering different failure mechanisms and utilization as a multivariate probabilistic method. Herein, the results were compared with the mentioned methods. MCSM is categorized in the full probabilistic level in risk assessment. Monte Carlo Simulation results are the most accurate ones that have the most precise results depending on the number of iterations. The results of other methods as the first levels showed good correlation though.

The study also reveals the sensitivity of different parameters in riprap design and sediment transport. The most sensitive mechanism of failure found as toe scouring which is related to the bed level variation. The bed level variation as the principal variable and the geometry and hydraulic parameters can change the state of the river bank riprap. This simulation method can be implemented on the water surface, and bed load calculation models. This allows applying the method on other rivers for computing the probability of failure based on prevailing sediment transport regime. The final goal is to have an assessment of the failure risk of riverbank riprap and other flood protection measures under changed flood and sediment yield scenario in the future under climate change.

.

Chapter 8

Application of Probabilistic Model on Swiss Rivers: Kleine Emme and Brenno

In this chapter the application of the model explained in chapter 7 on two Swiss rivers is presented. The chosen rivers, Kleine Emme and Brenno, are described and the development of the model based of sediment transport prediction and probabilistic simulations are explained. Finally, the example of modelling is presented to show the probability of failure in each section in different mechanisms for two rivers.

8.1 Introduction

To apply the probabilistic model on a real condition explained in chapter 7, two Swiss rivers, the Kleine Emme and the Brenno (Figure 8.1 and Figure 8.2) are selected. Bedload transport prediction of these two rivers has been studied in Swiss Federal Institute for Forest, Snow and Landscape Research (WSL) based on model sedFlow. (Heimann et al, 2015). Based on their study, the Kleine Emme was chosen since extensive data are available to validate the model sedFlow and could be the representative of pre-alpine river due to testing the model in this catchment. The Brenno river was selected as a case study to include a wide range of channel gradients as an alpine river. In this chapter, the river Kleine Emme which is located in the pre-alpine area of central Switzerland is analyzed to define the probability of failure in each section (Fig. 8.1). The river is located in an area of 477 km^2 with length of 58 km and drains into the Reuss at Reussegg (presented by Geoportal Kanton Luzern, 2013). The Kleine Emme is a mountain river catchment with mild slopes, with no glaciers inputs and with only the impact of hydropower installations, however, with variations by fluvial engineering. (FOEN, 2005) (Heimann et al, 2015).

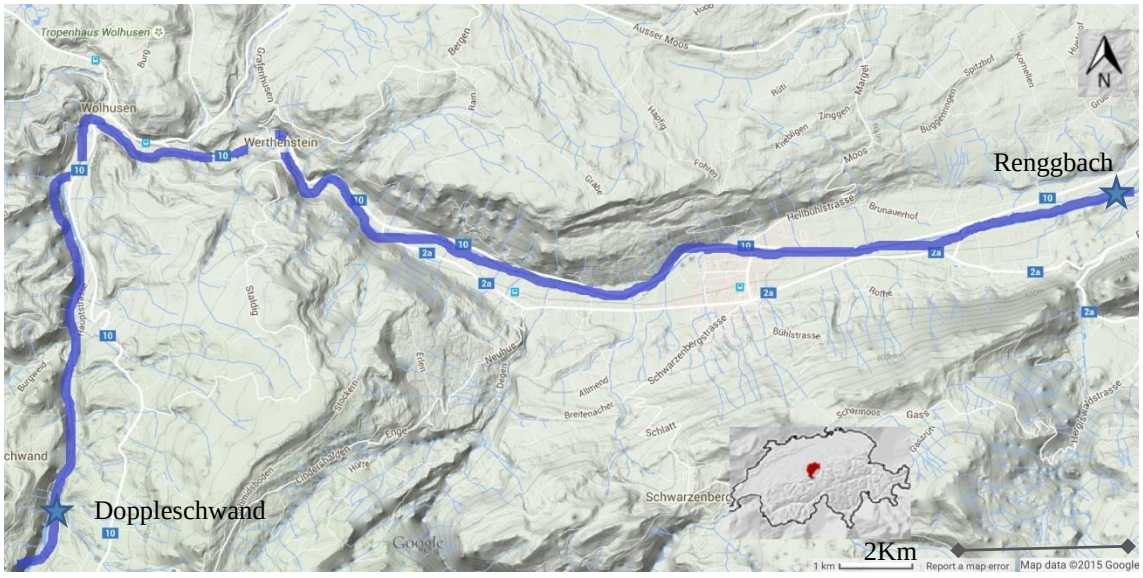

Figure 8.1 The Kleine Emme catchment in central Switzerland from Doppleschwand to the confluence with the Renggbach is shown by the blue line.

For the reach scale analysis, a total length of 20 km of the Kleine Emme was simulated by sedFlow, starting downstream of Entlebuch and continuing until Littau, which is located 5 km upstream of the confluence with the Reuss.

Figure 8.2 The Brenno catchment in southern Switzerland from Olivone to Biasca is shown by the blue line.

The Brenno is situated in southern Switzerland (Fig. 8.2) and flows into the river Ticino. Its drainage area is 397 km^2. The two catchments are impacted and show a range of engineering constructions like many mountain catchments. The Kleine Emme is marked by river training works, including numerous bottom sills and riprap revetments

in some locations. The Brenno is strongly influenced by controls on water and sediment delivery to the channel. The Brenno's hydrology is considerably influenced by hydropower production.

The two catchment areas have similar size but channel is steeper in the Brenno river than in the Kleine Emme. In the Kleine Emme, channel bank erosion is the most important parameter in feeding sediment to the transport system, in the Brenno lateral sediment input due to debris flows from tributaries was important during the calibration period (Heimann et al, 2015).

In summary, the two study catchments differ substantially and present a range of characteristics common to many mountain catchments. Several channel cross sections are periodically surveyed for both rivers. In the case of the Kleine Emme, they are measured by the Swiss Federal Office for the Environment (FOEN) and in the case of the Brenno, they are measured by the authorities of the canton of Ticino. Cross-sectional profiles are recorded at 200 m intervals in the Kleine Emme and at about 150 m intervals in the Brenno. For the Kleine Emme measurements from September 2000 to November 2005 is used. Measurements from April 1999 to June/July 2009 are used for the Brenno.

8.2 Model development

The probabilistic model developed in chapter 7 can be applied on the rivers according the output of WSL study.

A bivariate copula model fitting developed in WSL which has provided the probability of occurrence due to two parameters:

1. Flood volume which is defined as the sum of the complete discharge between the start and end of a flood. The start of a flood is defined as the point in time, at which discharge exceeds some threshold discharge, and the end of a flood is defined as the point in time, at which discharge again falls below the same threshold discharge. For example, in Kleine Emme the 2005 event volume is chosen to be folded to range of volume factors.
2. The peak of flood which is related to the return period.

The probability of occurrence for nine different volume factors (0.8 ~ 2.0 for Kleine Emme and 0.87 ~ 1.51 for Brenno) and nine return period peak factors (30 to 300 year floods) are obtained and model sedFlow were run for these. The shapes of flood volumes are chosen as three different historical flood events in each catchment. The other outputs were discharge, bed levels, channel slope and maximum flow depth for 154 reaches in Kleine Emme and 160 reaches in Brenno. Eighty-one probabilistic conditions for three different Scenarios (historical flood events shape) are developed.

For one flood scenario in one reach the probability of Toe Scouring, Overtopping, Direct block erosion and remaining Stable (in 4 different risk level) are obtained. Then the probability of 1) Most occurred mechanism and 2) First occurred mechanism are calculated. Then the probability calculation of all 81 conditions for three flood scenarios in two rivers are performed (totally 243 conditions). Safety factor regarding the direct block erosion is taken in 4 level of risk. From SF = 1 to 1.4 with elapse of 0.1.

The results are shown in following charts (Figure 8.4 to Figure 8.5) as examples based on three assumptions by varying block sizes, angle of repose, riprap bank slope and riprap foundation height represented in Table 8.1. Assumptions I, II and III are shown in Table 8.1 as well. Appendix 3 presents some of the results of simulations in both rivers.

Table 8.1 parameters notation of model

Notation	Description	Unit	Comments
r	River Id	—	
e	Elevation Reach Id	—	
s	Scenario Id	—	
c	Condition Id	—	
t	Time Elapsed	sec	
$H_{f_{re}}$	Riprap Foundation Height	m	$= (I)0.8, (II)0.4, (III)\ 0.2$
$D_{B_{re}}$	Block Size	m	$= (I)0.8, (II)0.65, (III)\ 0.5$
β_{re}	Riprap Bank Slope	°	$= (I)45, (II)\ 45, (III)\ 45$
φ_{re}	Angle of Repose	°	$= (I)60, (II)55, (III)\ 50$
$S_{B_{re}}$	Block Specific Gravity	—	$= 2.65$
P_{re}	Cross Section Point Id	—	
$x_{P_{re}}$	X of Cross Section Point	m	
$z_{P_{re}}$	Z of Cross Section Point	m	Level from origin
p_{rc}	Probability of Condition	—	
L_{resct}	Bed Elevation	m	Level from origin
J_{resct}	Bed Slope	—	
h_{resct}	Water Depth	m	
SF_{resct}	Safety Factor	—	
SS_{resct}	Safety or Failure State	—	TS Toe Scouring OT Over-topping DBE Direct Block Erosion S Stable
$p_{SS^F_{res}}$	Probability of First Occurrence of Safety State	—	
$p_{SS^M_{res}}$	Probability of Most Occurrence of Safety State	—	

Here is the model development in levels of defining probability of failure in each mechanism and final results in each reach.

For each r, e, s, c, t: (8.1)

$$L_{resct} < z_{B_{re}} - H_{f_{re}}$$
$$\rightarrow SS_{resct} = TS$$
$$\nrightarrow L_{resct} + h_{resct} > z_{T_{re}}$$
$$\rightarrow SS_{resct} = OT$$
$$\nrightarrow SF_{resct} < 1.4$$
$$\rightarrow SS_{resct} = DBE$$
$$\nrightarrow SS_{resct} = S$$

$$SF_{resct} = \frac{1}{2}\frac{\tan \varphi_{re}}{\tan \alpha_{re}}\left(\sqrt{\xi_{resct}{}^2 + 4} - \xi_{resct}\right)$$

$$\xi_{resct} = \frac{7.7 h_{resct} J_{resct} \tan \varphi_{re}}{\left(S_{B_{re}} - 1\right) D_{B_{re}} \sin \alpha_{re}} \text{Aggregation}$$

For each r, e, s, c, SS:

$$R_{SS_{resc}} = \frac{\underset{resc}{\text{count}}\, SS_{resct}}{\underset{resc}{\text{count}}\, r}$$

$$SS^{F}_{resc} = SS_{resct} \text{ where } t = \min_{resc} t_{SS_{resct}}$$

$$SS^{M}_{resc} = SS_{resct} \text{ where } R_{SS_{resc}} = \max_{resc} R_{SS_{resc}}$$

For each r, e, s, SS:

$$p_{SS^{F}_{res}} = \sum_{c}^{N_c} p_{re} \text{ where } SS_{resc} = SS^{F}_{resc}$$

$$p_{SS^{M}_{res}} = \sum_{c}^{N_c} p_{re} \text{ where } SS_{resc} = SS^{M}_{resc}$$

8.3 Results

The Figure 8.3 shows the limits of failure in one flood scenario. Figures 8.4 and 8.5 are the result of two assumptions in one flood scenario and one occurrence condition of failure.

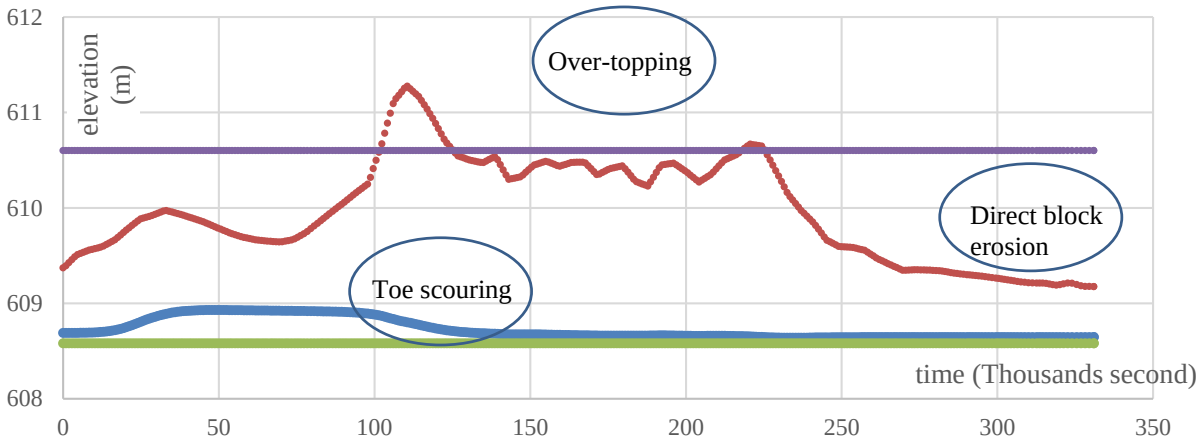

Figure 8.3 The limit of each failure mechanism during one flood.

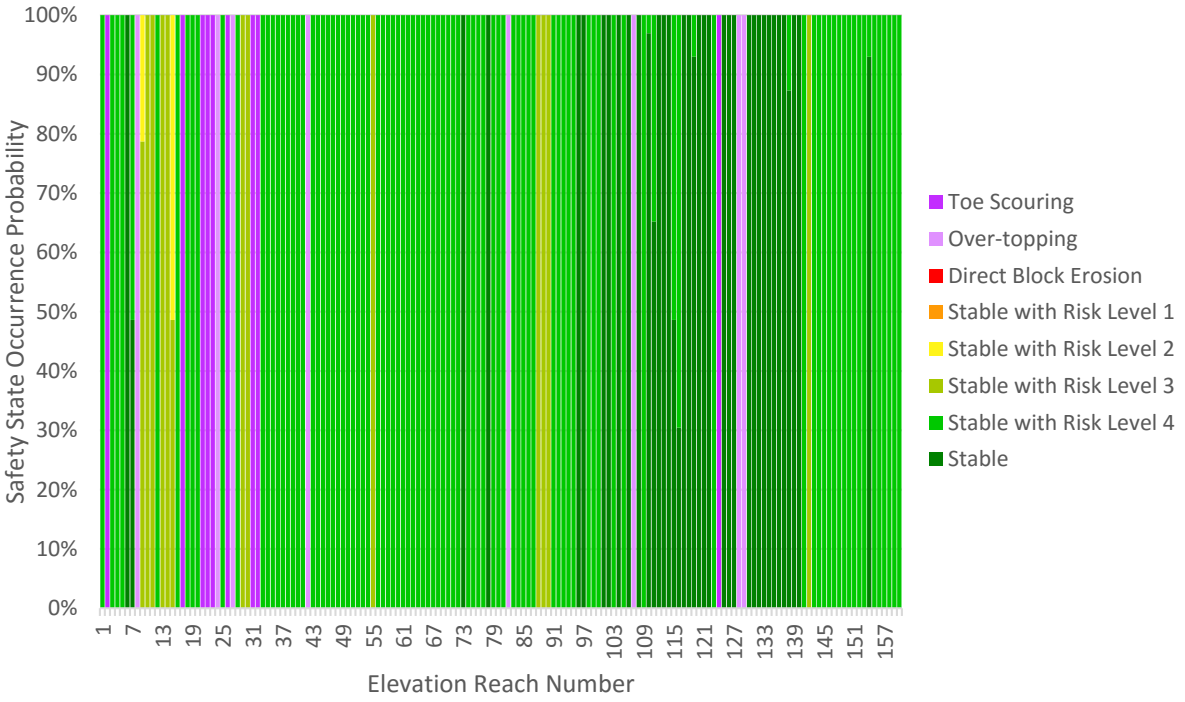

Figure 8.4 The probability of failure in different mechanism for the scenario of flood in Brenno in 1987, first occurrence mechanism and assumption I

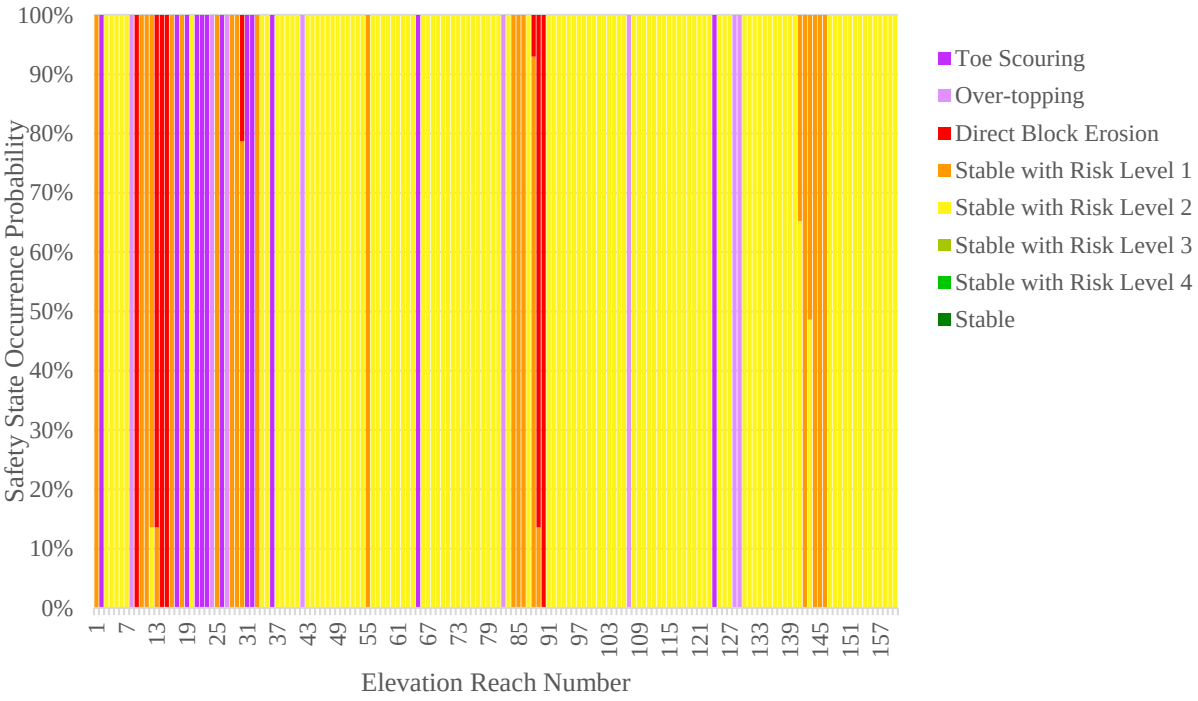

Figure 8.5 The probability of failure in different mechanism for the scenario of flood in Brenno in 1987, first occurrence mechanism and assumption II

8.4 Conclusion

This chapter presented the application of probabilistic model on two different rivers of Switzerland. The Kleine Emme which is located in pre-alpine catchment in centre of Switzerland and Brenno which is in southern part of this country are analysed to define the riprap failure status. The model was run based on the result of sedFlow model developed in WSL to predict the flood and sediment transport in river catchment due to flood regime changes in future. Critical parameters are derived to define the status of failure in terms of toe scouring, over-topping, direct block erosion and stability based on safety factor over one in four different risk levels. This results are based on bivariate probabilistic model of peak and volume of various floods in different return periods.

This method has the flexibility of defining different mechanisms of failure. The examples presented in this chapter and Appendix 3 show that how the failure status can be changed by varying the parameters. The vulnerability of the river reach can be measure in case of unexpected flood to rehabilitate and proactive actions of protecting river bank riprap. This model could be used to define risk maps for the application concerns.

Chapter 9

Conclusions and Recommendations

9.1 Introduction

Stream power in mountain rivers has impact on the channel stability and risk of scouring the bed and bank. Therefore, the erodible river banks need to be protected against the possible scouring, practically during the flood events. Among all kind of river bank protection measures, riprap is one of the most frequently used protection to avoid bank erosion. Destruction or collapsing of riverbank will result in uncontrolled flooding and lateral erosion with displacement of meanders and the formation of braided river patterns. These processes can have catastrophic consequences on urban areas and infrastructures especially along Alpine rivers. Thus, an optimum design which provide a safe condition is crucial. Riprap design has been developed for a long time. Thus, several methods of riprap sizing are mostly derived for dumped median size blocks. However, in mountain rivers and steep channels, extra stability can be provided by packing the large blocks and individually positioned riprap. This model of installation has been rarely studied and it was the motivation of current study to analyse the stability and design of such packed

riprap. In Chapter 1, main questions illustrated the motivation and concerns of the present research. The answers achieved based on the experimental data obtained in systematic laboratory tests and also the probabilistic modelling. The outcomes of this research is as following:

9.2 Sizing riprap

The sizing of large block riprap, i.e. the design of the required block weight, for river bank protection in steep mountain rivers was studied taking into account the minimum possible spaces among the blocks when they are placed individually. The involved parameters are the diameter of the riprap blocks *D*, the longitudinal channel slope *S*, the bank slope of the riprap β and the hydraulic conditions. The stability of packed riprap is evaluated and analysed through a vast dataset of 98 one layer riprap experiments carried out with varying flume slopes, bank slopes and size of the blocks. Thirty-four dumped riprap laboratory tests are also performed in order to have a comparison with existing design methods of dumped riprap.

By comparing the 34 dumped riprap tests with the existing design methods, good agreement with design equations of HEC-11 (1998) and EM-1601 (1994) was obtained confirming the experimental setup. The bank slope effect could be reproduced correctly regarding the limit between stable or failed condition. However, the existing equations for dumped riprap overestimated also the size of blocks in some of the tests performed with dumped riprap.

The failure occurs when the blocks are eroded and slide down; then the section becomes unstable. The detailed data analysis as well as the visual observations reveal that, under the same hydraulic conditions, the tests with packed blocks, are more stable and considerably delay the process of bank failure. The channel slope as a design parameter has the strongest effect on the block erosion rate and the failure time. The block erosion decreases significantly for packed riprap due to interlocking between the blocks when they are closely packed by individual placement in the prototype.

An empirical, new relationship between the relative roughness and the modified Froude number is proposed. The definition is based on the boundary between stability and failure providing the required size of the blocks remaining stable for certain hydraulic

conditions. This relationship results smaller block sizes for the stable condition for packed block riprap when comparing it with dumped blocks. The new empirical relationship can be also used to re-evaluate the stability of existing packed riprap facings. The following equation for designing the optimum block size for individually placed riprap, based on Froude number, relative roughness and bank slope modified by repose angle of blocks, is herein proposed:

$$D = 0.22 C_f \, h\left(\frac{V}{\sqrt{((S_B-1)gh)}}\right)^{0.88} \qquad \text{(cf. equation (4.11))}$$

Where h is flow depth, V is the mean velocity, and C_f is a factor of bank slope effect (cf. equations (4.13) and (4.14)). This study shows the significant effect of bank slope on the stability of the blocks. The results revealed that by increasing the bank slope the C_f increases and the size of the blocks should be greater to be resistant against the flood. The empirical relationship has been validated by a logistic classification approach comparing to the experimental transition condition.

9.3 Time to failure

The influence of the use of packed block riprap on the time to failure was analysed in detail. Particular attention was given to the time to failure defined as the duration of the experiment until the riprap collapsed totally over the whole bank height. A maximum duration of the flume tests of three hours was used which covers roughly a 15 hour flood duration when taking into account a typical scale factor of (1:25). This duration may be considered as sufficient for flood durations in typical Alpine rivers.

Classical stability criterion for dumped riprap are typically limited to the steady boundary condition which means that the total failure occurs at the time of the first movement as a direct block erosion. It means that the failure occurs very fast once the first blocks are eroded and transported downstream. For packed riprap, the criterion of failure is strongly linked to the time to failure. Complete sliding or erosion of the riprap over the whole bank height in a certain channel section, defined as complete failure, occurs only after a specific duration of block erosion. Thus, a time-dependent analysis of failure was implemented.

The time to failure depends on the tested parameters as block size, channel slope, and specific discharge. The slope of the channel has a significant effect on the characteristic time to failure for all tested block size. However, larger block sizes not only postponed the time to failure but also reduced the block erosion rate for a fixed longitudinal slope.

A clear relationship between the time to failure and the bed shear stress adimensionalized with the block size could be found. Nevertheless, the best results were obtained using an approach of adimensionalizing the time to failure based on the flow depth. The relationship gave the possibility of estimating roughly the time to failure for the tests which remained stable (cf. Figure 5.6). The results revealed that the range of erosion, which is defined as the number of eroded blocks, is not increased severely comparing to the predicted normalized time to failure.

9.4 Effect of a second layer in packed riprap

The effect of thickness, respectively the effect of a second layer on the stability of packed and packed riprap as riverbank protections was studied with 23 additional experiments with two layers of riprap. Empirical results are presented in terms of longitudinal channel slope, riprap side slopes and thickness of the protection layer. The influence of a second layer in the riprap protection is considered on both the time to failure and sizing of riprap.

For the same longitudinal channel slope and bank slope, the second layer had a stabilizing effect and postponed the failure. However, the block erosion rate is increased significantly, since the upper layer has to be eroded first and attachment between blocks are less than the blocks and filter.

By increasing the discharge, the effect of second layer reduced. It means that in the lower discharges, thus, the second layer has more influence on the stability of the riprap for lower failure discharge.

Regarding the riprap bank slope, a double layer riprap is more stable for higher bank slope comparing to a single layer. The longitudinal slope of the channel is the most dominant parameter. Nevertheless, the effect of the second layer in higher channel slope showed to be reduced comparing to the lower channel slope.

A time-dependent analysis shows that the characteristic time to failure has a functional relationship with dimensionless shear stress (τ^*) and the longitudinal slope. The two layer tests resist for higher bed shear stresses at the same time to failure. In the other word, for identical flow forces acting on the blocks, the characteristic time to failure is higher for a double layer riprap. The second layer is more stabilizing when the riprap bank slope becomes close to the repose angle of the blocks.

In this study, tests with the occurrence of failure and tests, which remained stable are compared, and the boundary between failed and stable tests is defined, representing the critical boundary for failure. The same functional relation proposed sizing stable riprap in equation (4.11) had good agreement with double layer tests results. Finally, as the second layer stabilizes the protection system considerably, in addition to delaying the failure time, in practical terms the blocks can be designed in a smaller size riprap with higher thickness.

9.5 Probability analysis of failure

The potential failure probabilities of ripraps have been evaluated by using MCSM and MAM as well as RPEM. The probability of failure is defined for the three different mechanisms of failure, namely toe scouring, overtopping and direct block erosion. The advantages of the probabilistic model are the flexibilities on covering different failure modes and utilization as a multivariate probabilistic method. MCSM is categorized in the full probabilistic level in risk assessment. Monte Carlo Simulation results are the most accurate ones, which has the most precise results depending on the number of iterations. The results of other method as the first levels showed a good correlation though.

This study also reveals the sensitivity of different parameters in riprap design and sediment transport. Toe scouring was found as the most sensitive mechanism of failure, which is strongly related to the bed level variation as a result of bed load transport conditions. The bed level variation as the principal variable and the geometry and hydraulic parameters can change the stability state of the river bank riprap. This probabilistic failure simulation method can be implemented in water surface and bed load calculation models. This allow to compute the probability of failure based on prevailing flow and sediment transport regime. The final goal is to have an assessment of the failure

risk of riverbank riprap and other flood protection measures under changed flood and sediment yield scenario in the future under climate change. The application of the model was run on two rivers of Switzerland Kleine Emme and Brenno. The input data of sediment transport in these two rivers was based on the model sedFlow developed in WSL and present the probability of failure for riverbanks as riprap protects them under flood uncertainties.

9.6 Recommendations for future research

The present investigation is inherently limited to a relatively small number of configurations that partially covers the broad range of influent factors on the stability of large and packed blocks. In addition, the experiments presented herein were conducted under idealized conditions, and the results only refer to supercritical flow and with fixed bed. To deepen the knowledge about the design of this arrangement of blocks applied in mountain rivers, the following topics are proposed for future laboratory and numerical investigations:

• Systematic laboratory experiments with mobile bed can be conducted in order to study the influence of this parameter on the time to failure of the riprap. Other mechanisms of failure in laboratory tests as toe scouring is possible to investigate by applying a mobile bed.

• Other configurations in terms of bank and bed slope, block size and gradation, variation of thickness and filter behind the riprap are further parameters which could be addressed.

• Most of the existent design methods for dumped riprap over-estimate the required block size in the case of packed riprap and result in a non-economical design. Field investigation regarding the porosity of packed riprap and angle of repose of large blocks can be the next step.

Finally, the probabilistic simulations to study of the risk of failure constitutes a quite challenging and interesting topic, which would provide an excellent tool for predicting the evolution of risk under flood uncertainties in future (e.g. climate change).

Bibliography

Abt, S.R., and Johnson, T.L. (1991). “Riprap design for overtopping flow.” *Journal of Hydraulic Engineering*, 117(8):959–972.

Abt, S.R., Thornton., C.I., Gallegos H.A., and Ullmann C.M. (2008). “Round-shaped riprap stabilization in overtopping flow.” *Journal of Hydraulic Engineering*, 134(8):1035. doi: 10.1061/(ASCE)0733-9429(2008)134:8(1035)

Ahmed, A.F. (1988). “Stability of riprap side slopes in open channels.” Thesis, University of Southampton, UK.

Anderson, A.G., Paintal, A.S., and Davenport, J.T. (1970). *Tentative design procedure for riprap lined channels*.” National Cooperative Highway Research Program Report, No. 108. University of Minnesota Minneapolis, MN.

Ang, A.H.S., and Tang, W.H. (2007). *Probabilistic concepts in engineering emphasis application to civil and environmental engineering*. John Wiley and Sons, New York.

Bedford, T., and Cooke, R. (2001). *Probabilistic risk analysis*. Cambridge University Press, UK.

Blodgett, J.C., and McConaughy, C.E. (1986). “Rock riprap design for protection of stream channels near highway structures; Volume 2, Evaluation of Riprap design procedures” *Water-Resources Investigations Report*, No. 86-4128. US Geological Survey, Sacramento, CA.

Bogardi, J.L. (1978). *Sediment transport in alluvial streams*. Akademiai Kiado, Budapest, Hungary.

Brown, S.A. and Clyde, E.S. (1989). Design of riprap revetment. *Hydraulic Engineering Circular*, 11. Federal Highway Administration, McLean, VA.

California Division of Highways (CDH). (1970). *Bank and shore protection in California highway practice.* California Department of Public Works, Sacramento, CA.

Cardoso, A., and Fael, C. (2009). “Protecting Vertical-Wall Abutments with Riprap Mattresses.” *Journal of Hydraulic Engineering*, 135(6):457–465.

Carter, A.C., Carlson, E.J., and Lane, E.W. (1953). “Critical Tractive Forces on Channel Side Slopes in Coarse, Non-Cohesive Material,” *Hydraulic Laboratory Report*, No. HYD-366. US Department of the Interior, Bureau of Reclamation, Denver, CO.

Center for Civil Engineering Research and Codes (CUR). (1995). *Manual on the use of rock in hydraulic engineering*. Rijkswaterstaat, Balkema, Rotterdam, Netherlands.

Chang, H. H. (1998). "Riprap stability of steep slopes." *International Journal of Sediment Research*, 13(2):40–50.

Conciatori, D., Brühwiler, E., and Morgenthaler, S. (2009). "Calculation of reinforced concrete corrosion initiation probabilities using the Rosenblueth method." *International Journal of Reliability and Safety*, 3(4):345–362.

De Almeida, G.A.M, and Martin-Vide, J.P. (2009). "Riprap stability: Transverse and longitudinal versus continues protections." *Journal of Hydraulic Engineering*, 135:447–456. doi: 10.1061/(ASCE)HY.1943-7900.0000031

Einstein, H.A. (1950). *The bed-load function for sediment transportation in open channel flows*. Technical Bulletin 1026, US Department of Agriculture, Soil Conservation Service, 70 pp.

Escarameia, M., and May, R. W. P. (1992). "Channel Protection. Turbulence downstream of structures." Report SR313. HR Wallingford, London.

Froehlich, D.C., and Benson, C.A. (1996). "Sizing dumped rock riprap." *Journal of Hydraulic Engineering*, 122(7):389–396.

Froehlich, D.C. (2011). "Sizing loose rock riprap to protect stream bank." *River Research and Application*, 29(2):219–235. doi: 10.1002/rra.1587

Froehlich, D.C., and Benson, C.A. (1996). Sizing dumped rock riprap. *Journal of Hydraulic Engineering*, 122(7):389–396. doi: 10.1061/(ASCE)0733-9429(1996)122:7(389)

Ghilardi, T., M. J. Franca, and A. J. Schleiss (2014). *Sediment transport in steep channels with large roughness elements*, River Flow 2014, Lausanne, Switzerland, Taylor & Francis Group, London, ISBN 978-1-138-02674-2.

Grace, J.L., Jr., Calhoun, C.C., Jr., and Brown, D.N. (1973). "Drainage and erosion control facilities: Field performance investigation." Miscellaneous paper H-73-6. US Army Engineer Waterways Experiment Station, Vicksburg, MS.

Graf, W.H. (1996). *Hydraulics of sediment transport*. Water resources publications, LLC, Colorado.

Haldar, A., and Mahadavan, S. (2000). *Probability, reliability and statistical methods in engineering design*. John Wiley and Sons, Inc.

Hartford, N.D., and Baecher, G.B. (2004). *Risk and uncertainty in dam safety*. Thomas Telford, London.

Hemphill, R.W., and Bramley, M.E. (1989). *Protection of river and canal banks*. Construction Industry Research and Information Association, Butterworths, London.

Heimann, F.U.M., Rickenmann, D., Böckli, M., Badoux, A., Turowski, J.M., and Kirchner, J.W. (2015). "Calculation of bedload transport in Swiss mountain rivers using the model sedFlow: Proof of concept." *Earth Surface Dynamics*, 3:35–54. doi: 10.5194/esurf-3-35-2015, 2015.

Hersberger, D.S. (2002). "Wall Roughness effects on flow and scouring in curved channels with gravel-bed." Communication 14 du Laboratoire de Constructions Hydrauliques (LCH), EPFL, Lausanne, pp. 413.

Iman, R.L., Helton, J.C., and Campbell, J.E. (1981). "An approach to sensitivity analysis of computer models, Part 1. Introduction, input variable selection and preliminary variable assessment." *Journal of Quality Technology*, 13(3):174–183.

Ippen, A.T., and Drinker, P. (1962). "Boundary Shear Stresses in Curved Trapezoidal Channels." *Journal of the Hydraulics Division*, 88(5):143–179.

Isbash, S.V. (1935). "Construction of dams by dumping stones in flowing water." A. Dovjikov, tr. War Department, US Engineer Office, Engineering Division, Eastport, ME.

Jafarnejad, M., Franca, M.J., Pfister, M., Schleiss, A.J. (2013). "Time dependent failure analysis of compressed riprap as riverbank protection." *Proceedings of 2013 IAHR Congress, Chengdu.*

Jafarnejad, M., Franca, M.J., Pfister, M., and Schleiss A.J. (2014). "Effect of compressed riprap thickness on the stability of river banks." in *Proceedings of the International conference on fluvial Hydraulics*. Taylor and Francis Group, CRC Press, London, pp. 2069–2074.

Jafarnejad, M., Pfister, M., and Schleiss, A.J. (2012). "Failure risk analysis of riverbank ripraps with Monte Carlo Simulation." in *Proceedings of the International conference on fluvial Hydraulics*. Taylor and Francis Group, CRC Press, London, pp. 1325–1330.

Julien, P.Y. (2002). *River mechanics*. Cambridge University Press, London.

Kassa, N.A. (2009). *Probabilistic safety analysis of dams- methods and applications.* Thesis, University of Dresden, Germany.

Kikkawa, H., Ikeda, S., and Kitagawa, A. (1976). "Flow and bed topography in curved open channels." *Journal of the Hydraulics Division*, 102(9):1372–1342.

Köplin, N., Schädler, B., Viviroli, D., and Weingartner, R. (2012). "Relating Climate Change Signals and Physiographic Catchment Properties to Clustered Hydrological Response Types." *Hydrology and Earth System Sciences*, 16(7):2267–2283. doi: 10.5194/hess-16-2267-2012.

Kuo, J.T., Yen, B.C., Hsu, Y.C., and Lin, H.F. (2007). "Risk analysis for dam overtopping-Feitsui reservoir as a case study." *Journal of Hydraulic Eng*ineering, 133(8):955–963.

Lagasse, P.F., Clopper, P. E., Zevenbergen, L. W., and Ruff, J. F. (2006). "Riprap Design Criteria, Recommended Specifications, and Quality Control" NCHRP Report 568. National Cooperative Highway Research Program, Transportation Research Board, National Academy of Sciences, Washington, DC.

Lane, E.W. (1955). "Design of stable channels." *Transactions,* 120(2776):1234–1279.

Lane, E.W. (1952). "Progress Report on Results of Studies on Design of Stable Channels," Hydraulic Laboratory Report No. HYD-352. Bureau of Reclamation, Denver, CO.

Li, R.M., Simons, D.B., Blinco, P.H., and Samad, M.A. (1976). Probabilistic approach to design of riprap riverbank protection. in *Rivers 76: Proceedings of the Symposium on Inland Waterways for Navigation, Flood Control, and Water Diversions*, Vol. I. American Society of Civil Engineering, Fort Collins, CO, pp. 1572–1591.

Maynord, S.T. (1992). "Riprap stability: Studies in near-prototype size laboratory channel." *Technical Rep. HL-92-5*, U.S. Army Engineer Waterways Experiment Station, Vicksburg, Miss.

Maynord, ST., and Neill, C. (2008). "Riprap Design". In *Sedimentation Engineering*, García, M.H., ed. ASCE Manual and Reports on Engineering Practice No. 110. American Society of Civil Engineering, Reston, VA, pp. 1037-1056. doi: 10.1061/9780784408148

Maynord, S.T., Ruff, J.F., and Abt, S.R. (1989). "Riprap design." *Journal of Hydraulic Engineering,* 115(7):937–949.

Maynord, S.T., Ruff, J.F., and Abt, S.R. (1991). Closure of Discussion on Riprap design. *Journal of Hydraulic Engineering,* 117:542–544.

Neill, C.R. (1967). "Mean velocity criterion for scour of coarse uniform bed-material." *International Association for Hydraulic Research, 12th Congress*, Paper C6, 3, C6.1-C6.9.

Papanicolaou, A.N., Diplas, P., Dancey, C.L., and Balakrishnan, M. (2001). "Surface roughness effects in near-bed turbulence implications to sediment entrainment." *Journal of Engineering Mechanics*, 127(3):211–218.

Permanent International Association of Navigation Congress (PIANC). (1987a). "Guidelines for the design of flexible revetments incorporating geotextiles for inland waterways." Supplement to Bulletin 57, Brussels, Belgium.

Permanent International Association of Navigation Congress (PIANC). (1987b). "Risk consideration when determining bank protection requirements." Report of permanent technical committee 1, Supplement to Bulletin 58. Brussels, Belgium.

Peterka, A.J. (1963). "Hydraulic design of stilling basins and energy dissipators." *Engineering Monograph No. 25*. US Bureau of Reclamation, Denver, CO.

Pilarczyk, K.W. (1990). “Coastal protection.” Short Course on Coastal Protection. Delft University of Technology. Balkema, Rotterdam, Netherlands.

Racin, J.A. (1996). “California bank and shore rock slope protection design: Practitioner`s guide and field evaluation of riprap methods.” Final Rep. FHWA-CA-TL-95-10, Caltrans Study F90TL03. Sacramento, CA.

Recking, A., and Pitlick, J. (2013). “Shields versus Isbash.” *Journal of Hydraulic Engineering*, 139(1), 51–54. doi: 10.1061/(ASCE)HY.1943-7900.0000647

Reese, A. (1984). “Riprap sizing four methods.” In *Proceedings of the ASCE Hydraulics Division Specialty Conference.* American Society of Civil Engineering, New York.

Richardson, E.V., and Davis, S.R. (2001). “Evaluating Scour at Bridges,” Hydraulic Engineering Circular No. 18 (HEC-18, Fourth Edition), Report FHWA NHI-01-001, Federal Highway Administration, Washington, DC.

Rickenmann, D. (1997). “Sediment transport in Swiss torrents.” *Earth Surface Processes and Landforms*, 22:937–951.

Robinson, K.M., Rice, C.E., and Kadavy, K.C. (1997). “Rock chutes for grade control.” Pp. 211–216 in *Proceedings of conference on management of landscapes disturbed by channel incision*. University of Mississippi, Oxford, MS.

Rosenblueth, E. (1975). “Point estimates of probability moments.” in *Proceedings of National Academy of Science*. Washington, DC, pp. 3812–3814.

Schleiss, A.J. (1998). “Bemessung und Gestaltung von Blockwürfen an Gebirgsflüssen [Design and landscape integration of riprapin mountain rivers].” *Interpraevent. Villach. Tagungspublikation,* 2:351–360.

Schleiss, A.J. (2007). *Amenagements de cours d'eau*, Note de cours. EPFL, Lausanne.

Simarro, G., Civeira, S., and Cardoso, A.H. (2012). “Influence of riprap apron shape on spillthrough abutments.” *Journal of Hydraulic Research*, 50(1):138–141.

Simons, D.B., and Senturk, F.Y. (1992). *Sediment Transport Technology*. Water Resources Publications, Fort Collins, CO.

Smart G.M. (1984). “Sediment transport formula for steep channels.” *Journal of Hydraulic Engineering*, 110(3):267–276.

Stephenson, D. (1979). *Rockfill in hydraulic engineering*. Elsevier, Amsterdam, Netherlands.

Stevens, M.A., Simons, D.B., and Lewis, G.L. (1976). “Safety factors for riprap protection.” *Journal of the Hydraulics Division,* 102(5):637–655.

Stevens, M.A., Simons, D.B., and Richardson, E.V. (1984). "Riprap stability analysis." *Transportation Research Board, Transportation Research Record* 2:209–216.

Straub, L.G. (1953). "Dredge fills closure of Missouri River at Fort Randall." in *Proceedings of Minnesota International Hydraulics Convention*. WMC Brown Co., Minneapolis, MN, pp. 61–75.

Terrell, P.W., and Borland, W.M. (1958). "Design of Stable Canals and Channels in Erodible Materials," *Transactions*, 123:101–115.

Thoft-Christensen, P., and Backer, M.J. (1982). *Structural reliability theory and its application*. Springer-verlag, Berlin.

Thoft-Christensen, P., and Murotsu, Y. (1986). *Application of structural system theory*. Springer-verlag, Berlin.

Townson, J.M. (1988). "The simulated motion of a loose revetment block." *Journal of Hydraulic Research*, 26(2):225–242. doi: 10.1080/00221688809499226

Turowski, J.M., Yager, E.M., Badoux, A., Rickenmann, D., and Molnar, P. (2009). "The impact of exceptional events on erosion, bedload transport and channel stability in a step-pool channel." *Earth Surface Processes and Landforms*, 34:1661–1673. doi:10.1002/esp.1855

Ulrich, T. (1987). "Stability of rock protection on slopes." *Journal of Hydraulic Engineering*, 113(7):879–891. doi: 10.1061/(ASCE)0733-9429(1987)113:7(879)

US Army Corps of Engineers (USACE). (1987). "Hydraulic design of navigation dams." EM 1110-2-1605. US Government Printing Office, Washington, DC.

US Army Corps of Engineers (USACE). (1990). "Hydraulic design of spillways." EM 1110-2-1603. US Government Printing Office, Washington, DC.

US Army Corps of Engineers (USACE). (1994). "Hydraulic design of flood control channels." EM 1110-2-1601. US Government Printing Office, Washington, DC.

Vulliet, L. (2011). *Fiabilité et sécurité de systèmes civils*. Polycopié du cours. EPFL, Lausanne.

Whittaker J.G. (1987). "Modelling bed-load transport in steep mountain streams, Erosion and sedimentation in the Pacific Rim." *Proceedings of the Corvallis Symposium*. IAHS Publication no. 165.

Wittler, R.J., and Abt, S.R. (1988). "Riprap design by modified safety factor method." in *Proceedings of the 1988 National Conference on Hydraulic Engineering*. American Society of Civil Engineering, Colorado Sprongs, CO, pp. 143–148.

Appendix 1

Pictures of Selected Experiments

Some examples of experimental procedure are presented in next pages. The first three photos show the longitudinal channel in time of starting the tests, the time that failure occurs and after finishing the test. Last two pictures present the front view of before and after the tests.

Table A1.1 Configuration of test Double 8

Series	Number of layers	Block Size (m)	Slope of Channel (%)	Slope of Riprap (–)	q (m^2s^{-1})	h (m)	t_f (min)
Double 8	two	0.037	1.5	3.5V-5H	0.408	0.229	73

Table A1.2 Configuration of test Double 21

Series	Number of layers	Block Size (m)	Slope of Channel (%)	Slope of Riprap (–)	q (m^2s^{-1})	h (m)	t_f (min)
Double 21	two	0.037	3	3V-5H	0.209	0.150	NB

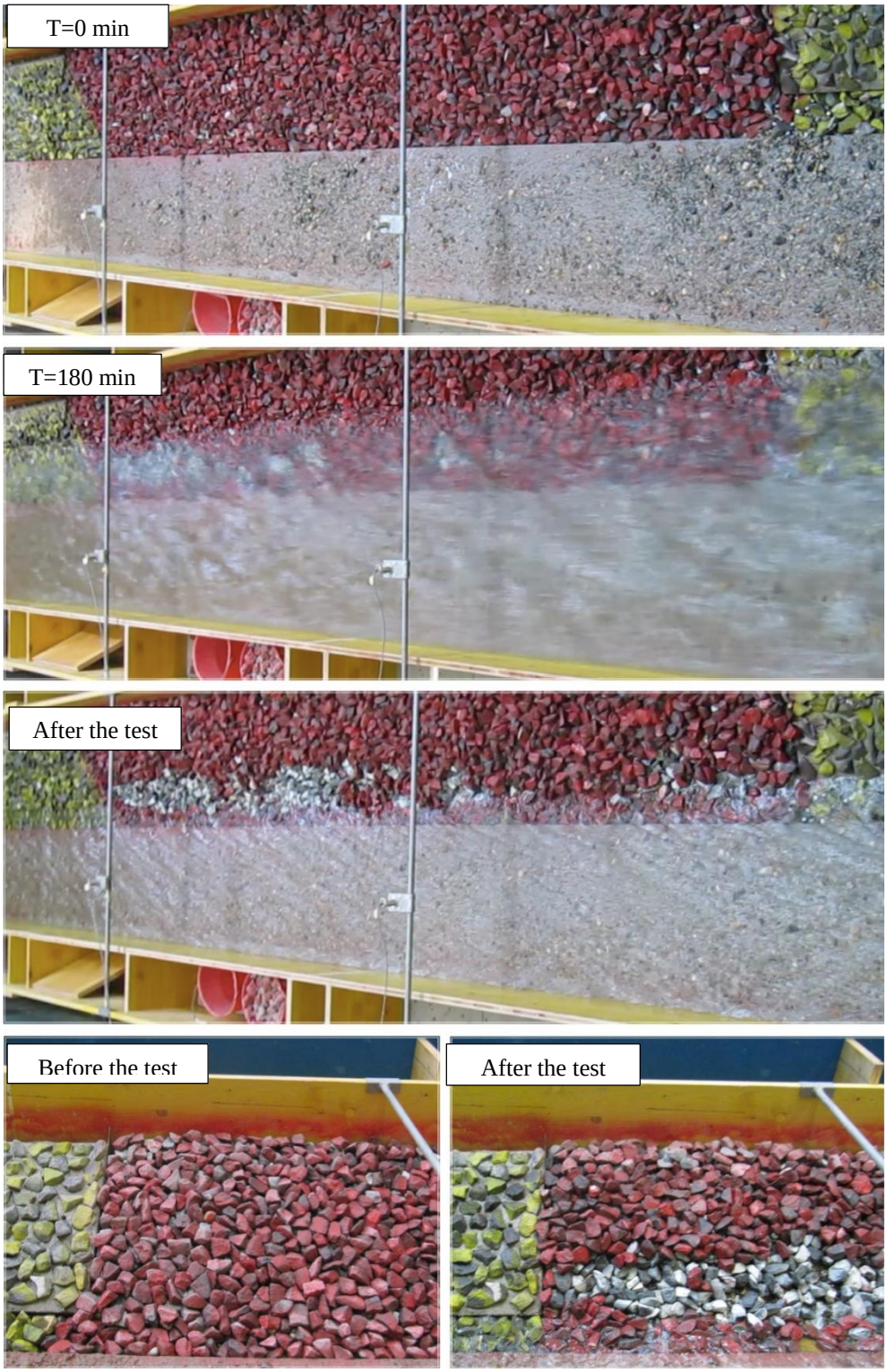

Table A1.3 Configuration of test 24

Series	Number of layers	Block Size (m)	Slope of Channel (%)	Slope of Riprap (–)	q (m^2s^{-1})	h (m)	t_f (min)
24	one	0.037	3	2.5V-5H	0.345	0.154	3

Table A1.4 Configuration of test 48

Series	Number of layers	Block Size (m)	Slope of Channel (%)	Slope of Riprap (–)	q (m^2s^{-1})	h (m)	t_f (min)
48	one	0.037	3	3V-5H	0.314	0.164	27

Table A1.5 Configuration of test 54

Series	Number of layers	Block Size (m)	Slope of Channel (%)	Slope of Riprap (–)	q (m^2s^{-1})	h (m)	t_f (min)
54	one	0.042	3	3V-5H	0.359	0.199	13

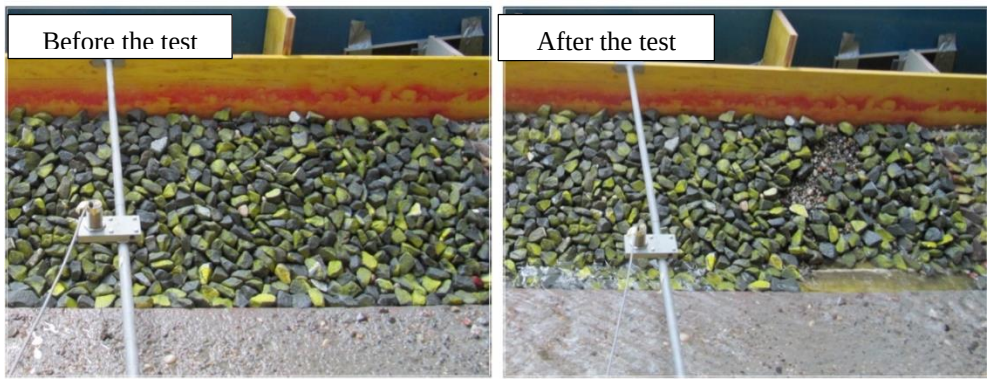

Table A1.6 Configuration of test 55

Series	Number of layers	Block Size (m)	Slope of Channel (%)	Slope of Riprap (–)	q (m^2s^{-1})	h (m)	t_f (min)
55	one	0.042	3	3V-5H	0.364	0. 201	6

Table A1.7 Configuration of test 43

Series	Number of layers	Block Size (m)	Slope of Channel (%)	Slope of Riprap (–)	q (m^2s^{-1})	h (m)	t_f (min)
43	one	0.047	3	3V-5H	0.438	0.205	148

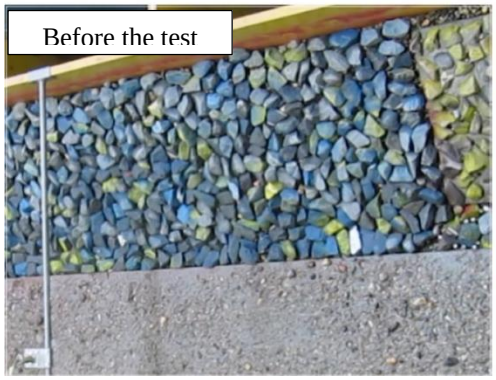

Table A1.8 Configuration of test 44

Series	Number of layers	Block Size (m)	Slope of Channel (%)	Slope of Riprap (–)	q (m^2s^{-1})	h (m)	t_f (min)
44	one	0.047	3	3V-5H	0.457	0.211	172

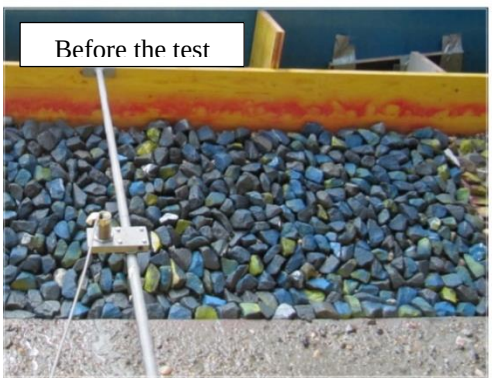

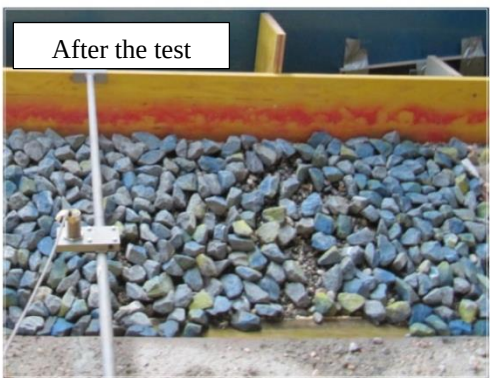

Appendix 2

Sensitivity Analysis of Monte Carlo Simulation

The Figures A2.1 to A2.3 show the variation of the probabilistic function of the failure probability. The sensitivity analysis for the case study indicates that the angle of riprap, shown in Figure A2.1 (left), has a relevant effect on the safety factor and direct block erosion while the other mechanisms can be neglected. However, the slope of the channel bed has also a significant impact on the failure of the riprap and not only changes the failure probability but also changes the failure mechanisms (Figure A2.1, right). Simulation shows that by decreasing the slope of channel the failure mode completely changes from overtopping to toe scouring. It means that the slope of channel is one of the dominant parameters. As shown in Figures A2.2 and A2.3, the rate of sediment supply and the height of riprap also have significant influences on the model. On the other hand, the grain size of the sediments (Figure A2.2 left) has no significant effect on failure of the riprap. The diameter of the blocks has an impact on probability of failure (Figure A2.3, left) but there is no significant change in failure modes. The sediment transport rate can influence the failure probability when it is reduced 20% (Figure A2.3 right). It can be witnessed that the failure mode changes totally from direct block erosion to toe scouring.

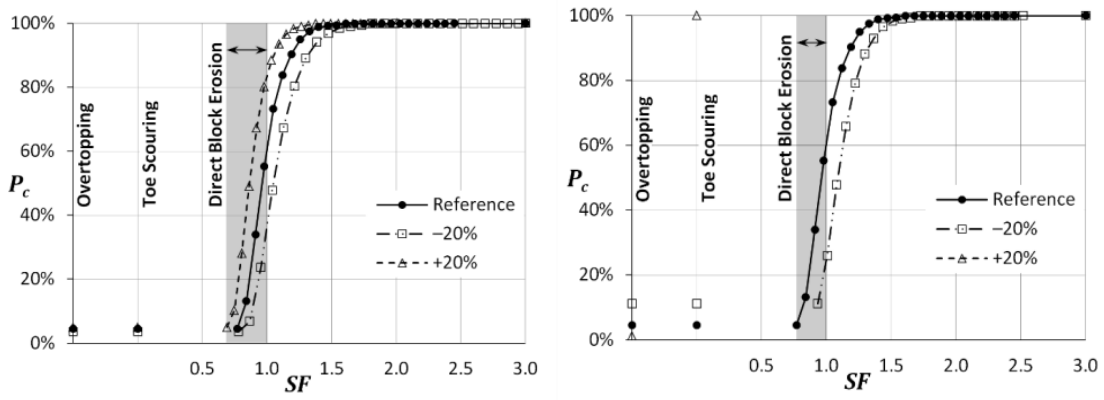

Figure A2.1 Probability of safety factor and failure modes with different slope angle of riprap (α) (left) and channel bed slope (S) (right)

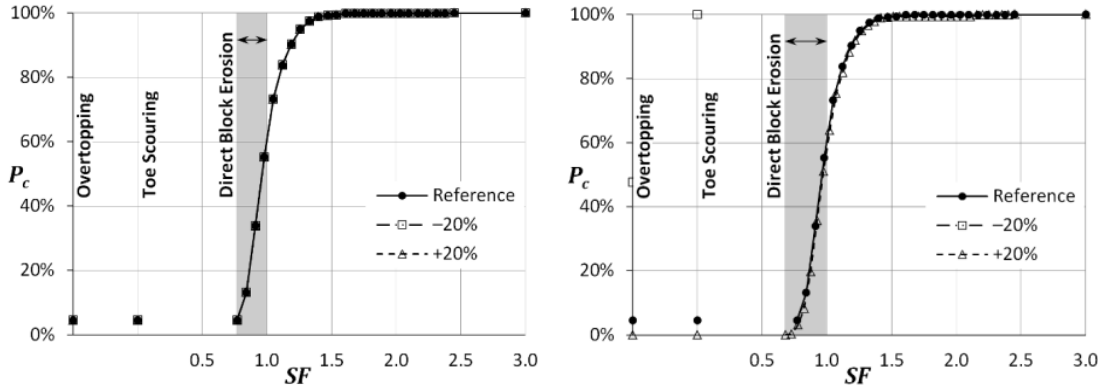

Figure A2.2 Probability values of safety factor and failure modes with different grain size (D_m) (left) and water level (h_i) (right)

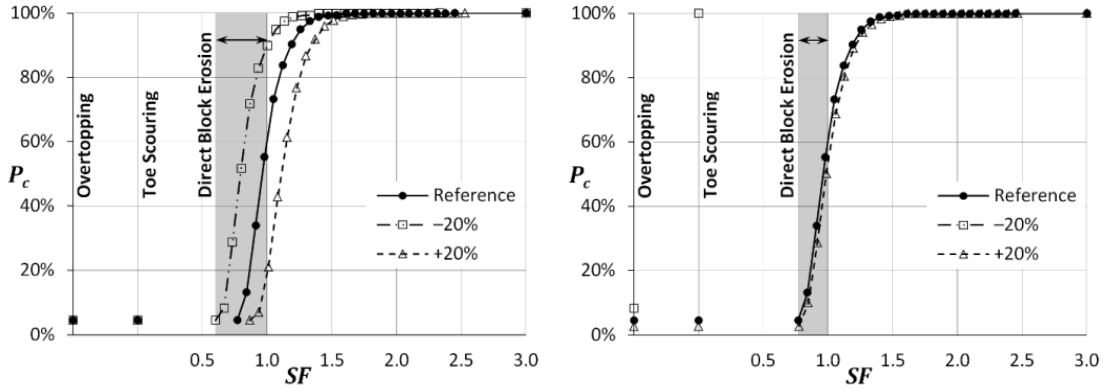

Figure A2.3 Probability values of safety factor and failure modes with different diameter of blocks (D_B) (left) and sediment transport rate (m_s) (right)

The potential failure probabilities of ripraps have been evaluated not only by Monte Carlo Simulation but also by First Order Second Moment analysis method. A sensitivity analysis of the case study showed that the most dominant parameters are slope of the

channel, height of the riprap and sediment transport rate. They change both the failure mechanisms and the probability of each failure modes. However, the diameters of the blocks and slope angle of riprap just have an impact on direct block erosion mode.

Appendix 3

Application of Probabilistic Model: Kleine Emme and Brenno

The application of the model explained in chapter 7 and 8 in two rivers are presented in Figures A3.1 to A3.15. Table A3.1 presents the definitions of failure status in different colours shown in Figures A3.1 to A3.15. The maps of Kleine Emme from Figure A3.1 to A3.7 are based on assumption of result set III, flood shape of November 1979 and as the first occurred condition. Table A3.2 shows that each reach is located in which distance from downstream of the Kleine Emme river.

The maps of Brenno from Figure A3.8 to A3.15 are based on assumption of result set II, flood shape of November 2002 and as the most occurred condition. Table A3.3 shows that each reach is located in which distance from downstream of the Brenno river.

Table A3.1 Definitions of failure status by colours used in results for both rivers

Mechanisms of Failure or Stability	Status Colour
Toe scouring	
Over-topping	
Direct block erosion	
Stable condition with risk level 1	
Stable condition with risk level 2	
Stable condition with risk level 3	
Stable condition with risk level 4	
Stable	

A3.1 Kleine Emme

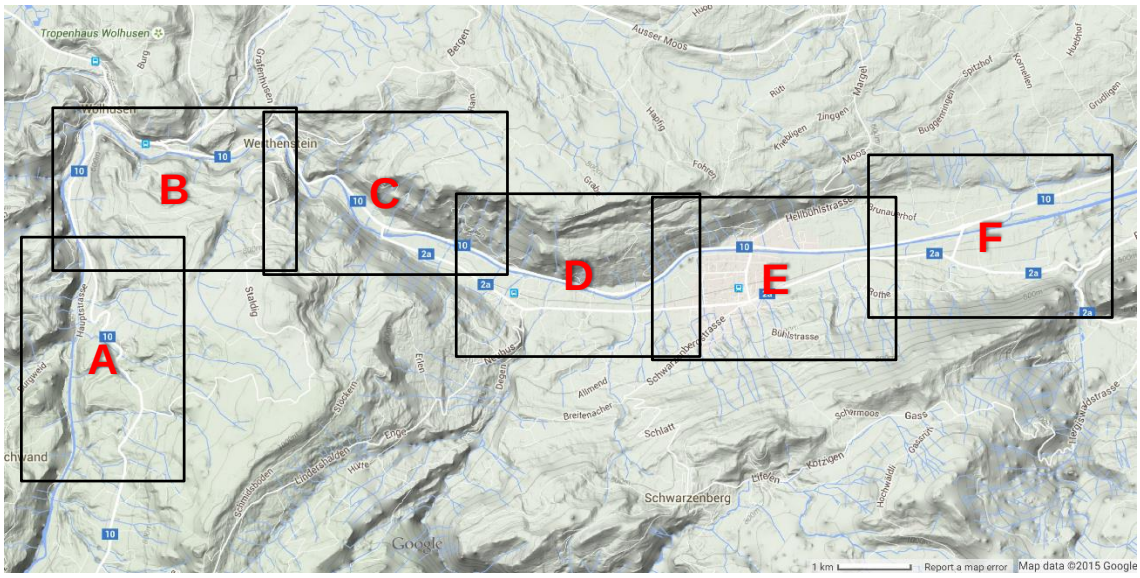

Figure A3.1 Kleine Emme Sheets

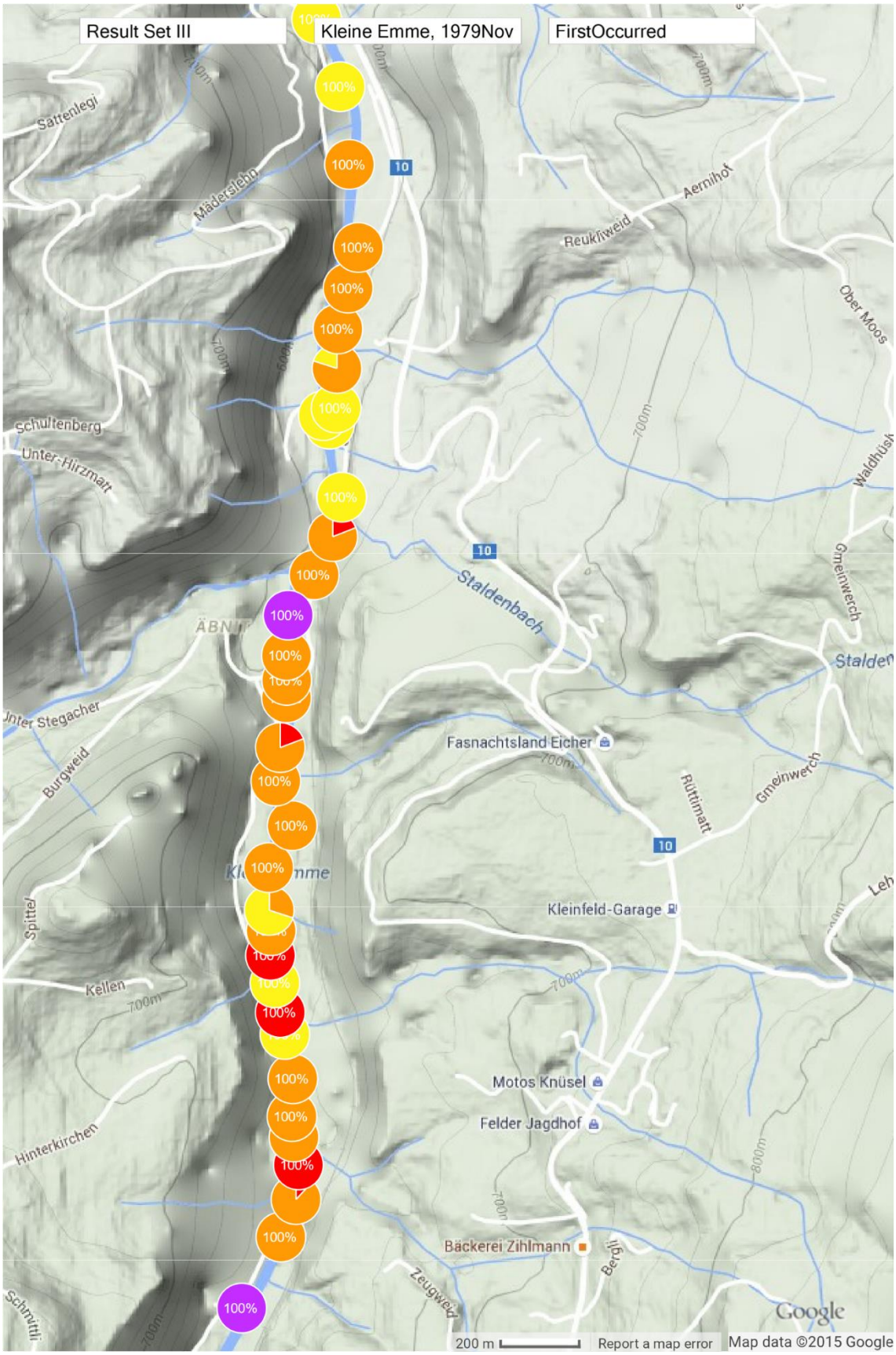

Figure A3.2 Kleine Emme Sheet A

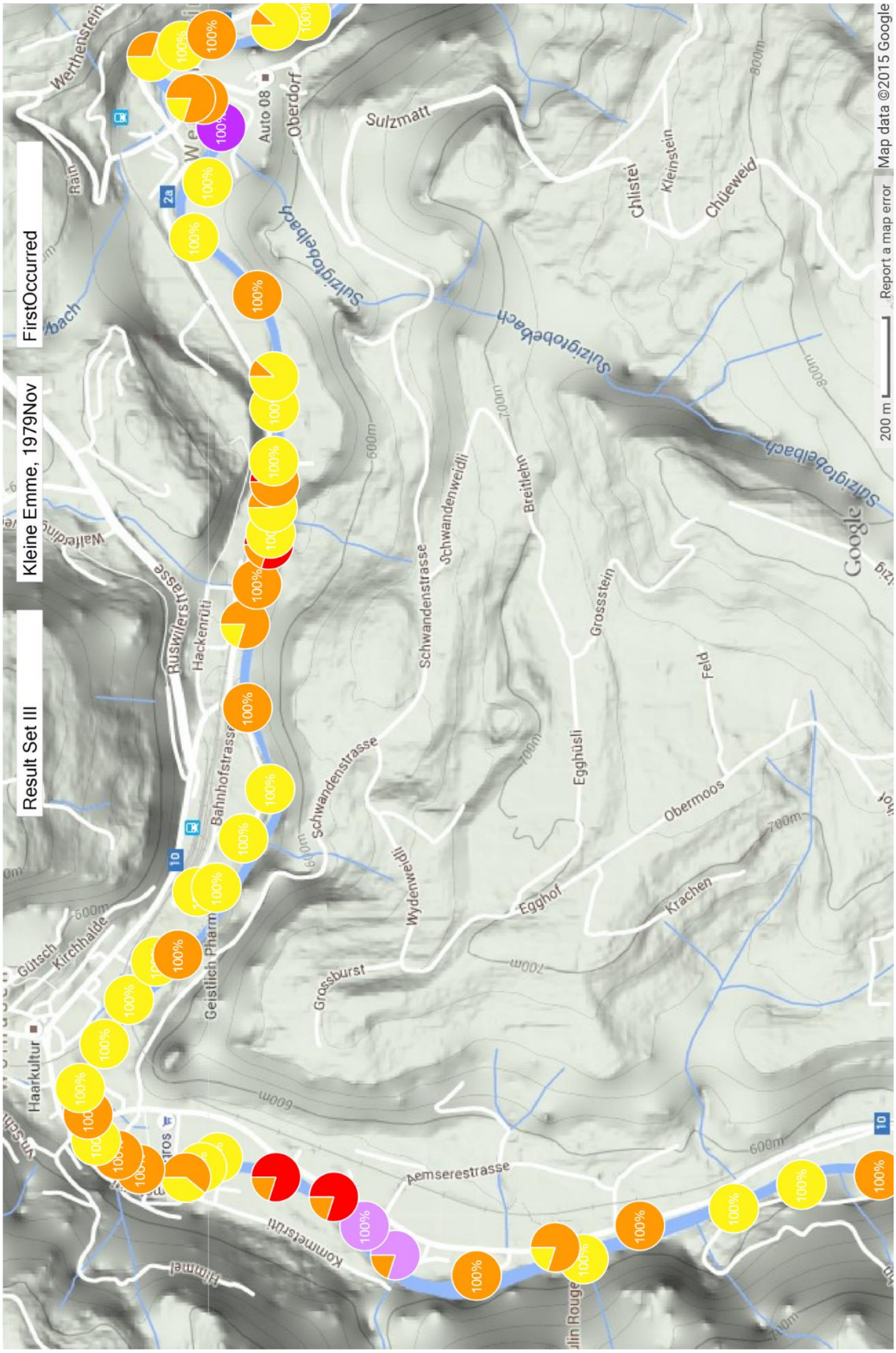

Figure A3.3 Kleine Emme Sheet B

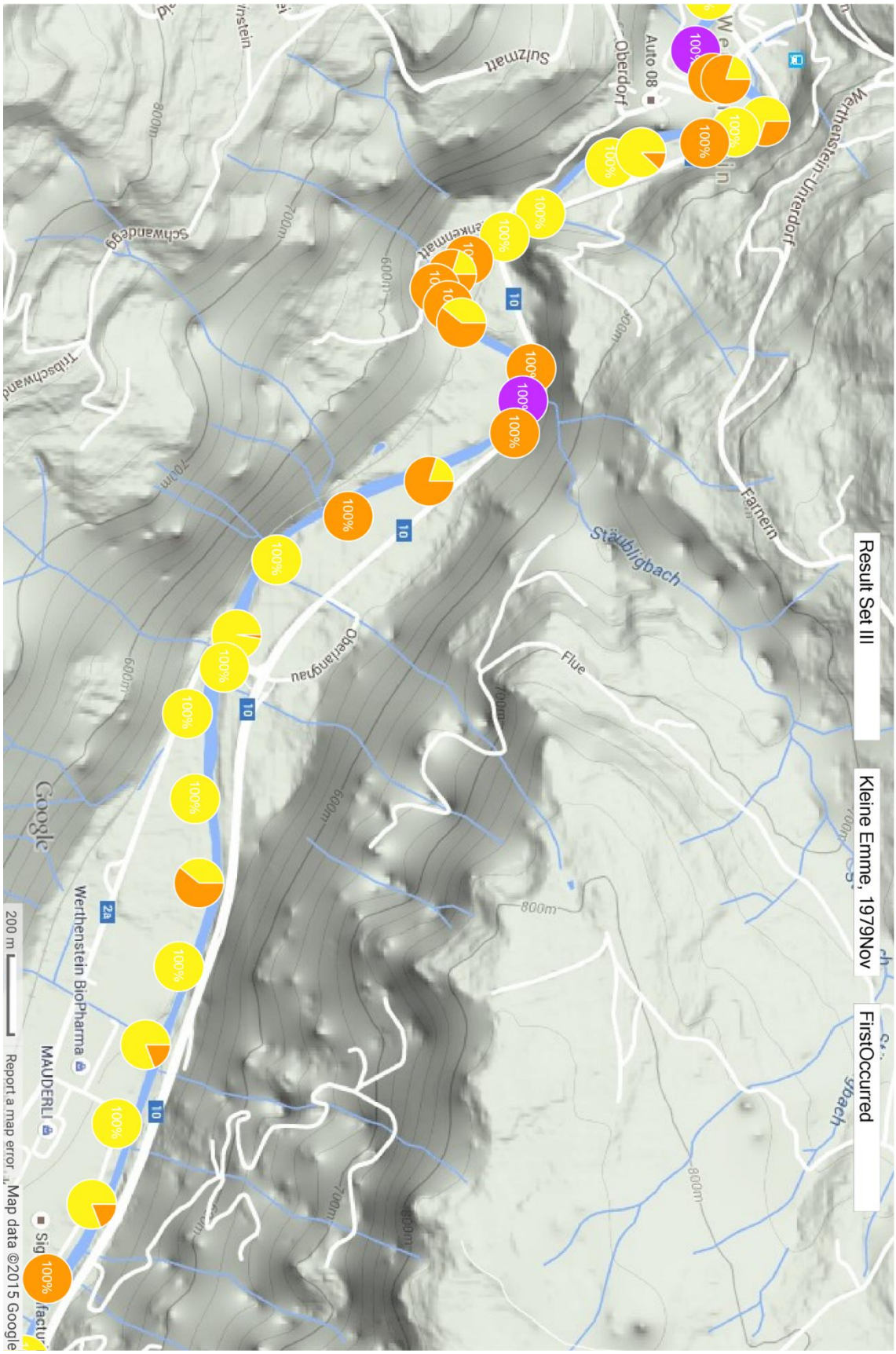

Figure A3.4 Kleine Emme Sheet C

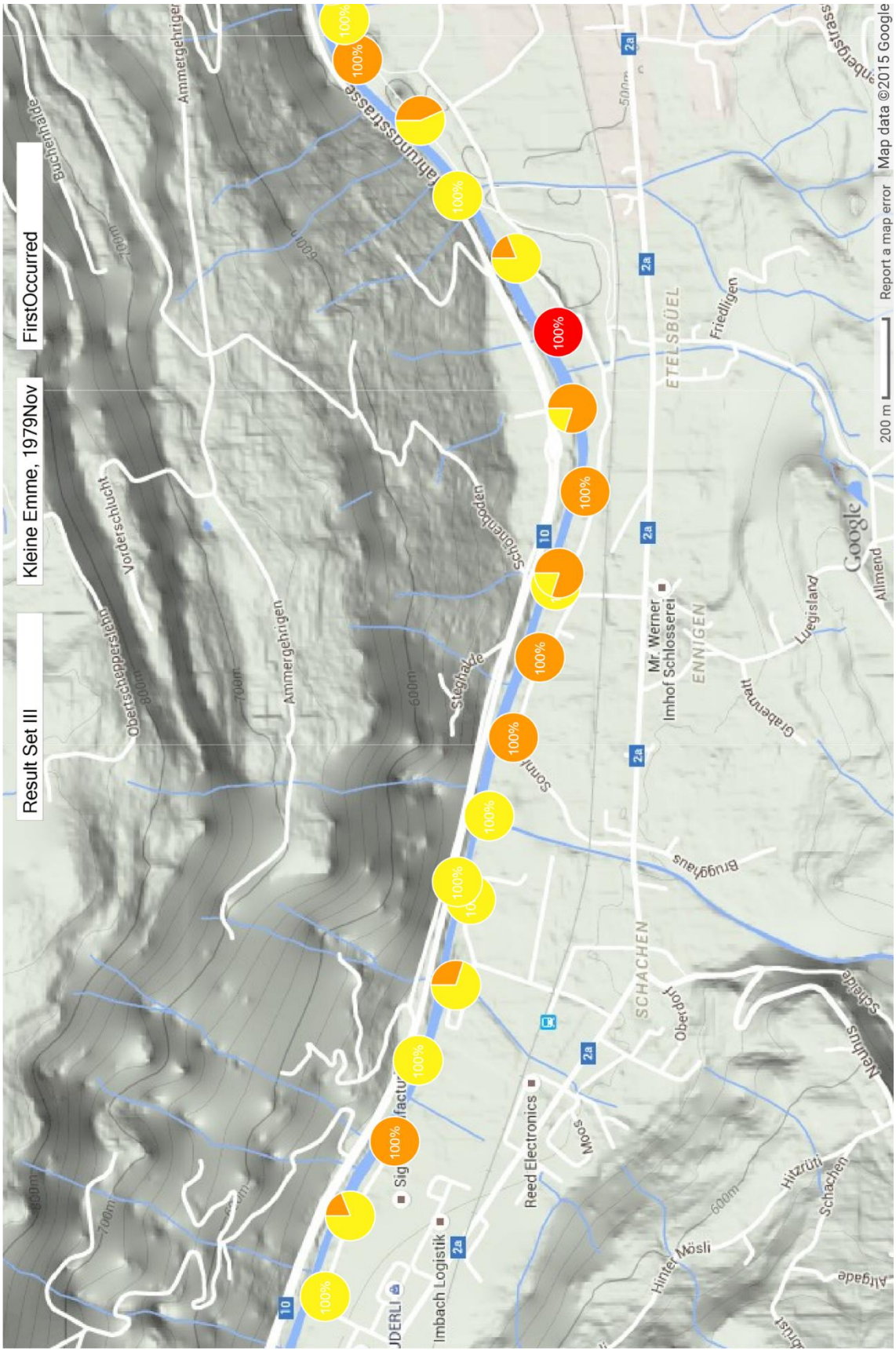

Figure A3.5 Kleine Emme Sheet D

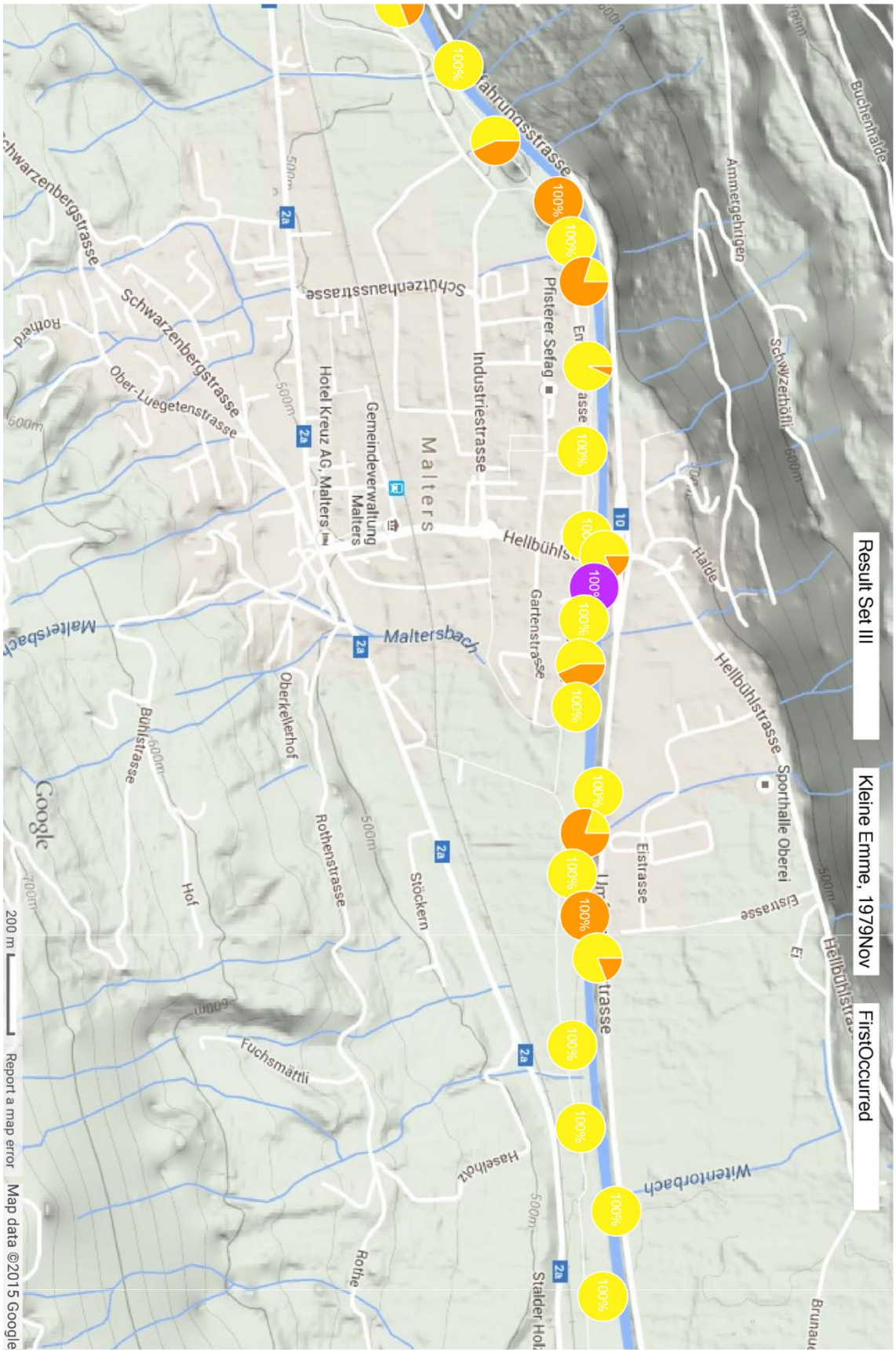

Figure A3.6 Kleine Emme Sheet E

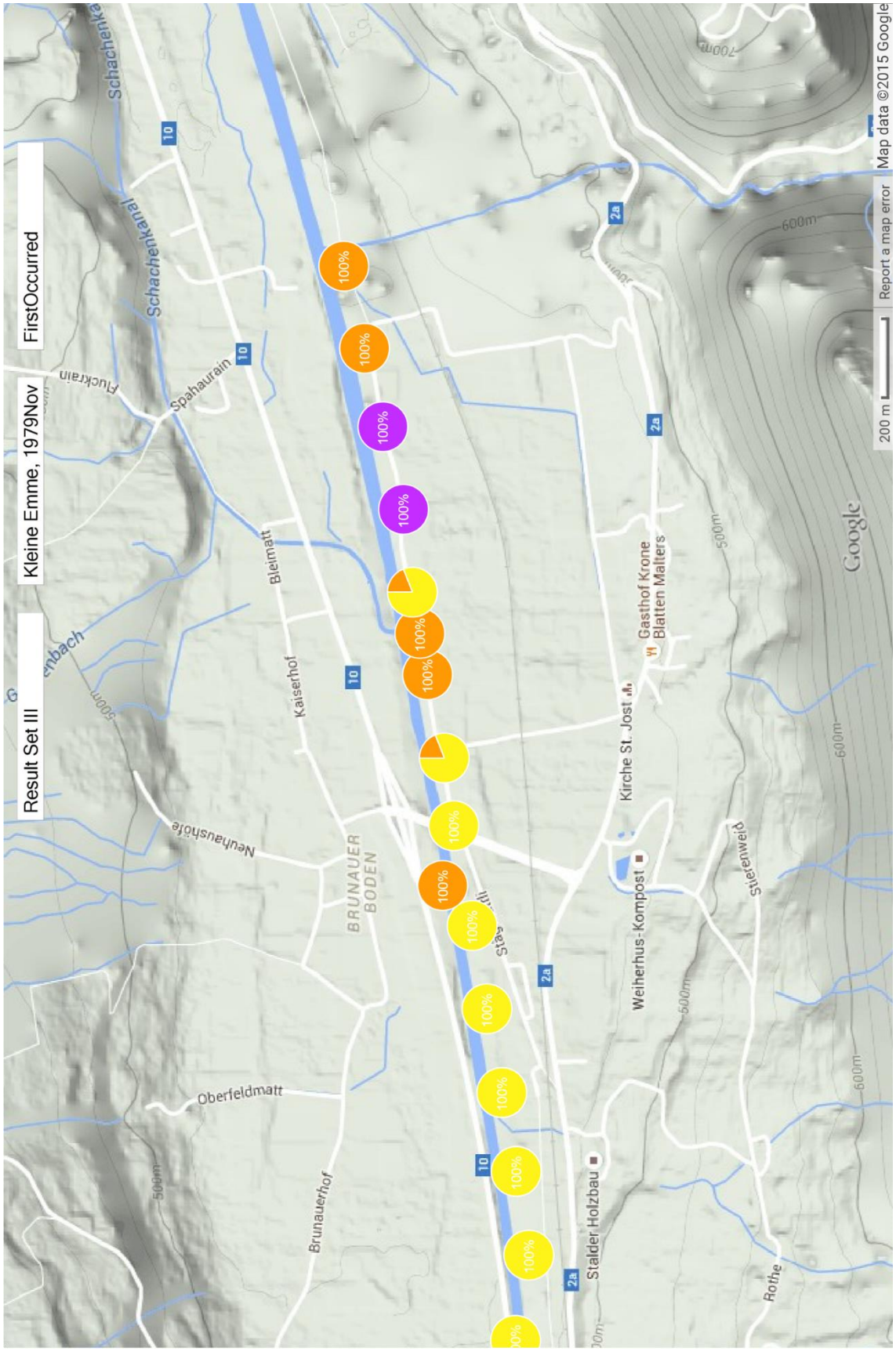

Figure A3.7 Kleine Emme Sheet F

Table A3.2 The Kilometrage of Kleine Emme Reach Ids

Reach Id	Km	Reach Id	Km	Reach Id	Km	Reach Id	Km
1	25.000	41	20.850	81	16.735	121	10.600
2	24.800	42	20.800	82	16.600	122	10.474
3	24.700	43	20.615	83	16.496	123	10.400
4	24.616	44	20.500	84	16.400	124	10.200
5	24.550	45	20.460	85	16.350	125	10.000
6	24.500	46	20.410	86	16.300	126	9.800
7	24.400	47	20.325	87	16.250	127	9.752
8	24.300	48	20.270	88	16.194	128	9.718
9	24.245	49	20.180	89	16.000	129	9.600
10	24.184	50	20.115	90	15.911	130	9.425
11	24.105	51	20.050	91	15.831	131	9.400
12	24.048	52	19.985	92	15.600	132	9.200
13	24.000	53	19.818	93	15.400	133	9.144
14	23.900	54	19.800	94	15.200	134	9.000
15	23.800	55	19.650	95	15.000	135	8.845
16	23.700	56	19.500	96	14.918	136	8.800
17	23.620	57	19.450	97	14.800	137	8.600
18	23.500	58	19.317	98	14.600	138	8.400
19	23.455	59	19.200	99	14.400	139	8.200
20	23.400	60	19.000	100	14.200	140	8.000
21	23.300	61	18.800	101	14.000	141	7.800
22	23.200	62	18.750	102	13.800	142	7.600
23	23.300	63	18.600	103	13.600	143	7.400
24	23.100	64	18.590	104	13.400	144	7.200
25	23.000	65	18.576	105	13.200	145	7.100
26	22.873	66	18.448	106	13.000	146	6.951
27	22.800	67	18.400	107	12.800	147	6.800
28	22.785	68	18.277	108	12.762	148	6.600
29	22.625	69	18.200	109	12.600	149	6.470
30	22.600	70	18.000	110	12.600	150	6.400
31	22.439	71	17.800	111	12.400	151	6.200
32	22.400	72	17.606	112	12.200	152	6.000
33	22.200	73	17.500	113	12.031	153	5.800
34	22.000	74	17.400	114	12.000	154	5.600
35	21.811	75	17.359	115	11.800		
36	21.600	76	17.200	116	11.600		
37	21.460	77	17.065	117	11.400		
38	21.400	78	17.034	118	11.200		
39	21.200	79	16.878	119	11.000		
40	21.000	80	16.800	120	10.783		

A3.2 Brenno

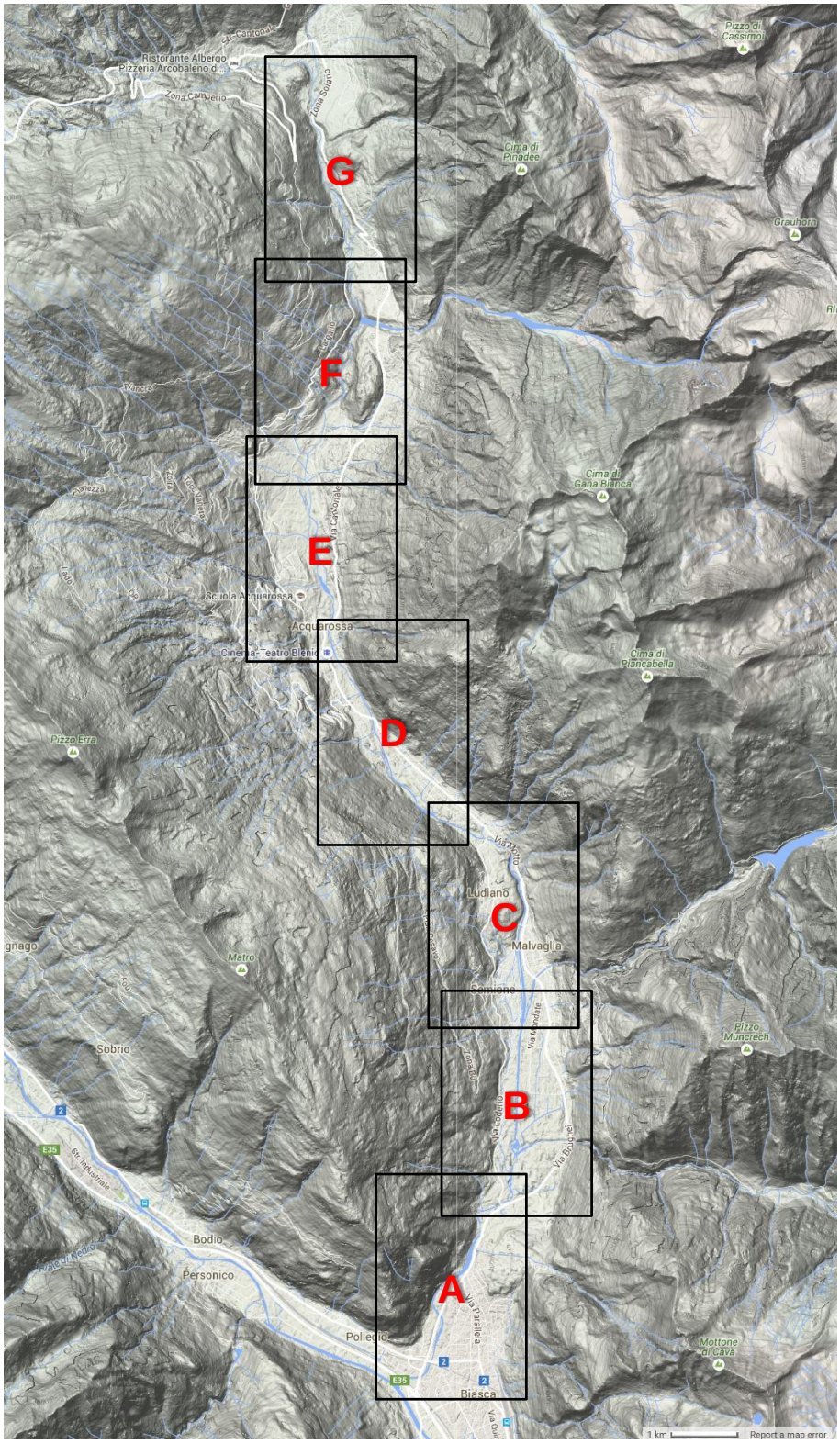

Figure A3.8 Brenno Sheets

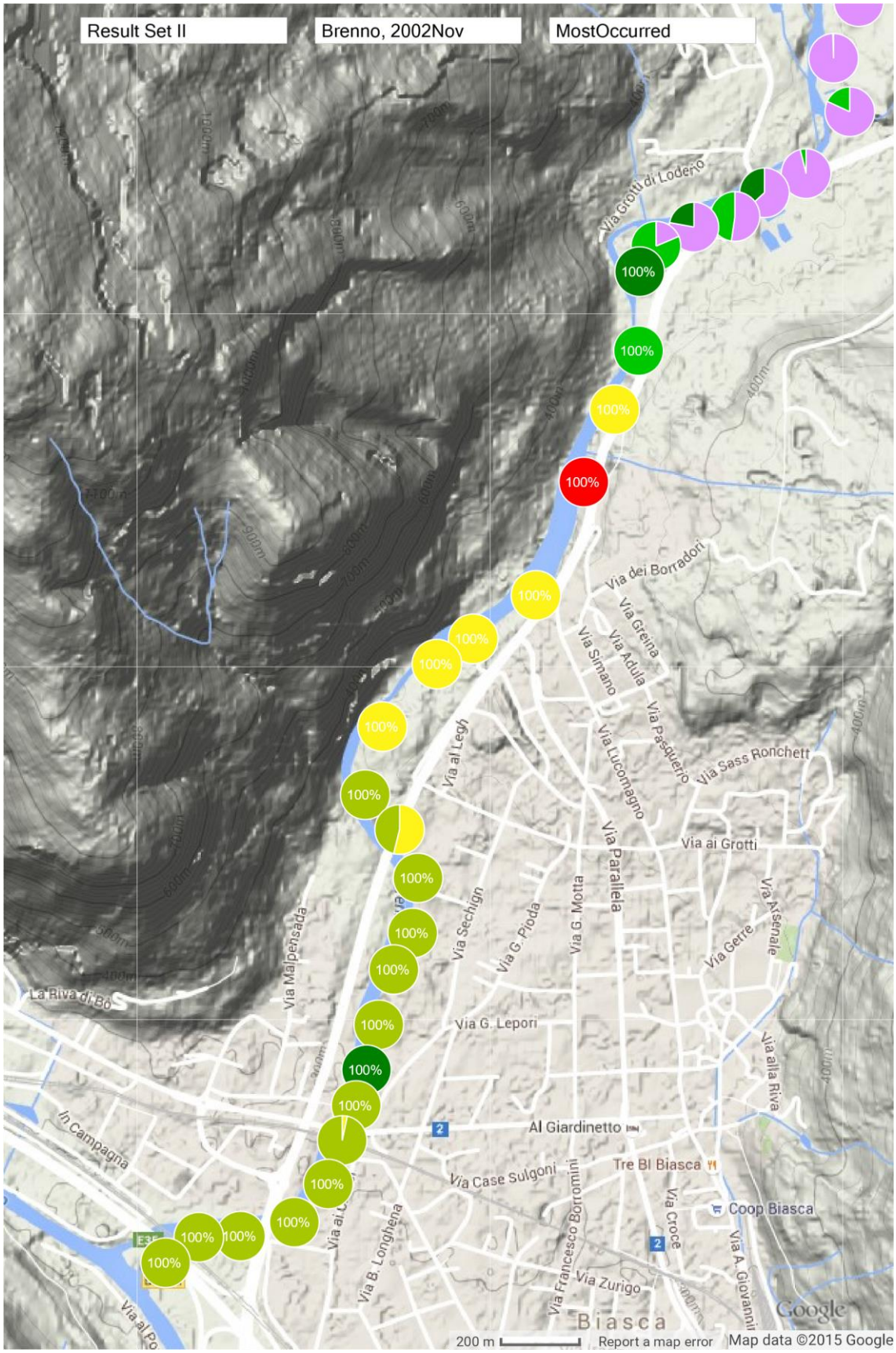

Figure A3.9 Brenno Sheet A

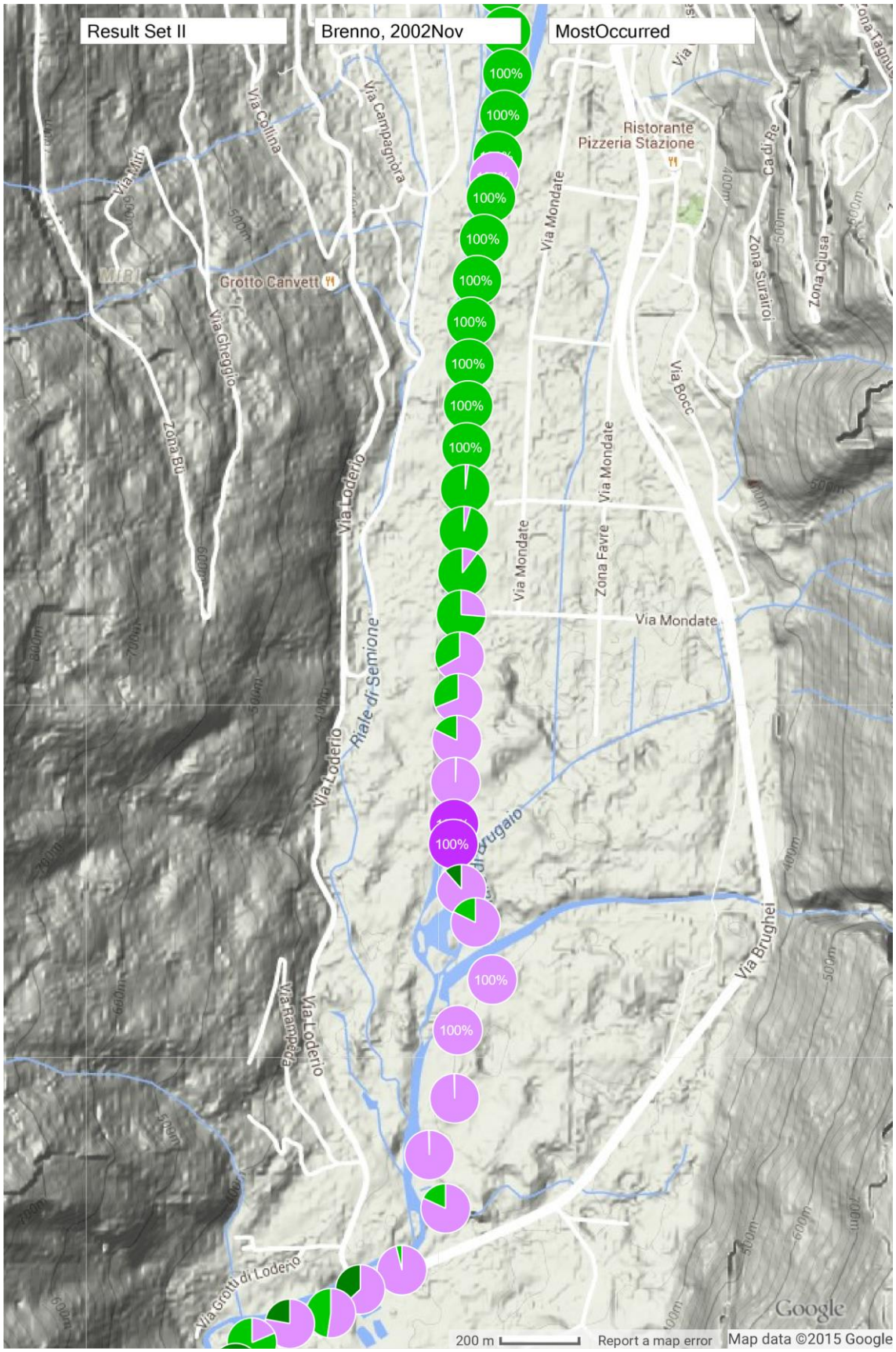

Figure A3.10 Brenno Sheet B

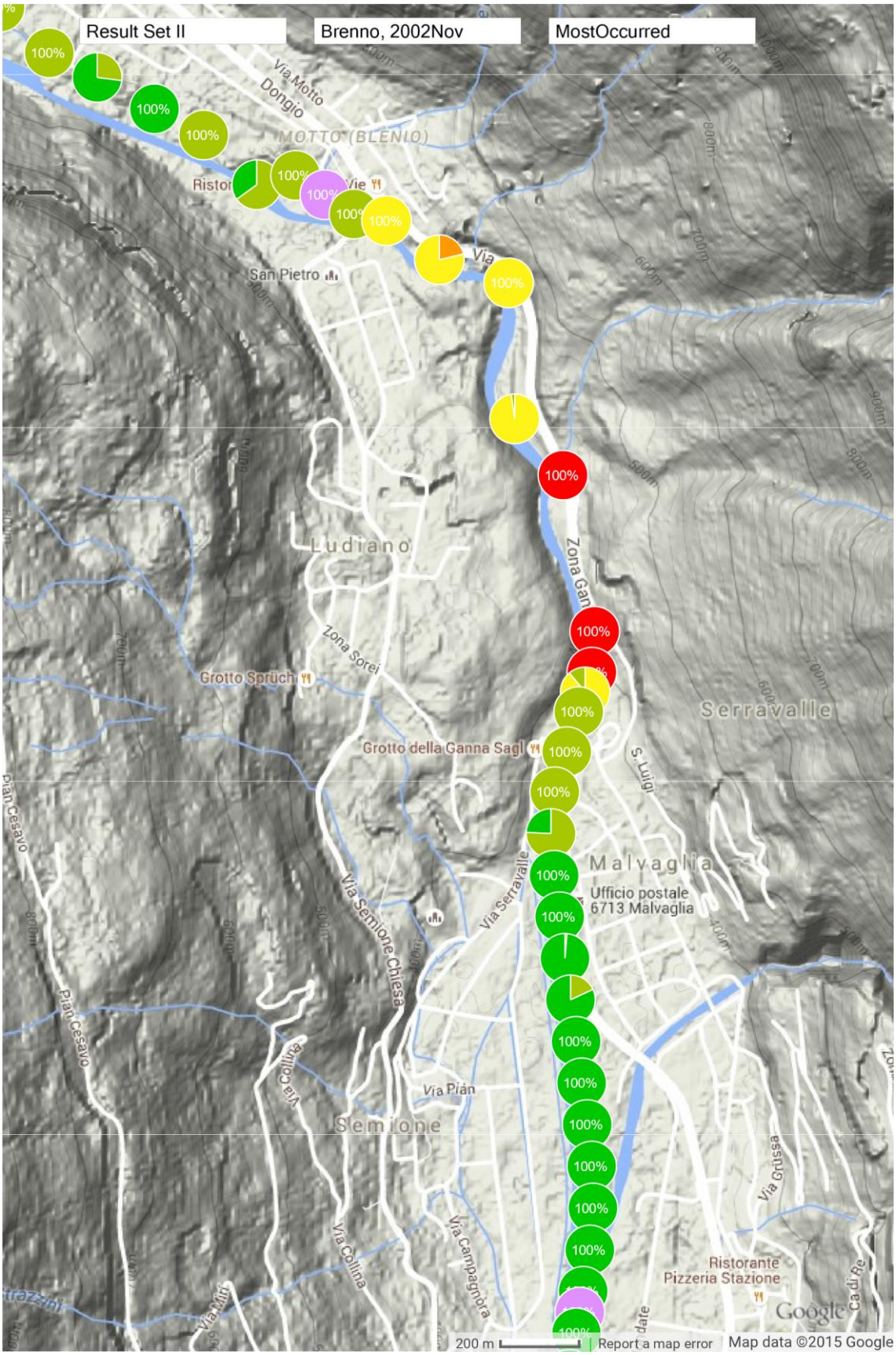

Figure A3.11 Brenno Sheet C

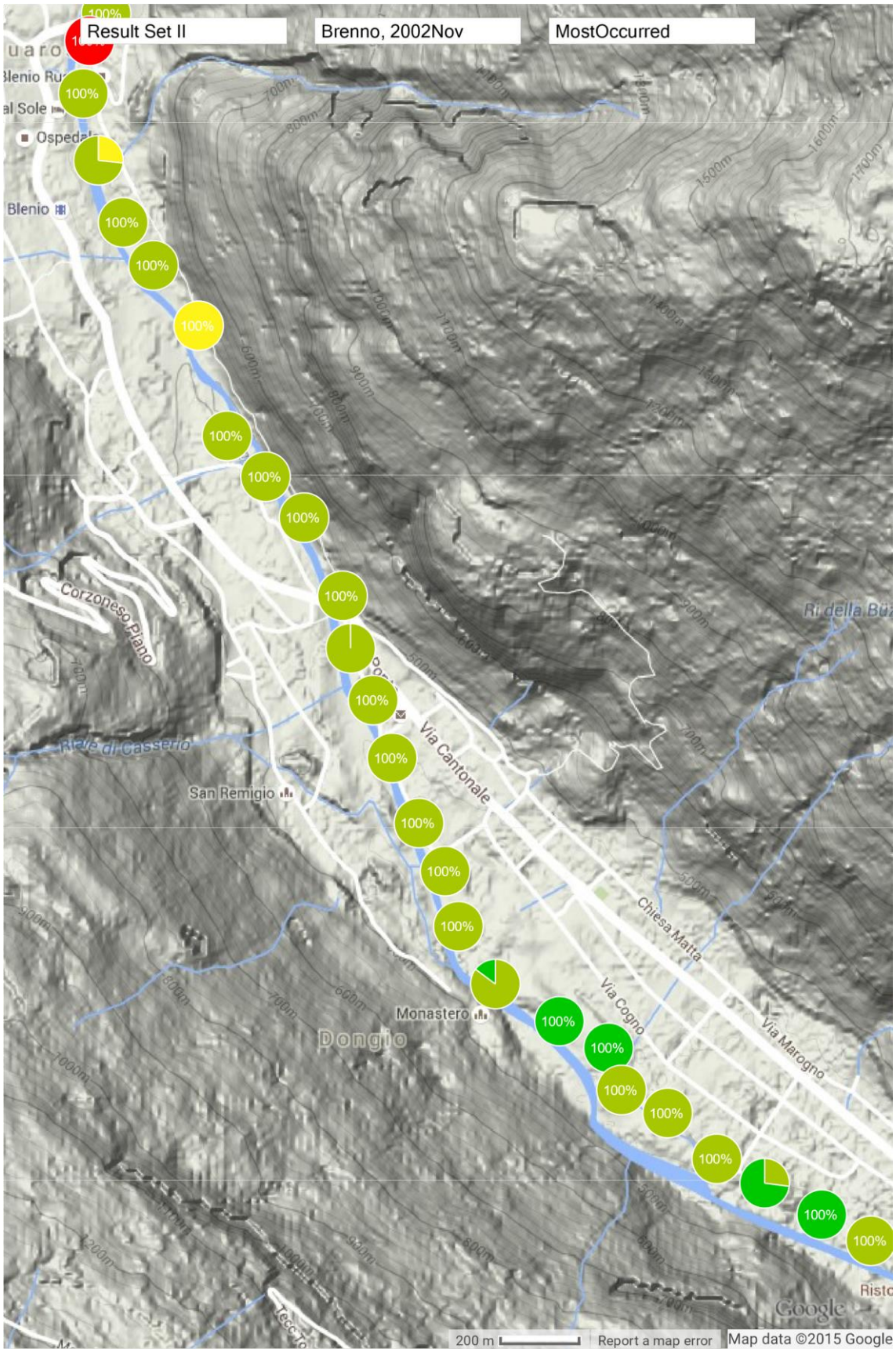

Figure A3.12 Brenno Sheet D

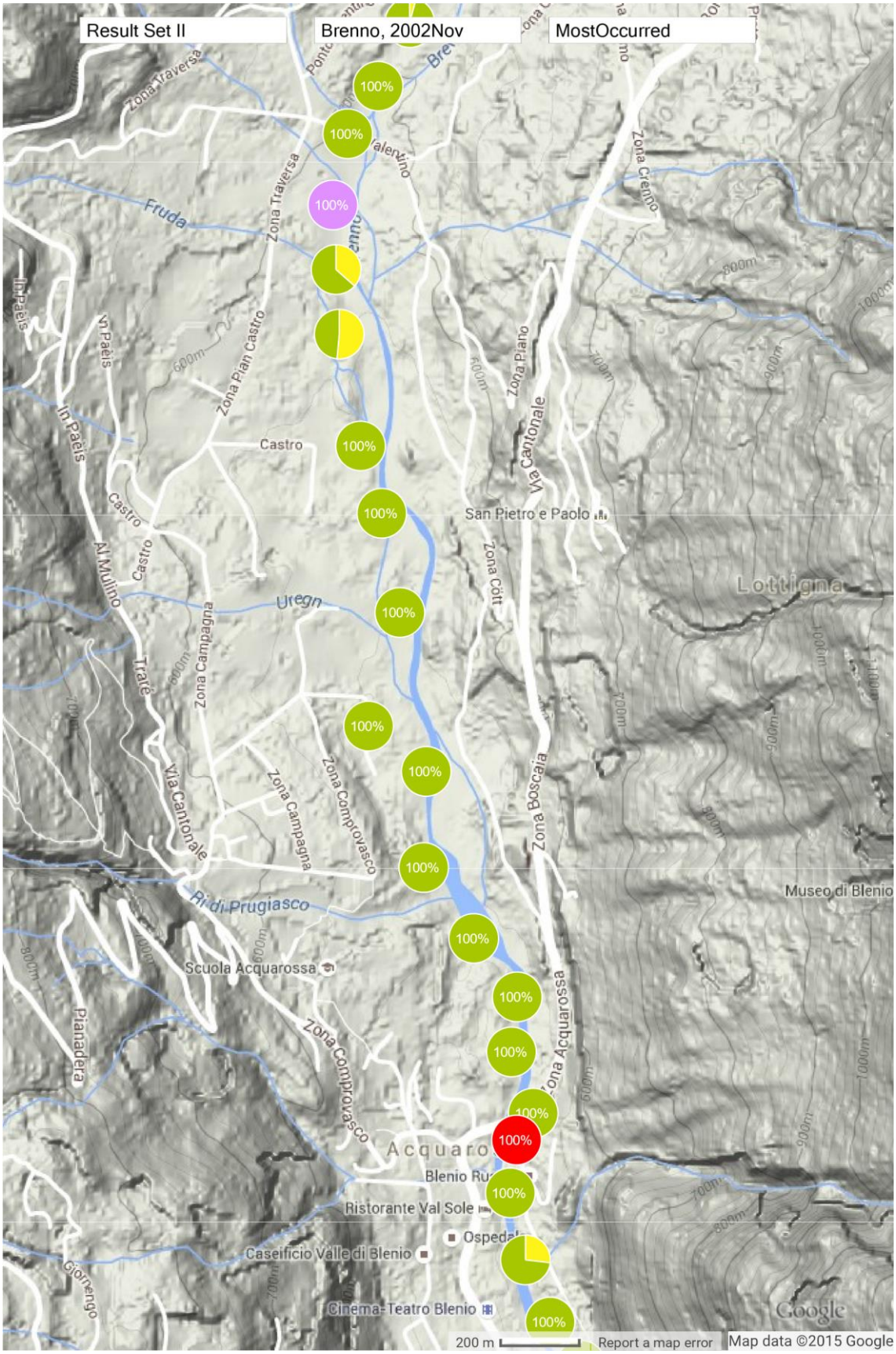

Figure A3.13 Brenno Sheet E

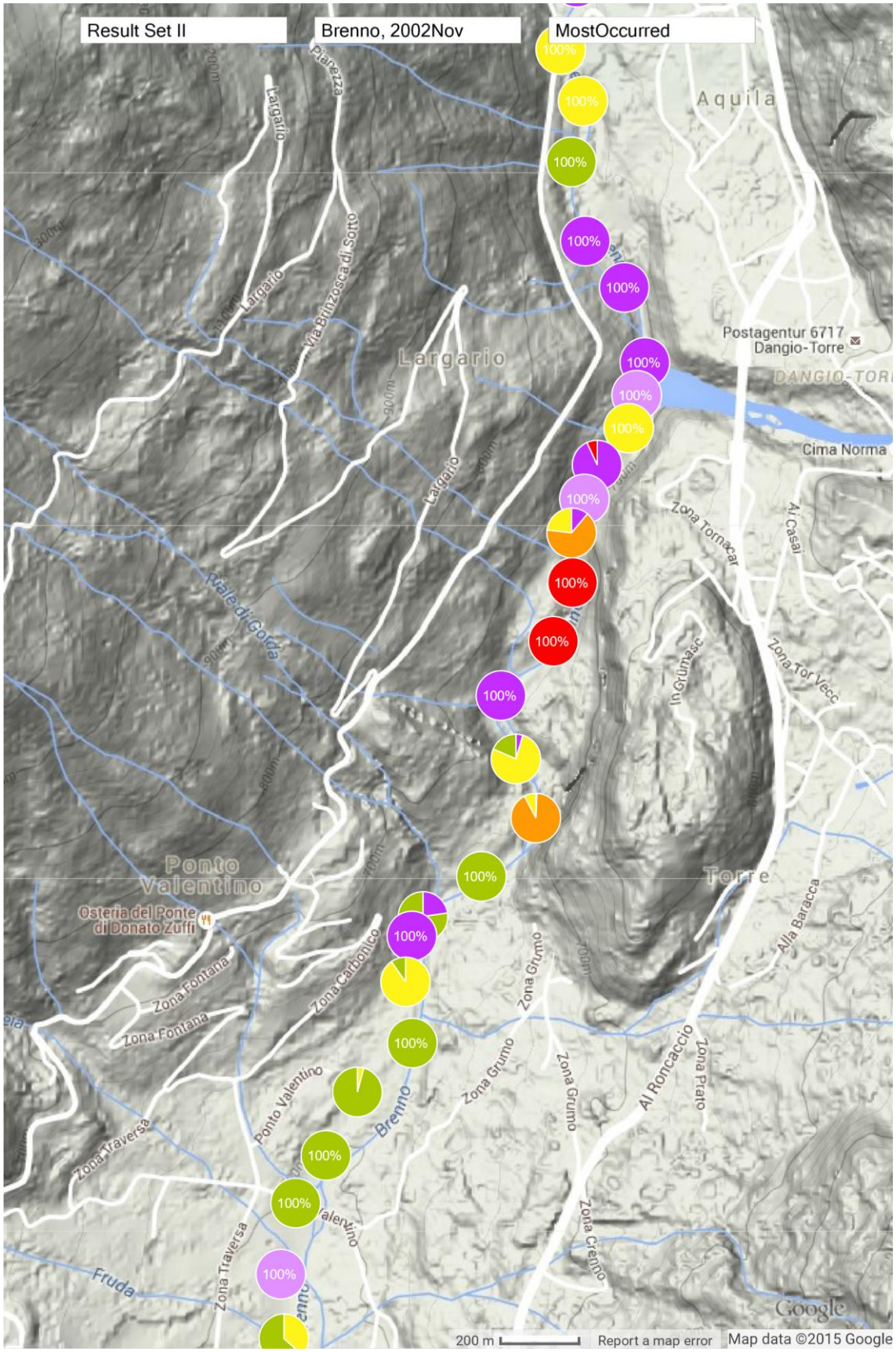

Figure A3.14 Brenno Sheet F

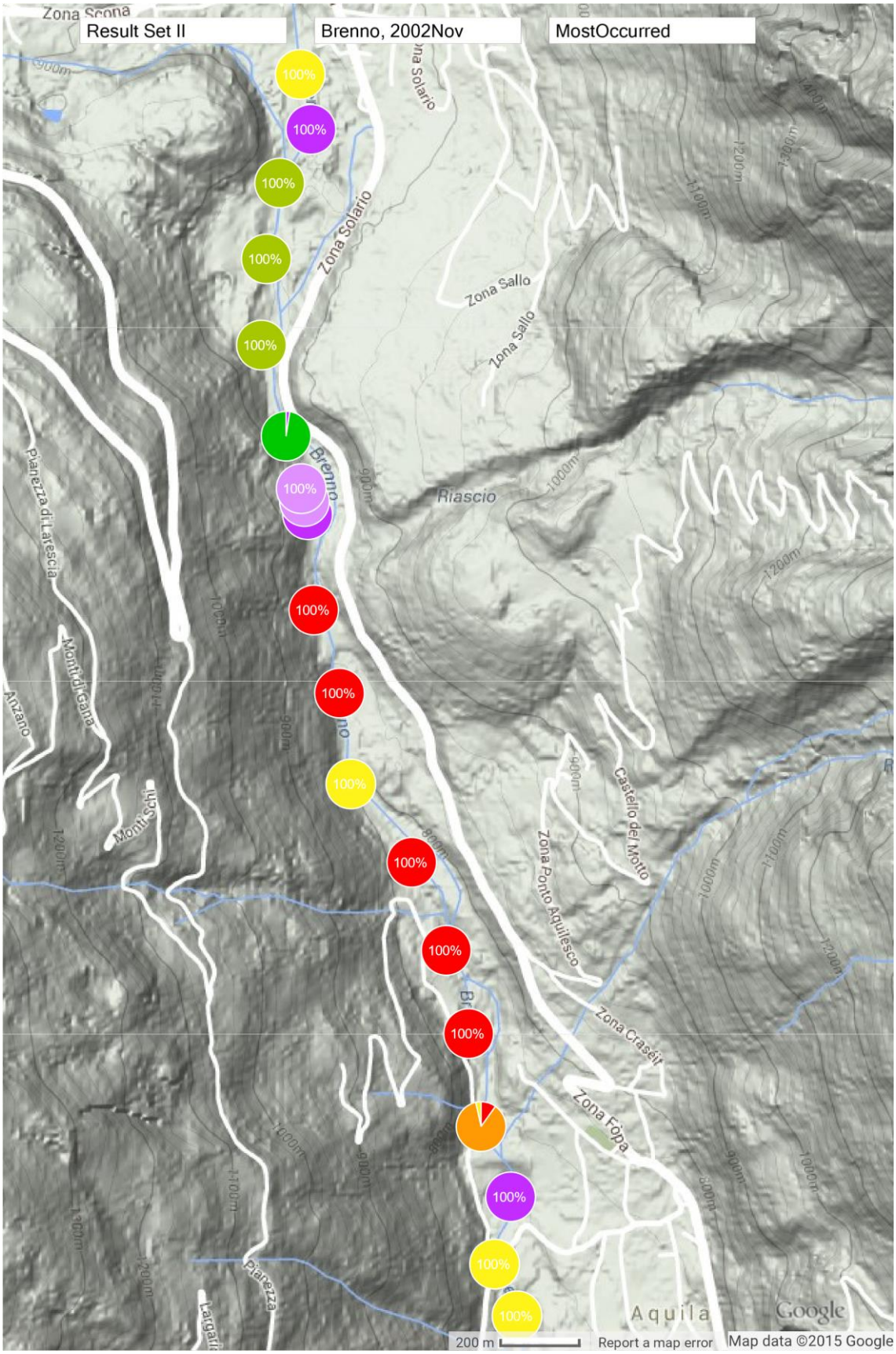

Figure A3.15 Brenno Sheet G

Table A3.3 The Kilometrage of Brenno Reach Ids

Reach Id	Km	Reach Id	Km	Reach Id	Km	Reach Id	Km
1	22.105	41	15.760	81	9.310	121	4.858
2	22.106	42	15.595	82	9.260	122	4.758
3	21.830	43	15.595	83	9.160	123	4.658
4	21.640	44	15.320	84	9.082	124	4.610
5	21.425	45	15.025	85	8.918	125	4.505
6	21.235	46	14.870	86	8.748	126	4.433
9	20.975	47	14.580	87	8.406	127	4.295
8	20.785	48	14.363	88	8.226	128	4.461
7	20.980	49	14.252	89	7.858	129	4.395
10	20.785	50	14.030	90	7.758	130	4.170
11	20.565	51	13.810	91	7.708	131	4.008
12	20.340	52	13.632	92	7.658	132	3.862
13	20.110	53	13.482	93	7.558	133	3.692
14	19.860	54	13.345	94	7.458	134	3.573
15	19.640	55	13.260	95	7.358	135	3.479
16	19.440	56	13.140	96	7.258	136	3.373
17	19.240	57	12.960	97	7.158	137	3.274
18	19.050	58	12.805	98	7.058	138	3.175
19	18.925	59	12.650	99	6.958	139	3.097
20	18.742	60	12.490	100	6.858	140	2.903
21	18.585	61	12.340	101	6.758	141	2.753
22	18.415	62	12.155	102	6.658	142	2.556
23	18.225	63	11.975	103	6.558	143	2.302
24	18.155	64	11.765	104	6.458	144	2.086
25	18.055	65	11.635	105	6.358	145	1.964
26	17.866	66	11.495	106	6.258	146	1.768
27	17.790	67	11.345	107	6.258	147	1.549
28	17.720	68	11.180	108	6.158	148	1.420
29	17.580	69	11.070	109	6.058	149	1.313
30	17.433	70	10.915	110	5.958	150	1.200
31	17.245	71	10.735	111	5.858	151	1.100
32	17.105	72	10.565	112	5.758	152	0.959
33	16.920	73	10.440	113	5.658	153	0.846
34	16.720	74	10.330	114	5.558	154	0.757
35	16.535	75	10.175	115	5.458	155	0.666
36	16.495	76	10.025	116	5.358	156	0.558
37	16.375	77	9.900	117	5.258	157	0.451
38	16.235	78	9.760	118	5.158	158	0.320
39	16.050	79	9.608	119	5.058	159	0.229
40	15.885	80	9.465	120	4.958	160	0.092

Communications du Laboratoire de Constructions Hydrauliques ISSN 1661-1179
Ecole Polytechnique Fédérale de Lausanne
Editeur: Prof. Dr A. Schleiss

N° 49 2011 F. Hachem
Monitoring of steel-lined pressure shafts considering water-hammer wave signals and fluid-structure interaction

N° 50 2011 J.-M. Ribi
Etude expérimentale de refuges à poissons aménagés dans les berges de rivières soumises aux éclusées hydroélectriques

N° 51 2012 W. Gostner
The Hydro-Morphological Index of Diversity:
a planning tool for river restoration projects

N° 52 2012 M. Bieri
Operation of complex hydropower schemes and its impact on the flow regime in the downstream river system under changing scenarios

N° 53 2012 M. Müller
Influence of in- and outflow sequences on flow patterns and suspended sediment behavior in reservoirs

N° 54 2013 V. Dugué
Influencing river morphodynamics by means of a bubble screen: application to open-channel bends

N° 55 2013 E. Person
Impact of hydropeaking on fish and their habitat

N° 56 2013 T. Cohen Liechti
Influence of dam operation on water resources management under different scenarios in the Zambezi River Basin considering environmental objectives and hydropower

N° 57 2014 A. M. da Costa Ricardo
Hydrodynamics of turbulent flows within arrays of circular cylinders

N° 58 2014 T. Ghilardi
Sediment transport and flow conditions in steep rivers with large immobile boulders

N° 59 2014 R. Duarte
Influence of air entrainment on rock scour development and block stability in plunge pools

N° 60 2014 J. P. Matos
Hydraulic-hydrologic model for the Zambezi River using satellite data and artificial intelligence techniques

N° 61 2015 S. Guillén Ludeña
Hydro-morphodynamics of open-channel confluences with low discharge ratio and dominant tributary sediment supply

N° 62 2016 M. Jafarnejad Chaghooshi
Time-dependent failure analysis of large block size riprap as bank protection in mountain rivers

ISSN 1661-1179

DOI: 10.5075/epfl-lchcomm-62

Prof. Dr A. Schleiss
Laboratoire de constructions hydrauliques - LCH
EPFL, Bât. GC, Station 18, CH-1015 Lausanne
http://lch.epfl.ch
e-mail: secretariat.lch@epfl.ch